First-Principles Models for van der Waals Interactions in Molecules and Materials: Concepts, Theory, and Applications

Jan Hermann[1], Robert A. DiStasio Jr.[2,*], and Alexandre Tkatchenko[1,3,*]

[1]*Fritz-Haber-Institut der Max-Planck-Gesellschaft, Faradayweg 4–6, 14195 Berlin, Germany*
[2]*Department of Chemistry and Chemical Biology, Cornell University, Ithaca, NY 14853, USA*
[3]*Physics and Materials Science Research Unit, University of Luxembourg, L-1511 Luxembourg*
[*]email: alexandre.tkatchenko@uni.lu, distasio@cornell.edu

Abstract

Noncovalent van der Waals (vdW) or dispersion forces are ubiquitous in nature and influence the structure, stability, dynamics, and function of molecules and materials throughout chemistry, biology, physics, and materials science. These forces are quantum-mechanical in origin and arise from electrostatic interactions between fluctuations in the electronic charge density. Here, we explore the conceptual and mathematical ingredients required for an exact treatment of vdW interactions, and present a systematic and unified framework for classifying the current first-principles vdW methods based on the adiabatic-connection fluctuation–dissipation (ACFD) theorem (namely the Rutgers–Chalmers vdW-DF, Vydrov–Van Voorhis (VV), exchange-hole dipole moment (XDM), Tkatchenko–Scheffler (TS), many-body dispersion (MBD), and random-phase approximation (RPA) approaches). Particular attention is paid to the intriguing nature of many-body vdW interactions, whose fundamental relevance has recently been highlighted in several landmark experiments. The performance of these models in predicting binding energetics as well as structural, electronic, and thermodynamic properties is connected with the theoretical concepts and provides a numerical summary of the state-of-the-art in the field. We conclude with a roadmap of the conceptual, methodological, practical, and numerical challenges that remain in obtaining a universally applicable and truly predictive vdW method for realistic molecular systems and materials.

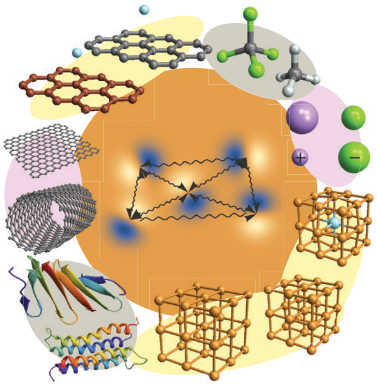

Contents

1 Introduction **2**
2 Conceptual understanding of vdW interactions in molecules and materials **3**
3 Experimental evidence for the nonlocal and non-additive nature of van der Waals dispersion interactions **9**
4 Theoretical framework for van der Waals models **11**
4.1 From point polarizability to nonlocal polarizability and back . . . 12
4.2 Exact correlation energy from nonlocal dynamic polarizability . . . 13
4.3 Local effective polarizability from the electron density . . . 16
4.3.1 Anisotropy of $\alpha_{\mathrm{eff}}(\mathbf{r})$ . . . 17
4.3.2 Harmonic oscillator model of dynamic response . . . 18
4.4 Classification of approximate van der Waals methods . . . 19
4.4.1 Coarse-graining the ACFD formula and Dyson equation . . . 19
4.4.2 Truncating the many-body expansion of the long-range correlation energy . 20
4.5 Methods based on random-phase approximation 20
4.5.1 Range-separated random-phase approximation . . . 21
4.5.2 Approximate exchange-correlation kernels . . . 21
4.5.3 Renormalized perturbation theory to second order . . . 21
4.6 Nonlocal density functionals . . . 22
4.6.1 A simple nonlocal functional . . . 23
4.6.2 vdW-DF functional . . . 23
4.6.3 Variations of vdW-DF . . . 24
4.7 Fragment-based pairwise methods . . . 25
4.7.1 Fragment-based pairwise models from the ACFD formula . . . 25
4.7.2 Models for C_6 dispersion coefficients and other vdW parameters . . . 26
4.8 Many-body dispersion framework . . . 29
4.8.1 Many-body dispersion framework from the ACFD formula . . . 29
4.8.2 Range-separated many-body dispersion method . . . 30
4.8.3 General remarks about MBD and *n*-body expansions . . . 30

5 Models for vdW interactions: Applications 31
5.1 Benchmark databases 31
5.2 Structural and electronic properties 35
5.3 Molecular dynamics 37
6 Challenges and outlook 39
7 Concluding remarks 41

1 Introduction

The ongoing challenges associated with modeling increasingly large and more complex molecular and condensed-phase materials have led to the universal realization that van der Waals (vdW) dispersion interactions (Langbein, 1974; Parsegian, 2005; Kaplan, 2006; Stone, 2013), commonly considered to be only a small contribution to the total energy, are in fact a crucial ingredient of both a qualitatively correct and quantitatively accurate description of the binding properties in a majority of molecular systems (Grimme, 2011; Klimeš and Michaelides, 2012; Reilly and Tkatchenko, 2015) and materials (French et al., 2010; Tkatchenko, 2015; Woods et al., 2016). In fact, it has become increasingly more apparent that the relevance of vdW interactions extends well beyond binding and cohesive energies, encompassing the structural (Tkatchenko, 2015; Reilly and Tkatchenko, 2015), mechanical (Shtogun and Woods, 2010; Gao and Tkatchenko, 2015), spectroscopic (Reilly and Tkatchenko, 2014b), kinetic (Gao and Tkatchenko, 2013), and even electronic (Ferri et al., 2015; Brémond et al., 2014) signatures of condensed matter. With an influence that ranges from drug binding in proteins and double-helix stability in DNA (DiStasio et al., 2012) to pedal adhesion in geckos (Autumn et al., 2000, 2002) and cohesion in asteroids (Rozitis et al., 2014; Scheeres et al., 2010), these nonbonded forces are quantum mechanical in origin and arise from the electrostatic interactions between the constantly fluctuating electron clouds which constitute molecules and materials (Ambrosetti et al., 2016). As such, vdW dispersion interactions are strongly nonlocal, extending to distances exceeding 10 nm in nanoscale materials (Dobson et al., 2006; Loskill et al., 2012, 2013; Ambrosetti et al., 2016), or even further in mesoscopic materials (Klimchitskaya et al., 2009; Rodriguez et al., 2011; Bordag et al., 2006).

With this context, the importance of understanding and modeling vdW interactions in realistic systems can hardly be overemphasized. However, our ability to accurately model these interactions from first principles is severely impeded by the prohibitively high computational cost of the high-level wavefunction methods of quantum chemistry, as well as the lack of efficient yet accurate approximations to the many-body electron correlation problem for large systems (Szabo and Ostlund, 1989). In light of this fact, the sophistication of approximate models for describing vdW interactions has been steadily increasing, especially within the context of electronic structure methods based on density-functional theory (DFT). The majority of these commonly used vdW-inclusive methods finds a theoretical basis in the quantum-mechanical treatment of two fragments A and B (*e.g.*, atoms, localized orbitals, or infinitesimal regions of the electron density) separated by a distance, R_{AB}, that places them outside of density or orbital overlap, for which second-order perturbation theory predicts the vdW interaction energy to be proportional to R_{AB}^{-6} (to leading order). Only recently have more advanced theoretical models been developed which go beyond this pairwise-additive approximation, resulting in quantitative improvements in the predictive capabilities of vdW-inclusive DFT calculations and novel conceptual insights into the nature of many-body vdW interactions. At this point, the existence of advanced theoretical models for describing vdW interactions coupled with the rapid increase in available computational resources has allowed us to achieve the accuracy needed for meaningful prediction of binding energetics between small organic molecules (Grimme et al., 2016) and vdW-inclusive methods are now even being extended towards quantitative predictions of the properties and functions of technologically and biologically relevant materials (Tkatchenko, 2015; Woods et al., 2016).

Meanwhile, the steep rise in the number of applications of vdW-inclusive methods to larger and more complex systems has led to a more comprehensive understanding of their inherent strengths and weaknesses, as well as a rough delineation of their respective ranges of applicability. Despite such substantial progress in the field of modeling vdW interactions, many questions still remain unanswered and significant further development is required before a universally applicable approach emerges. For instance, the aforementioned pairwise-additive interatomic vdW methods are frequently used to describe adsorption of organic molecules on inorganic surfaces (Mercurio et al., 2010; Atodiresei et al., 2009; Tonigold and Groß, 2010; Stradi et al., 2011). Despite the fact that such an approach effectively ignores the relatively strong electrodynamic response screening present in bulk materials, the results often have a reasonable level of accuracy. Another example comes in the form of use of the nonlocal vdW-DF family of functionals (Dion et al., 2004; Lee et al., 2010; Vydrov and Van Voorhis, 2009b; Berland et al., 2015) to describe binding between molecules, which can lead to an acceptable level of accuracy even though one would not expect the employed homogeneous dielectric approximation to work well for molecules. These examples highlight the need for a deeper understanding of the physical reasons for why these different approaches often yield relatively good results outside their expected domains of applicability, as this is a determining factor in the development of more robust approximations.

In general, vdW interactions can be remarkably sensitive to the geometry and electronic structure of a given system. Therefore, these interactions not only affect the structure and dynamics of the system, but can also have a visible effect on the electronic charge distribution and other properties derived from the charge density (*e.g.*, multipole moments, work functions, polarizabilities, electron affinities, etc.) (Ferri et al., 2015), in accordance with the theoretical insight into vdW interactions advocated by Feynman (Feynman, 1939). This observation highlights the need for first-principles based methods—vdW methods that explicitly depend on the charge density or orbitals—in which the vdW interactions are treated in a fully self-consistent manner; as such, these methods are the main focus of this work.

In this review, we will use the terms "van der Waals (vdW) interactions" and "dispersion interactions" interchangeably. Originally, vdW interactions encompassed (especially in the chemistry literature) electrostatic (permanent moment–permanent moment), induction (permanent moment–induced moment), and dispersion (induced moment–induced moment) interactions. In the current work, however, this trio is increasingly being referred to as noncovalent interactions, while vdW interactions are reserved specifically for the dispersion interactions, thus aligning the terminology with the physics literature. This has perhaps been motivated by the ever increasing overlap between chemistry and condensed-matter physics in the field of vdW interactions. Another matter of terminology that extends well beyond semantics concerns the use of the phrase "many-body"; here the communities significantly differ in their association of a given physical (or mathematical) entity with the label "body". For example, a body would typically refer to a molecule in the field of molecular modeling, although it could also refer to an atom, as demonstrated by the literature on the Axilrod–Teller–Muto three-body (three-atom) potential (Axilrod and Teller, 1943; Muto, 1943). In the quantum chemistry community, the coupled-cluster hierarchy is a particular class of methods within many-body perturbation theory, and in this case, the bodies are electrons (electronic excitations). In this review, we will use the term many-body when referring to interactions between more than two bodies (*i.e.*, beyond pairwise), as the point of this term is to delineate the degree of coupling in a given model. The meaning of the term body will therefore change according to the context and we hope that our exposition will make it clear why such a fluidic use of this term is indeed helpful in defining a general conceptual and mathematical framework for describing vdW interactions.

This review concentrates on the conceptual, methodological, mathematical, and numerical aspects of various approaches for treating vdW interactions based on first principles. For the plethora of other aspects associated with vdW interactions, we refer the interested reader to the following set of reviews, which is by no means an exhaustive list but includes many works which are complementary to that presented here (Langreth et al., 2009; Johnson et al., 2009; Tkatchenko et al., 2010; Grimme, 2011; Ruzsinszky and Perdew, 2011; Cohen et al., 2012; Burke, 2012; Klimeš and Michaelides, 2012; Dobson and Gould, 2012; Dobson, 2014; DiStasio et al., 2014b; Tkatchenko, 2015; Reilly and Tkatchenko, 2015; Wagner and Schreiner, 2015; Grimme et al., 2016).

This review begins with a conceptual introduction to the treatment of vdW interactions in molecules and materials of increasing complexity, showcasing the critical ingredients necessary for a qualitatively correct and physically sound description of these interactions in different classes of systems. We then proceed with a brief discussion of several recent landmark experiments that clearly highlight the nontrivial nature of vdW interactions at the nanoscale and demonstrate that our understanding of these quantum-mechanical phenomena is only beginning to emerge. This is followed by a comprehensive theoretical basis for the description of vdW interactions that provides a systematic classification scheme and derivation of many of the popular first-principles based methods within the framework of the adiabatic-connection fluctuation–dissipation (ACFD) theorem. A critical assessment of the performance of these models in predicting binding energetics, structural and electronic properties, as well as equilibrium quantities from *ab initio* molecular dynamics is then discussed, as we introduce the many challenges that arise when these methods are applied to increasingly realistic and experimentally relevant systems. We conclude this review by presenting an outlook which not only summarizes the achievements in the field of modeling vdW interactions in the last decade, but also highlights the many remaining challenges that we expect will keep this exciting field quite active for some time to come.

2 Conceptual understanding of vdW interactions in molecules and materials

In this section, we discuss the current conceptual understanding of noncovalent vdW interactions in molecules and materials. By considering a set of fundamental systems, we demonstrate how the vdW energy depends on local (additive or weakly nonadditive) and nonlocal (nonadditive) effects that originate from the underlying electronic structure of the system. Our focus here is on identifying and analyzing the ingredients (Figure 1) that are necessary to correctly describe vdW interactions across a wide array of systems characterized by markedly different structural features (*e.g.*, size, dimensionality, geometry/topology), electronic properties (*e.g.*, covalent/ionic bonding, hybridization, oxidation state, charge transfer), and environmental effects (*e.g.*, solvation, interfaces, external pressure).

Currently available vdW-inclusive methods are able to describe how these structural, electronic, and environmental considerations affect the vdW energy only to a certain extent which varies from method to method. In general, the methods can be classified based on the approximations that they use for the two central quantities required for description of vdW interactions, namely the nonlocal microscopic frequency-dependent polarizability $\alpha(\mathbf{r}, \mathbf{r}', u)$ and the effective interaction potential $v(\mathbf{r}, \mathbf{r}')$ between points $\mathbf{r}$ and $\mathbf{r}'$ in space. This classification scheme is illustrated in Figure 2 and includes (a) the exact treatment of the electron correlation via the adiabatic-connection fluctuation–dissipation (ACFD) theorem (McLachlan and Ball, 1964; Harris and Jones, 1974; Langreth and Perdew, 1977), (b) fragment-based (or coarse-grained) many-body vdW methods (Tkatchenko et al., 2012; Silvestrelli, 2013), (c) fragment-based (or coarse-grained) pairwise vdW methods (Grimme, 2004; Grimme et al., 2010; Becke and Johnson, 2007; Tkatchenko and Scheffler, 2009; Steinmann and Corminboeuf, 2010), and (d) nonlocal two-point (fine-grained) density-functional approximations (Dion et al., 2004; Lee et al., 2010; Vydrov and Van Voorhis, 2009b, 2010b). For quick overview, we present a condensed description of the most widely used vdW methods in Table 1, which includes a brief synopsis of each method as well as a critical assessment of their performance in treating different aspects of vdW interactions. Throughout this section we discuss the different scenarios that

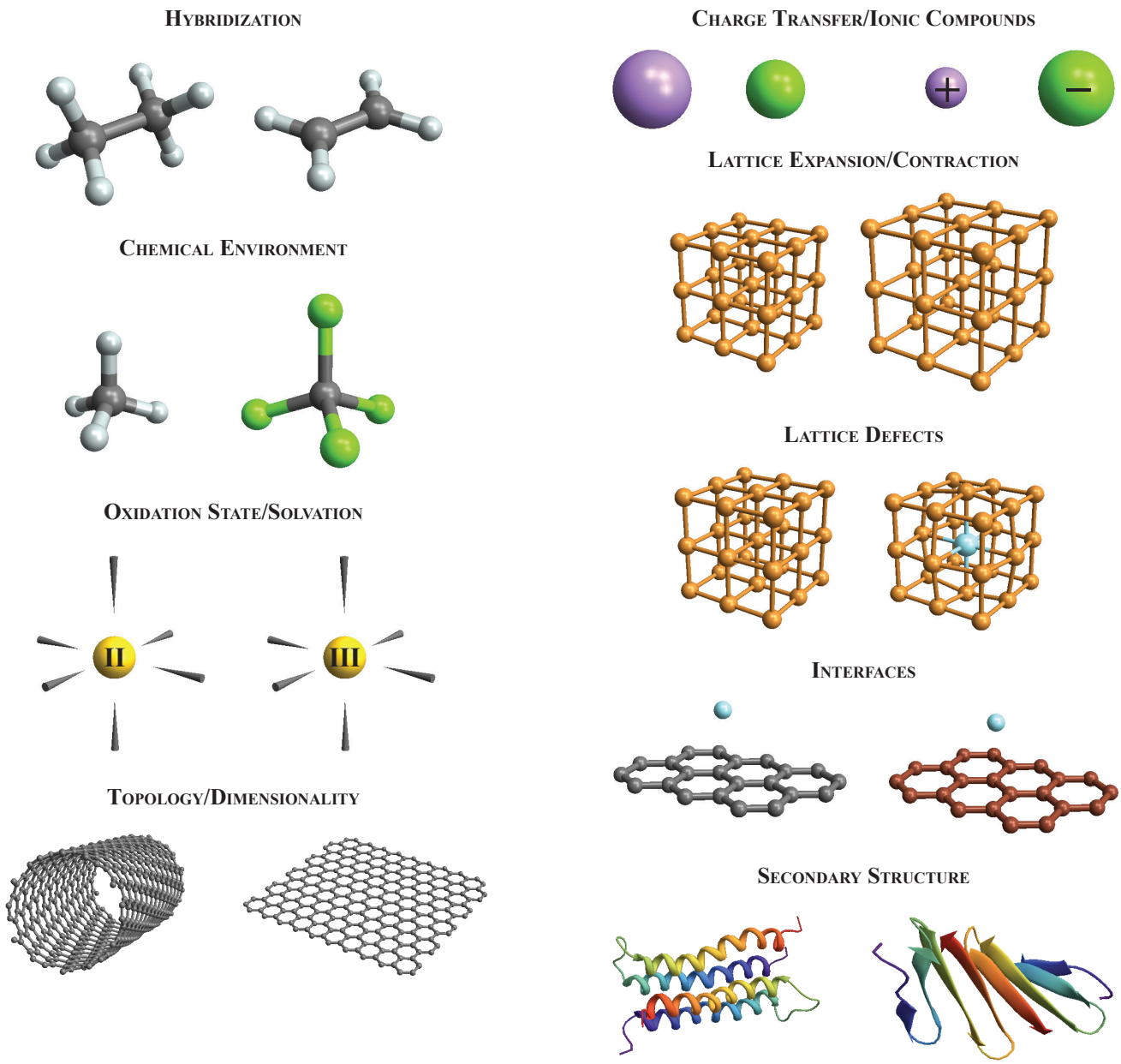

Figure 1. Structural features, electronic properties, and environmental effects of relevance to noncovalent vdW interactions. Each of these distinct system characteristics affects the underlying electronic structure and therefore the associated vdW interactions, leading to the complications in accurate modeling of these interactions in realistic systems. A seamless and universally applicable vdW method must meet this challenge and accurately describe these effects across a wide range of systems found in chemistry, biology, and physics.

arise in the modeling of the polarizability and interaction potential in systems of increasing complexity. While this section focuses on a conceptual picture of vdW interactions, Section 4 will address these issues from a mathematical point of view. We aim to dispel several myths about vdW interactions and note that many of the points will be revisited and reinforced by the more formal presentation in Section 4.

The exact solution of the electronic Schrödinger equation would automatically incorporate the exact vdW contribution to the total energy of a many-electron system, as this contribution is strictly contained in the electron correlation energy. However, the explicit solution of the Schrödinger equation for a system containing more than a few electrons is still a computationally prohibitive task, even when many approximations are used. For this reason, modeling of realistic materials often starts with more tractable mean-field models, such as the Hartree-Fock (HF) approximation, or the alternative suite of density-functional approximations (DFAs), which use the three-dimensional electron charge density, $n(\mathbf{r})$, instead of the exceedingly more complicated many-electron wave function.

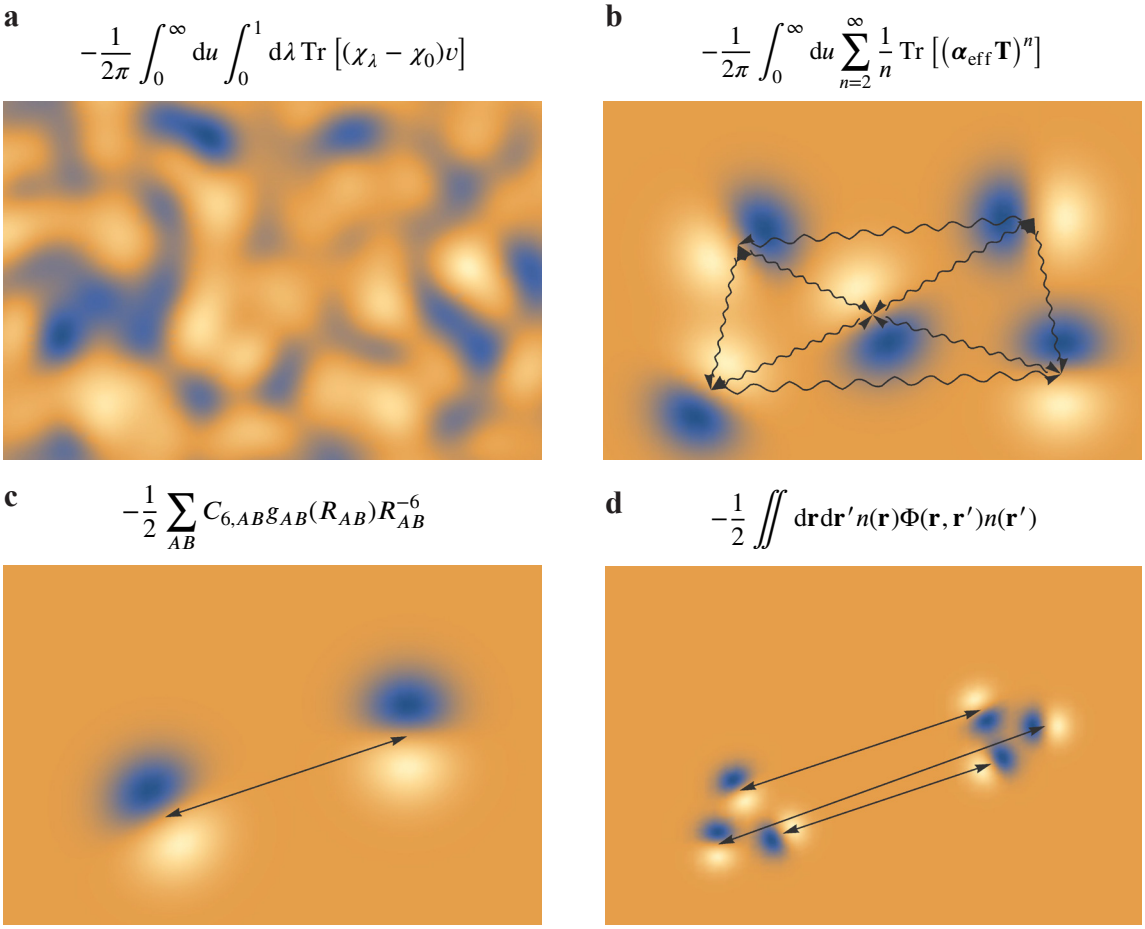

Figure 2. Theoretical approaches used by different vdW models based on first principles. **(a)** Exact treatment of the correlation energy in the framework of the adiabatic-connection fluctuation–dissipation (ACFD) theorem, which uses the full nonlocal response function $\chi_\lambda(\mathbf{r}, \mathbf{r}', u)$. This response function can be viewed as describing the propagation of fluctuations throughout the molecule or material. **(b)** Fragment-based (coarse-grained) many-body methods correlate fluctuations to infinite order by using model response functions in the ACFD formula. **(c)** Fragment-based (coarse-grained) two-body methods compute the pairwise contribution to the vdW energy by correlating only two dipoles (or multipoles) at a time. **(d)** Long-range pairwise functionals use an infinitesimal (fine-grained) representation of dipolar fluctuations and correlate only two dipoles at a time.

However, these common approximations are unable to describe the long-range electron correlation energy and therefore fail to describe vdW interactions. This is true even for the more advanced semi-local meta-GGA functionals (**?**Peverati and Truhlar, 2011; Sun et al., 2015).

Even in the simple case of an isolated many-electron atom, an accurate calculation of its (frequency-dependent) polarizability is a complicated many-body problem. However, substantial progress has been made in this regard with the development of post-HF quantum-chemical methods and time-dependent DFT (TD-DFT) calculations that can provide reliable estimates of the dipole polarizability and dipole–dipole vdW coefficients for all atoms between hydrogen and plutonium ($Z = 1$ to 102) (Chu and Dalgarno, 2004; Grimme et al., 2010; Zhang and Mitroy, 2007; Mitroy and Zhang, 2007; Gould and Bučko, 2016). Calculations that treat explicitly many-electron correlation effects (either wave-function or more recently TD-DFT methods) yield electronic response properties with an accuracy of 2% to 10% for gas-phase atoms (Larsen et al., 1999; Chu and Dalgarno, 2004; Zhang and Mitroy, 2007; Mitroy and Zhang, 2007; Babb, 2015). This high level of accuracy makes the available free-atom polarizabilities and vdW coefficients useful as reference data for vdW methods in more complex systems, as for example in the Tkatchenko–Scheffler (TS) (Tkatchenko and Scheffler, 2009) and exchange-hole dipole moment (XDM) (Becke and Johnson, 2007) methods. But because the resulting atoms-in-molecules coefficients are inevitably approximate, we are faced with the question of how the errors in asymptotic vdW coefficients affect the binding energy at equilibrium distances.

The binding energy is a result of an interplay between the Pauli repulsion and vdW attraction, so vdW energy alone is often larger (more attractive) than the net binding energy itself. As an illustration, consider noble gas atom dimers, for which interaction potentials of spectroscopic accuracy can be constructed solely from highly accurate vdW coefficients in conjunction with mean-field HF calculations (Aziz, 1993; Tang and Toennies, 1984). One can then simply calculate that an error of 20% in the asymptotic vdW coefficients of the xenon

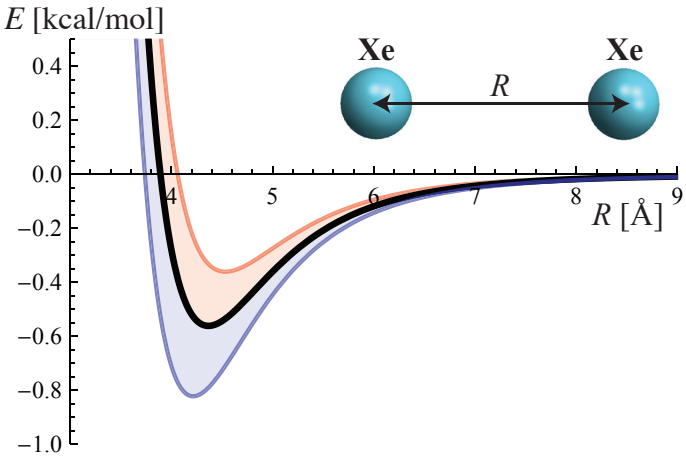

Figure 3. Potential energy curve of the xenon dimer as a function of the interatomic distance *R*. The black curve represents the exact potential energy curve (Tang and Toennies, 2003), while the blue (red) curve was obtained by increasing (decreasing) all (C_6, C_8, C_{10}) vdW coefficients by 20%. This change in the vdW coefficients yields an error of ±40% in the binding energy at the equilibrium distance, illustrating the importance of highly accurate asymptotic vdW coefficients for equilibrium predictions.

atom results in an error of approximately 40% in the equilibrium binding energy (Figure 3). Already this simple example highlights the importance of accuracy in the parameters used for including vdW interactions in electronic structure calculations. Even errors of 10%, which are typical, may lead to unacceptable errors of 20% in the corresponding binding energies. A common way to circumvent these errors is via fitting free parameters of a method to reference binding energies, but this strategy is likely to fail for systems outside the data set used for the fitting. As one might expect, these levels of uncertainty in the asymptotic vdW coefficients lead to even more serious problems in larger and more polarizable systems. The vdW contribution to the binding energy of a diindenoperylene molecule ($C_{32}H_{16}$) adsorbed on the Cu(111) surface is approximately 5.3 eV (Bürker et al., 2013). In this case, an error of 20% in the vdW coefficient would translate to the error of 1.0 eV in the equilibrium binding energy—exceeding the energy of thermal fluctuations (kT) at room temperature by a factor of 35. We note that in popular pairwise vdW corrections, vdW coefficients of molecules on metal surfaces can be overestimated by as much as 500%, because these approaches miss the complex polarization effects in the extended surface that are typically responsible for reducing the vdW coefficients of atoms in metals by 50–500% with respect to the free-atom values (Ruiz et al., 2012, 2016).

The discrepancies in the vdW energy caused by small errors in asymptotic coefficients can lead to qualitatively incorrect conclusions about relative stabilities (not absolute energies) as well, such as when studying molecular crystal polymorphs (Marom et al., 2013). In systems of increasing size, the binding arises from an interplay of short- and long-range interactions, so an accurate and reliable vdW method must be able to describe the binding at least at both equilibrium and asymptotic separations, as well as everything in-between, on equal footing. For these reasons, the accuracy of asymptotic vdW coefficients must be given a significant weight when evaluating the performance of vdW-inclusive methods.

While accurate vdW parameters can now be obtained for isolated gas-phase atoms, the situation in real molecules and materials is vastly more complicated. Even for small molecules, the molecular polarizability and vdW coefficients cannot be accurately represented simply as a sum over free-atom parameters. Dobson (Dobson, 2014) calls this difference between a free atom and an atom in a molecule type-*A* nonadditivity—it is caused by the increased kinetic energy of the valence electrons due to the confining molecular (instead of atomic) external potential. In many organic molecules (see Hybridization in Figure 1), the main effect is that orbital hybridization (*i.e.*, a relatively local effect) reduces the effective polarizability and vdW coefficients of the atoms. For example, the C_6 coefficient of an isolated carbon atom is 46.6 (a.u.), but this value is reduced to 29.8 for an sp-bonded atom and 22.1 for an sp^3-bonded atom (Wu and Yang, 2002). However, the hybridization (coordination number) concept alone is insufficient to fully account for the influence of the local chemical environment on vdW coefficients. For example, consider the methane (CH_4) and carbon tetrachloride (CCl_4) molecules. In both these molecules, the carbon atoms are sp^3-hybridized with fourfold coordination, and are therefore identical according to these two measures of the local chemical environment. Yet the local chemical environments experienced by these atoms are substantially different, with the C–H bond distance of 1.1 Å in CH_4 compared to the C–Cl distance of 1.8 Å in CCl_4. This results in increased volume and lowered kinetic energy of the valence electrons in CCl_4 compared to CH_4. The TS method is able to capture these local environment effects and yields a C_6^{C-C} coefficient of 43.1 in CCl_4 and 24.1 in CH_4. As these local chemical effects are important in capturing qualitative trends in vdW parameters, they are now captured by most vdW-inclusive methods (see Table 1). Indeed, it is quite remarkable that the C_6 coefficients of small molecules can be obtained very accurately (*i.e.*, to within 5.5%) only from the knowledge of the relative volume of an atom in its environment compared to the corresponding gas-phase atom (Tkatchenko and Scheffler, 2009).

The local chemical environment (volume scaling) is only the first effect in a series of electronic structure contributions to vdW parameters. Another mostly local effect is caused by charge transfer and different oxidation states in many-electron systems (see Oxidation State/Solvation and Charge Transfer/Ionic Compounds in Figure 1). In rock salt (NaCl), being a classical example of charge transfer simple, volume-based models cannot be used to calculate vdW coefficients unambiguously, because there are multiple ways to assign atomic densities to the Na and Cl atoms. One limit assumes that NaCl consists of a superposition of Na and Cl free-atom densities, yielding a polarizability of 182.7 (a.u.) per unit cell. The other limit assumes Na^+ and Cl^- ions, yielding a significantly reduced polarizability of 21.6 (Zhang et al., 2011b). The large difference between these two limits is caused by the change in the polarizability from 167.7 for neutral Na atom to 0.9 for

Na^+. Measurements of dielectric properties (Tessman et al., 1953) and high-level calculations (Fowler et al., 1994) demonstrate that the polarizability of NaCl solid is in fact closer to the sum of Na^+ and Cl^- ions. Large changes in vdW parameters occur also for different oxidation states of metal atoms in molecules and solids (Moellmann et al., 2012; Hansen et al., 2014; Johnson, 2011). In contrast to the hybridization effects, charge transfer and oxidation states can only be treated seamlessly by vdW methods that explicitly use electronic structure information (Becke and Johnson, 2007; Tkatchenko and Scheffler, 2009; Tkatchenko et al., 2012; Dion et al., 2004; Lee et al., 2010; Vydrov and Van Voorhis, 2010b). Methods that rely on atomic fragments require sophisticated definitions of atomic fragment densities to yield quantitative accuracy for charge transfer and oxidation states (Bučko et al., 2014, 2013a).

Another manifestation of electronic structure in vdW parameters is their dependence on the contraction or expansion of the crystal lattice (see Lattice Expansion/Contraction in Figure 1). For instance, Zhang *et al.* demonstrated a substantial linear dependence of α_{Si} and $C_6^{\text{Si-Si}}$ in zincblende sillion on the lattice constant using TD-DFT calculations (Zhang et al., 2011b). This behaviour cannot be explained by the coordination of the sillicon, because this is unchanged throughout the lattice contraction, but rather can be related to the change in the electronic band gap. Nonlinear dependence of vdW parameters on the lattice constant can be observed in semiconductors, such as Ge, where the small band gap becomes zero upon metallic phase transition induced by the lattice contraction. Such effects are reliably reproduced only by methods that explicitly consider electronic orbitals and their energies (*e.g.* RPA and TD-DFT methods). Consistent treatment of vdW interactions in systems with widely varying band gaps remains challenging because the electronic response is difficult to extract from the electron density alone. The linear increase of the polarizability with lattice constant in semiconductor solids is reproduced quantitatively by the many-body dispersion (MBD) method (Tkatchenko et al., 2012; Ambrosetti et al., 2014b), which models the response of valence electrons by overlapping quantum harmonic oscillators, qualitatively by nonlocal density functionals, in which the polarizability depends on the electron density and its gradient (Dion et al., 2004; Vydrov and Van Voorhis, 2010b), and not at all by pairwise fragment-based methods (Grimme, 2004; Grimme et al., 2010; Becke and Johnson, 2007; Tkatchenko and Scheffler, 2009).

All effects discussed so far were mostly local: local behaviour of the electron density is often sufficient to describe coordination, charge transfer, oxidation states, and variation of vdW parameters with small changes in structure. However, the frequency-dependent polarizability is a nonlocal function that explicitly depends on two points, $\mathbf{r}, \mathbf{r}'$, in space: $\alpha(\mathbf{r}, \mathbf{r}', u)$. The many effects in vdW interactions that require explicit nonlocal description have necessarily a nonadditive many-body nature. For instance, the prototypical benzene molecule has a strongly anisotropic response, with the in-plane component of the polarizability being twice as large as the out-of-plane component. This effect stems from the anisotropy of the π orbitals below and above the benzene ring. Already this well-known nonadditive contribution is neglected by most vdW methods, which rely on an isotropic definition of vdW parameters (Grimme, 2004; Grimme et al., 2010; Becke and Johnson, 2007; Tkatchenko and Scheffler, 2009; Dion et al., 2004; Vydrov and Van Voorhis, 2010b). But many of these isotropic pairwise methods are able to quite accurately approximate binding energies between small molecules, and this suggests that the effects of anisotropy might be partially compensated by the empirical damping functions used in these methods and by the lack of many-body vdW energy terms (Axilrod–Teller and higher order). The importance of nonadditive effects increases dramatically with system size and lower dimensionality. For example, the in-plane component of the polarizability increases in a strongly nonlinear fashion in polycyclic aromatic hydrocarbons (Marques et al., 2007; Krishtal et al., 2011). This nonlinear increase of polarizability then translates into vdW coefficients being strongly nonadditive (Ruzsinszky et al., 2012; Gobre and Tkatchenko, 2013; Tao et al., 2015).

Dobson calls these effects type-B nonadditivity (Dobson, 2014), and it depends sensitively on the size, structure, and dimensionality of a given system. To illustrate these effects, we calculated the nonlocal fully interacting polarizability tensor $\alpha(\mathbf{r}, \mathbf{r}', u = 0)$ of three molecules (Figure 4): adamantane $C_{10}H_{16}$, naphthalene $C_{10}H_{14}$, and decapentaene $C_{10}H_{12}$. The polarizability matrix is constructed using a self-consistent coupled dipole approach (Thole, 1981; Mayer, 2007; Tkatchenko et al., 2012), which models the response of valence electrons to an internal electric field by a projection to a set of overlapping and interacting dipole oscillators. Although the polarizability matrix in Figure 4 is not the exact $\alpha(\mathbf{r}, \mathbf{r}', u = 0)$, as could be obtained by TD-DFT calculations, it provides a reliable approximation to the polarization, as has been demonstrated in numerous studies (Jensen et al., 2002; Mayer, 2007; Jensen and Jensen, 2009; Tkatchenko et al., 2012; Gobre and Tkatchenko, 2013). The polarizability tensor is a dense matrix for all three molecules and a diagonal isotropic approximation of such a tensor, used in many vdW methods, is clearly incomplete. The dependence of polarization on the geometry and bonding is nontrivial, with a much slower decay in decapentaene compared to naphthalene and adamantane. The possible effects of such nonlocal behavior on the polarizability can be illustrated on two different orientations of the benzene dimer: the sandwich and T-shaped configurations. The plots in Figure 5 show, for instance, that the higher symmetry of the sandwich configuration makes the xz component of the polarizability tensor vanish, whereas this is not the case for the T-shaped structure. The isotropic pairwise approximation would be unable to capture the full complexity of these polarization effects.

Polarization effects scale nonlinearly and so much stronger effects can be observed in nanoscale molecules and materials compared to the illustrative case of the benzene dimer. The stability and mobility of defects in solids (Gao and Tkatchenko, 2013), polymorphism in molecular crystals (Reilly and Tkatchenko, 2013b, 2014b, 2015; Kronik and Tkatchenko, 2014), adsorption of atoms and molecules on surfaces (Liu et al., 2015; Carrasco et al., 2014), self-assembly of nanostructured materials (Gobre and Tkatchenko, 2013; Gao and Tkatchenko, 2015), and relative stability of secondary structure motifs in peptides and proteins (Rossi et al., 2015) have all been

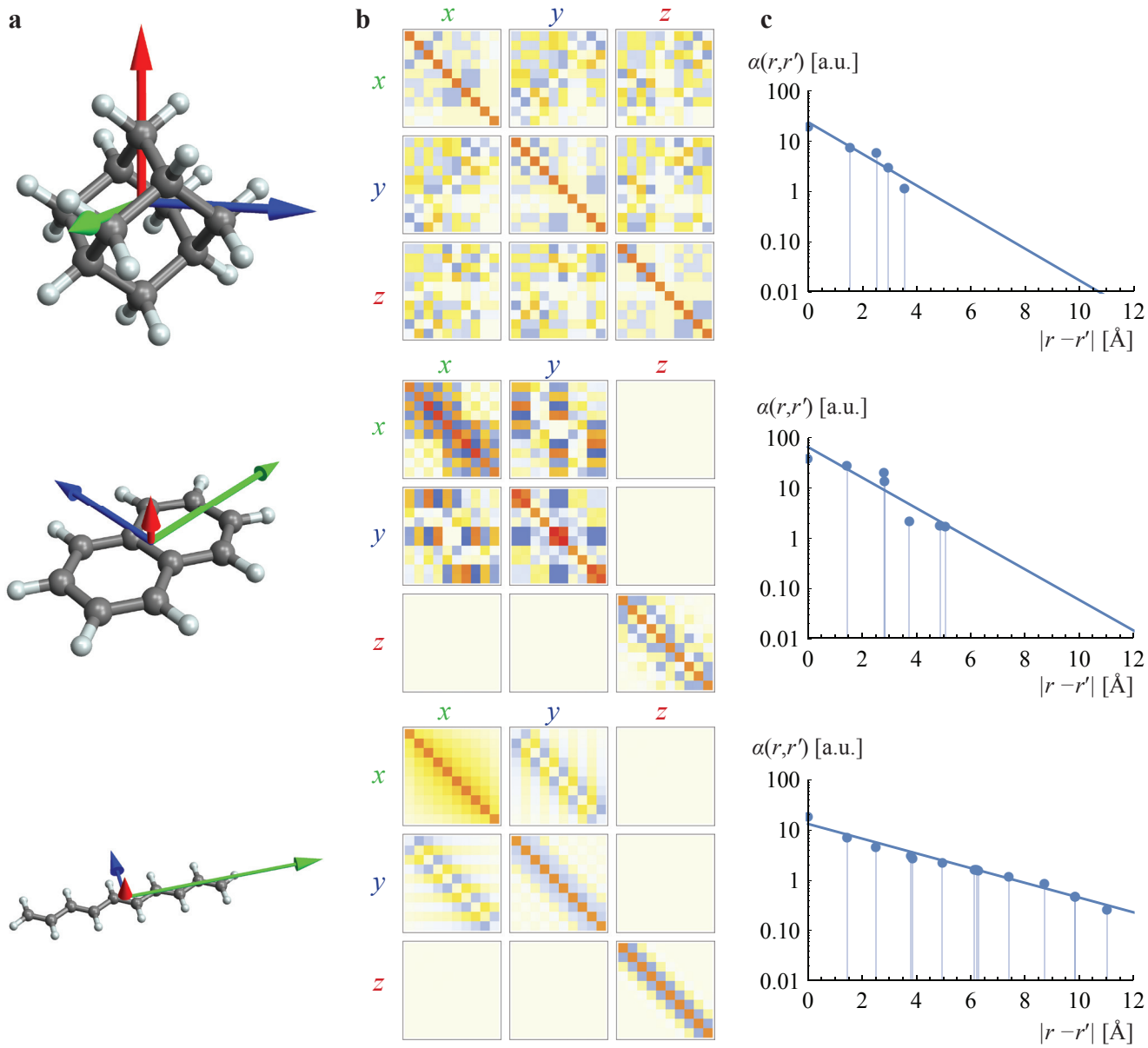

Figure 4. Nonlocal polarizability α_{AB} of three hydrocarbon molecules with 10 carbon atoms: bulky, saturated adamantane; planar, aromatic naphthalene; and linear, conjugated decapentaene. Solution of the dipole screening equation gives the nonlocal polarizability $\boldsymbol{\alpha}_{AB} \equiv \alpha^{ij}_{AB}$ (A, B label atoms, i, j Cartesian coordinates). Three different visualizations of this quantity are shown: (**a**) Molecular structures and Cartesian components of the total molecular polarizability $\sum_{AB} \boldsymbol{\alpha}_{AB}$. x, y and z components are encoded with green, blue, and red color, respectively. All arrows have the same scale. (**b**) Visualization of α^{ij}_{AB} for the subset of A and B being carbon atoms. Each 10-by-10 matrix corresponds to the α^{ij}_{AB} matrix with i and j fixed. The color encodes the sign (red for positive, blue for negative) and the intensity encodes the magnitude of a given matrix element. (**c**) Dependence of the magnitude of α^{ij}_{AB} on the distance between carbon atoms A and B in a log plot. The data points are fitted with a single exponential curve.

shown to require explicit nonlocal and nonadditive treatment of polarizability and vdW interactions. In general, the presence of any environment (be it liquid phase, crystal, or presence of edges and surfaces), will strongly affect the polarizability and vdW interactions within and between molecules and materials. Last but not least, electromagnetic fields can also change the electron density distribution and its response, thereby potentially influencing vdW interactions. Our understanding of these complex polarization effects is still fairly limited, and much current work is dedicated to the study of the behavior of intermolecular interactions in complex environments.

Particularly strong nonadditive and nonlocal effects (called type-C by Dobson (Dobson, 2014)) occur in nanoscale materials of reduced dimensionality (Dobson, 2014; Dobson et al., 2006), such as in fullerenes, nanotubes, nanoribbons, and multilayered graphene, or in materials without cubic (spherical)

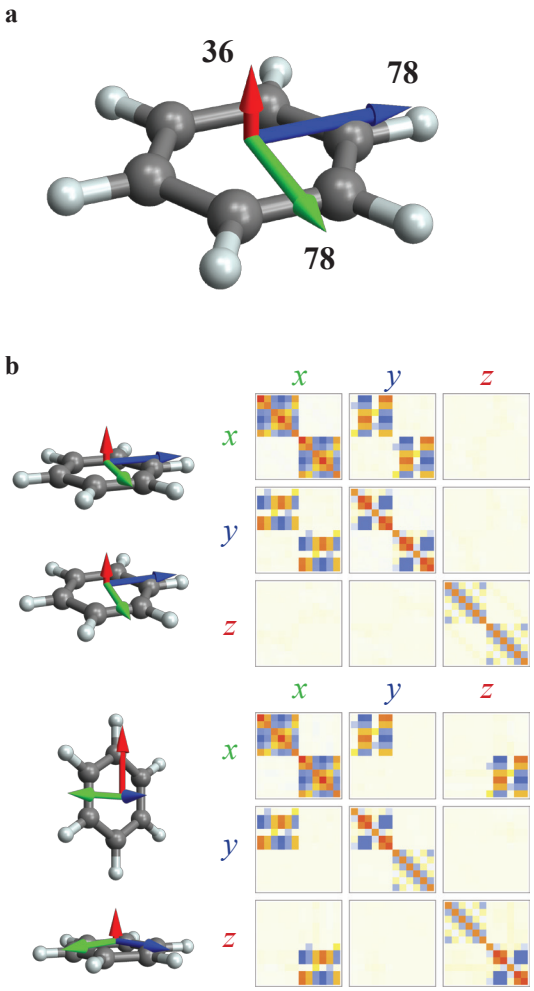

Figure 5. Nonlocal polarizability α_{AB} of two essential configurations of the benzene dimer: T-shaped and sandwich geometry. (**a**) A single benzene molecule and the Cartesian components of the total molecular polarizability $\sum_{AB} \alpha_{AB}$. x, y and z components are encoded with green, blue, and red colors, respectively. All arrows have the same scale. (**b**) Visualization of the full nonlocal polarizability α_{AB}^{ij} of the T-shaped and sandwich configurations of the benzene dimer with A and B restricted to carbon atoms. See the caption of Figure 4b for a detailed description.

symmetry. The coupling between many electrons over extended length scales leads to farsighted quantum-mechanical fluctuations (as opposed to nearsighted correlation (Prodan and Kohn, 2005)) that are responsible for long-range vdW forces (Ambrosetti et al., 2016). The inherent delocalization of free electrons in metals coupled with low dimensionalty leads to an especially slow decay of the vdW force between metallic chains and layers as a function of their separation (Dobson et al., 2006), a modification of the conventional asymptotic behavior which dominates at very large distances (*e.g.*, beyond 10–20 nm in bilayer graphene) (Dobson et al., 2014). In this context, Misquitta *et al.* (Misquitta et al., 2010, 2014) demonstrated that upon closure of the band gap, semiconducting nanowires may also exhibit unconventional power-law behavior at intermediate separations, followed by asymptotic convergence to the pairwise-additive limit.

The preceding discussion concentrated on describing many-body effects in the vdW energy that stem from the nonadditivity of polarizability in complex molecules and materials. This is often the dominant many-body effect, but there are other types of many-body contributions to the vdW energy, which can be understood using higher-order perturbation theory on isotropic fragments with fixed polarizability. This approach was originally used by Axilrod and Teller (Axilrod and Teller, 1943), and independently by Muto (Muto, 1943), resulting in the so-called Axilrod–Teller–Muto (ATM) three-body term, with a characteristic decay of R_{ABC}^{-9} where R_{ABC} is the geometric mean of the three mutual distances between fragments A, B, and C. By continuing this perturbative expansion, one can derive expression for four-body and higher-order terms that decay faster with respect to the distance between the objects. Because of this short-range nature of higher-order terms, it is common to argue that many-body terms beyond the three-body ATM term are negligible for realistic interatomic distances found in molecules and materials. However, the ATM expansion was derived assuming fixed isotropic fragments and additive localized polarizabilities—assumptions that are not general enough, as discussed above. In general, a subtle interplay between nonadditive polarization and higher-order vdW energy terms determines the many-body contributions to the vdW energy, which can in turn be both attractive or repulsive. The sign will sensitively depend on the topology, size, dimensionality, and polarizability density distribution. An empirical way to account for this interplay is to renormalize the dispersion coefficients that enter the pairwise and ATM terms. However, such procedure cannot be transferable and more sophisticated methods have been developed that include both nonadditive polarization and higher-order many-body effects by construction. This intriguing nature of many-body effects and coupling between different terms in the many-body expansion is analysed in the theoretical part of this review, especially in Section 4.8.3.

While the exact ACFD formulation (see Figure 2(a)) is able to seamlessly include all the described nonadditive contributions to noncovalent vdW interactions, this is not the case for many approximate methods discussed in this section. For quick guidance, Table 1 provides a succinct description of a range of approximate methods for modeling vdW interactions, together with their ability to treat some nonadditive aspects of these forces. We hope that this table together with the discussion in this and the next two sections will help to understand the reasons behind good performance of some methods for particular classes of systems, and failures of varying degree for other molecules and materials.

3 Experimental evidence for the nonlocal and nonadditive nature of van der Waals dispersion interactions

Our understanding of vdW interactions in complex systems relies mostly on theoretical concepts and the analysis of the

Table 1. Approximate vdW methods in terms of their general properties and the degree to which they incorporate some effects influencing vdW interactions.

Method[a]	Hybridization, coordination & chemical environment	Ions/oxidation states	Accuracy of C_6 coefficients of small organic molecules	Polarization in materials	Nonadditive polarizability
D1/D2	No	No	20%	No	No
D3	Only coord. effects	Requires separate parametrization	5–10%	No	No
XDM	Yes	Yes, but strong charge transfer requires parametrization	12%	No	Short-range
TS	Yes	Yes, but strong charge transfer requires parametrization	5.5%	No	Short-range
MBD	Yes	Yes, but strong charge transfer requires parametrization	6.2%	Yes	All ranges
vdW-DF1	Yes	Yes	20%	No	Short-range
vdW-DF2	Yes	Yes	60%	No	Short-range
VV10	Yes	Yes	12%	No	Short-range
RPA	Yes	Yes	10%	Yes	All ranges

Method	Anisotropy in vdW parameters	Many-body vdW energy	Computational cost	Amount of fitting	Applicability
D1/D2	No	No	Very low	High	Small molecules
D3	No	Three-body Axilrod–Teller can be added	Very low	Intermediate	Small and mid-size molecules
XDM	No	Three-body Axilrod–Teller can be added	Low	Low	Small and mid-size molecules
TS	No	Three-body Axilrod–Teller can be added	Low	Low	Small and mid-size molecules
MBD	Yes	Infinite order	Low	Low	Broadly applicable. Take care with metals
vdW-DF1	No	No	Intermediate	None	Small molecules and bulk solids, sensitive to exchange functional
vdW-DF2	No	No	Intermediate	Low	Small molecules and bulk solids, sensitive to exchange functional
VV10	No	No	Intermediate	Low	Small and mid-size molecules
dRPA	Yes	Infinite order	High	None	Broadly applicable

[a]D1 (Grimme, 2004), D2 (Grimme, 2006), and D3 (Grimme et al., 2010) are popular vdW methods that do not use electronic structure as input but are presented for comparison. XDM is the exchange-hole dipole moment method (Becke and Johnson, 2007). TS is the Tkatchenko–Scheffler method (Tkatchenko and Scheffler, 2009). MBD is the many-body dispersion method (Ambrosetti et al., 2014b). vdW-DF1 (Dion et al., 2004) and vdW-DF2 (Lee et al., 2010) are the nonlocal vdW density functionals. VV10 is the vdW functional of Vydrov and van Voorhis (Vydrov and Van Voorhis, 2010b). dRPA is the direct RPA method, see for example ref. 91.

results of computer modeling. However, several recent seminal experiments find unexpected collective behavior in vdW interactions that simple models based on pairwise approximations are unable to explain satisfactorily. These experimental results are discussed here; taken together, they indicate a need to revise our understanding of vdW interactions based on a rigorous, explicit, nonlocal, and many-body description.

The group led by Stefan Tautz directly measured the force gradients caused by the interaction of a single molecule attached to a tip of an atomic force microscope with clean (111) terraces of a gold surface (Wagner et al., 2014). The high precision of these measurements allowed them to confirm the well-known Lifshitz–Zaremba–Kohn (LZK) (Lifshitz, 1956; Zaremba and Kohn, 1976) Z^{-3} power law for the interaction of a molecule with an underlying surface as a function of their separation Z. This study also validated the LZK approximation for a range of increasingly large molecules derived from perylene. The most remarkable finding is that the vdW attraction of perylene derivatives with the gold surface scales nonlinearly with the number of carbon atoms. This finding was attributed to a superlinear increase of the polarizability with size, and explained using calculations at the RPA level of theory (Wagner et al., 2014).

Stronger nonlocality was observed in experiments carried out in the group of Karin Jacobs, who studied the interaction of nanoscale, mesoscale, and macroscale objects with polarizable heterointerfaces composed of SiO_2 thin films grown on Si surface (Loskill et al., 2012, 2013). They studied the force between nanoscale proteins, mesoscale bacteria, and macroscale gecko feet and SiO_2/Si interfaces by varying the thickness of the SiO_2

thin film. This allows determining the critical SiO_2 thickness at which the underlying Si surface becomes "invisible" for the interacting object. The conventional pairwise treatment of vdW interactions yields a critical thickness of approximately 1 nm, after which the vdW interaction should vanish. Remarkably, the experiments indicate that the measured force converges only when a thickness of 10–20 nm is reached, indicating that vdW interactions are more nonlocal and farsighted than expected from simple models. In contrast, explicit many-body models for vdW interactions predict much slower convergence of vdW forces for heterointerfaces with complex dielectric profiles (Gobre and Tkatchenko, 2013). Such interfaces are characterized by electric fields that propagate far into the vacuum, which explains the observed order-of-magnitude slower decay of vdW interactions.

Another manifestation of many-body effects is the recently observed complete screening of vdW interactions by a single-layer graphene or MoS_2 adsorbed on SiO_2 surface by Tsoi *et al.* (Tsoi et al., 2014). This group carried out atomic-force microscopy experiments on top of the SiO_2 surface and the same surface covered by a single-layer graphene or MoS_2. Whereas for a pristine SiO_2 surface the usual Lifshitz theory explains the experimental observations, covering the surface with graphene or MoS_2 leads to measurements that can only be explained by assuming that the tip interacts exclusively with the adsorbed single layer. A possible explanation for this behavior is that the covering layers are characterized by strongly anisotropic polarizability tensor, with in-plane fluctuations having a dominant role. Because these fluctuations are not significantly modified by adsorption on the insulating SiO_2 substrate, the tip–substrate force is dominated by the interaction with the 2D in-plane fluctuations, making any contribution of the underlying SiO_2 surface negligible.

The nonlocality and nonadditivity of vdW interactions is also manifested in nontrivial behavior of nanoclusters adsorbed on extended nanostructures (Rance et al., 2010; Batista et al., 2015). A simple additive model would lead to a linear dependence of the adsorption density on the accessible nanotube surface area. Instead, Rance *et al.* observed quadratic dependence (Rance et al., 2010). Furthermore, the attractive interactions increased nonlinearly for larger, more polarizable gold nanoparticles.

While all these experiments provide a strong evidence for the many-body nature of vdW interactions in complex materials, it is expected that they are just the "tip of the iceberg" in the ocean of molecules and materials. The complex interplay of size, dimensionality, and polarization response will continue to surprise us and lead to new insights into vdW interactions, and ultimately to better control of the self-assembly of complex polarizable molecules and materials into useful ensembles (Batista et al., 2015).

4 Theoretical framework for van der Waals models

After summarizing general concepts behind the current understanding of vdW interactions in the previous section, we now present a mathematical framework for discussing these concepts and for describing the different vdW models with a single terminology. We start with the exact adiabatic-connection fluctuation–dissipation (ACFD) theorem for the electron correlation energy and formulate a general classification of currently used approximations to this expression. We will be concerned only with models that treat the correlation between electrons explicitly via an interacting potential and in which this potential has a correct asymptotic power-law behavior. In this regard, we will not discuss semi-local density functionals that, to some degree, capture the short-range part of the correlation energy responsible for vdW interactions, such as the Minnesota family of functionals (**?**Peverati and Truhlar, 2011), or the class of explicit vdW models which can only be applied in situations with non-negligible electron density overlap, such as the method of von Lilienfeld *et al*. based on atomic pseudopotentials (von Lilienfeld et al., 2004, 2005; Tapavicza et al., 2007; DiLabio, 2008; Karalti et al., 2014). We also do not discuss *ab initio* methods that are based on symmetry-adapted perturbation theory (SAPT) (Jeziorski et al., 1994; Szalewicz, 2012), since such approaches use a different definition of the noninteracting reference system that can only be applied to systems with distinct interacting fragments (although this limitation has been a focus of recent work (Parrish et al., 2015)).

Although the framework presented here is general and could be used to discuss the modeling of vdW interactions even in fully empirical methods such as classical force fields, we will focus only on first-principles approximations, that is, methods which explicitly take into account the electronic structure of a molecule or material via the electron density or orbitals. As such, we limit the scope of this review to the context of electronic structure methods, in particular density-functional theory (DFT). In this case, a vdW model can be included in the self-consistent Kohn–Sham (KS) equations via its dependence on the electron density or orbitals, and hence can predict not only the effect of the long-range electron correlation on the total energy, but also on the electronic structure. This observation is closely related to the well-known Feynman picture of vdW interactions (Feynman, 1939), which essentially provides a phenomenological connection between these two effects, and which does not apply to models that depend only on the geometry and topology of a molecule or material. (The Hellmann–Feynman theorem applied to the electronic Hamiltonian of two well-separated fragments implies that the long-range electron correlation slightly disturbs the fragment electron densities, and in a fully self-consistent method, these distortions can be used to alternatively express the vdW forces on atoms as pure electrostatic attraction between the nuclei and the surrounding electron density. However, an electron correlation method is needed to calculate the distortions in the first place, so the Feynman picture does not practically solve that problem.)

We begin this section with the introduction and discussion of different variants of the polarizability—quantity that is central to the description of the long-range electron correlation. This is followed by a detailed analysis of the ACFD formula and related equations, and by the presentation of a theoretical framework for the development of systematic approximations to this formula based on range-separation and the quantum harmonic

oscillator model. Finally, we introduce a general classification scheme for such approximations and apply it to the currently used vdW models, which are then reviewed individually in detail in the subsequent sections.

4.1 From point polarizability to nonlocal polarizability and back

The electrical polarizability, α, indicates the willingness of a molecule or a material to respond (become polar) under the influence of a perturbation of the electric field. As such, α is only one of several commonly used response functions for describing this behavior, each of which differs by expressing the perturbation (cause) and polarization (effect) as different quantities. Other typical response functions are the density response function χ and the relative electric permittivity ε. Originally, these quantities of classical electrodynamics were considered as macroscopic, that is, they were "smoothed" over the rapid variations in the fields and densities that occur in a material on the length scale of individual atoms. But they can in fact also be used in the microscopic regime, now phenomenologically describing the behavior of the electrons that can be fully explained only by quantum mechanics. In its simplest form, the (point) polarizability α_{pt} determines the (point) dipole $\mathbf{p}$ of a molecule or a crystal unit cell that is induced by an external electric field $\mathbf{E}$,

$$\mathbf{p} = \alpha_{\text{pt}}\mathbf{E}. \tag{1}$$

We will now generalize the point polarizability to a continuous nonlocal time-dependent tensor quantity, $\boldsymbol{\alpha}(\mathbf{r}, \mathbf{r}', t, t')$, relate this form to the simple one above and to other response functions, comment on why this is still not the full picture, and finally show why this has anything and everything to do with vdW interactions.

First, the field and the induced dipole may not have the same direction in a general anisotropic material. In other words, the induced dipole in some Cartesian direction, p_i, may not depend only on the component of the perturbing field in that direction, E_i, but also on the other components, E_j. This can be captured mathematically by considering the polarizability as a tensor quantity $\boldsymbol{\alpha}$ with Cartesian components α_{ij}, as was discussed in Section 2 and shown illustratively in Figures 4 and 5. Second, we switch to a continuous time-dependent description, where both the external field and the response depend on the position in space and in time. When a small perturbation in the external potential $\Delta\phi(\mathbf{r}, t)$ (or the corresponding field $\mathbf{E}(\mathbf{r}, t) = -\boldsymbol{\nabla}(\Delta\phi(\mathbf{r}, t))$) is applied, assuming fixed nuclear charges, the material responds with a change in the electron (charge) density $\Delta n(\mathbf{r}', t')$. The time-dependent point dipole $\mathbf{p}(t) = \int \mathrm{d}\mathbf{r}\Delta n(\mathbf{r}, t)\mathbf{r}$ has its continuous analog in the polarization density $\mathbf{P}(\mathbf{r}, t)$, which can also be understood as a dipole density, $\mathbf{p}(t) = \int \mathrm{d}\mathbf{r}\mathbf{P}(\mathbf{r}, t)$. We note that there is no nontrivial point counterpart to Δn, because the total charge in a material cannot be changed by an applied external field, $\int \mathrm{d}\mathbf{r}\Delta n(\mathbf{r}) = 0$ (unless the field is strong enough to produce emission, which is a completely different kind of effect). The induced charge density and polarization density are related by

$$\Delta n(\mathbf{r}, t) = -\boldsymbol{\nabla} \cdot \mathbf{P}(\mathbf{r}, t). \tag{2}$$

The response of the material is in general nonlocal, that is, the polarization here and now does not depend only on the field here and now. This effect can be captured with $\boldsymbol{\alpha}$ being a nonlocal function. In fact, it is this sole ability of the polarizability to relate the response at a point $\mathbf{r}$ to a perturbation at a point $\mathbf{r}'$, which enables it to capture the electron correlation. Thus, in the most general form, the relationship between the polarization density and the polarizing electric field is

$$P_i(\mathbf{r}, t) = \int \mathrm{d}\mathbf{r}' \int \mathrm{d}t' \sum_j \alpha_{ij}(\mathbf{r}, \mathbf{r}', t, t')E_j(\mathbf{r}', t'), \tag{3}$$

where the integrals are over all space and time and the sum over Cartesian components can be understood as multiplication of the matrix $\boldsymbol{\alpha}$ and the vector $\mathbf{E}$. In what follows, we will often drop the explicit sum and enumeration over Cartesian components and simply write $\sum_j \alpha_{ij}E_j = (\boldsymbol{\alpha}\mathbf{E})_i$. Eq. (3) would thus be written as

$$\mathbf{P}(\mathbf{r}, t) = \int \mathrm{d}\mathbf{r}' \int_{-\infty}^{t} \mathrm{d}t'\boldsymbol{\alpha}(\mathbf{r}, \mathbf{r}', t, t')\mathbf{E}(\mathbf{r}', t'). \tag{4}$$

Although $\boldsymbol{\alpha}$ is the dipole polarizability, one can recover all the higher induced multipoles from its fully nonlocal form, by first calculating $\mathbf{P}$, followed by Δn via Eq. 2, and from that any induced multipole moment.

Now we follow the path back to the molecular isotropic polarizability. To do so, one must first assume a static electric field, and drop the dependence on time, *i.e.*, $\mathbf{E}(\mathbf{r})$. (This will be discussed in more detail later when discussing the vdW energy.) Second, one must assume a spatially homogeneous electric field, $\mathbf{E}(\mathbf{r}) = \mathbf{E}$, for which

$$\mathbf{P}(\mathbf{r}) = \left(\int \mathrm{d}\mathbf{r}'\boldsymbol{\alpha}(\mathbf{r}, \mathbf{r}')\right)\mathbf{E} = \boldsymbol{\alpha}_{\text{loc}}(\mathbf{r})\mathbf{E}, \tag{5}$$

where we introduced a new quantity, $\boldsymbol{\alpha}_{\text{loc}}(\mathbf{r})$, termed here as a local polarizability. Although $\boldsymbol{\alpha}_{\text{loc}}$ is now formally a local quantity, it effectively contains the integrated nonlocal response at point $\mathbf{r}$ to the (homogeneous) field at all points $\mathbf{r}'$. This is analogous to how the local exchange-correlation energy density in the homogeneous electron gas is formally a local quantity at point $\mathbf{r}$, but contains integrated correlation contributions from all points $\mathbf{r}'$. Integrating over $\mathbf{r}'$ in $\boldsymbol{\alpha}(\mathbf{r}, \mathbf{r}')$ reduces the amount of information contained in $\boldsymbol{\alpha}$; hence, $\boldsymbol{\alpha}_{\text{loc}}$ is no longer able to completely describe the response of a material to a general inhomogeneous field. Indeed, using $\boldsymbol{\alpha}_{\text{loc}}$ to get a full response of a material subject to an inhomogeneous perturbation would be an approximation, akin to using the local density approximation (LDA) in DFT when treating inhomogeneous systems such as molecules.

Next, if one requires only the knowledge of the total point dipole of a molecule or material in a homogeneous field, then

$$\mathbf{p} = \int \mathrm{d}\mathbf{r}\,\mathbf{P}(\mathbf{r}) = \left(\int \mathrm{d}\mathbf{r}\boldsymbol{\alpha}_{\text{loc}}(\mathbf{r})\right)\mathbf{E} = \boldsymbol{\alpha}_{\text{pt}}\mathbf{E}, \tag{6}$$

where $\boldsymbol{\alpha}_{\text{pt}}$ is now the anisotropic point polarizability, obtained by integrating over both $\mathbf{r}$ and $\mathbf{r}'$ in $\boldsymbol{\alpha}(\mathbf{r}, \mathbf{r}')$, *i.e.*, $\boldsymbol{\alpha}_{\text{pt}} =$

$\iint \mathrm{d}\mathbf{r}\mathrm{d}\mathbf{r}'\boldsymbol{\alpha}(\mathbf{r},\mathbf{r}')$. Finally, if one assumes an isotropic material, for which the response is the same in all directions, $\alpha_{\mathrm{pt},ij} = \alpha_{\mathrm{pt}}\delta_{ij}$, then

$$\mathbf{p} = \alpha_{\mathrm{pt}}\mathbf{E}, \tag{7}$$

which brings us back to the point polarizability in Eq. (1).

The nonlocal polarizability $\boldsymbol{\alpha}(\mathbf{r},\mathbf{r}')$ is related to other response functions, such as χ or ε by simple formulas, which mirrors the fact that all these response functions carry essentially the same information. The density response χ relates a perturbation in the external potential to a response in terms of the induced density,

$$\Delta n(\mathbf{r},t) = \int \mathrm{d}\mathbf{r}' \int_{-\infty}^{t} \mathrm{d}t' \chi(\mathbf{r},\mathbf{r}',t,t')\Delta\phi(\mathbf{r}',t'). \tag{8}$$

By comparing equations Eqs. (8) and (3), and using the relationships between $\Delta\phi$, Δn, $\mathbf{E}$, and $\mathbf{P}$, we arrive at

$$\begin{aligned}\chi(\mathbf{r},\mathbf{r}',t,t') &= \boldsymbol{\nabla}_{\mathbf{r}} \cdot \boldsymbol{\nabla}_{\mathbf{r}'} \cdot \boldsymbol{\alpha}(\mathbf{r},\mathbf{r}',t,t') \\ &= \sum_{ij} \frac{\partial}{\partial r_i}\frac{\partial}{\partial r'_j}\alpha_{ij}(\mathbf{r},\mathbf{r}',t,t').\end{aligned} \tag{9}$$

That is, the density response is the result of the divergence operator applied to both $\mathbf{r}$ and $\mathbf{r}'$ of the nonlocal polarizability. We note that whereas $\boldsymbol{\alpha}$ is a tensor, χ is only a scalar. As in the case of Δn, χ has no nontrivial point analog, because $\iint \mathrm{d}\mathbf{r}\mathrm{d}\mathbf{r}'\chi(\mathbf{r},\mathbf{r}',t,t') = 0$ by charge conservation. For this reason, we will use $\boldsymbol{\alpha}$ rather than χ throughout this review. The relationship between the density response χ (and hence the nonlocal polarizability) and the relative permittivity ε is obtained directly from their macroscopic definitions in the context of the Maxwell equations, and in atomic units ($\varepsilon_0 = 1/4\pi$) reads as

$$\varepsilon(\mathbf{r},\mathbf{r}',t,t')^{-1} = 1 + \int \mathrm{d}\mathbf{r}'' v(\mathbf{r},\mathbf{r}'')\chi(\mathbf{r}'',\mathbf{r}',t,t'), \tag{10}$$

where $v(\mathbf{r},\mathbf{r}') = |\mathbf{r}-\mathbf{r}'|^{-1}$ is the Coulomb potential.

Although $\boldsymbol{\alpha}$, χ, and ε are fully nonlocal time-dependent response functions, they still do not describe the response of a material in its full complexity, but only within the linear regime. In general, the response of a material is a nonlinear functional of the perturbation, and the response functions presented above are the corresponding first functional derivatives of these quantities,

$$\boldsymbol{\alpha}(\mathbf{r},\mathbf{r}',t,t') = \frac{\delta\mathbf{P}(\mathbf{r},t)}{\delta\mathbf{E}(\mathbf{r}',t')}, \quad \chi(\mathbf{r},\mathbf{r}',t,t') = \frac{\delta n(\mathbf{r},t)}{\delta\phi(\mathbf{r}',t')}. \tag{11}$$

This additional complexity is however not significant for a discussion of the electron correlation energy, because the electron pair density, $n_2(\mathbf{r},\mathbf{r}')$, from which the correlation energy can be calculated directly, can be fully recovered from the linear response functions only. The fundamental reason for this is that the Coulomb potential $1/|\mathbf{r}-\mathbf{r}'|$ acts between two points in space, whereas the higher functional derivatives of the nonlinear response depend on three or more positions in space. Thus, these quantities essentially carry more information about the electronic system than is needed for the calculation of the correlation energy.

Before proceeding further, the final step is to transform the response functions from the time domain to the frequency domain. All approaches discussed in this review are concerned with systems in equilibrium (stationary states in quantum mechanics). Then, the response depends only on the time difference $t - t'$. This allows one to Fourier-transform the polarizability $\boldsymbol{\alpha}(\mathbf{r},\mathbf{r}',t-t')$ to the frequency domain, $\boldsymbol{\alpha}(\mathbf{r},\mathbf{r}',u)$, with the frequency denoted as u; namely:

$$\boldsymbol{\alpha}(\mathbf{r},\mathbf{r}',t,t') = \boldsymbol{\alpha}(\mathbf{r},\mathbf{r}',t-t',0) \xrightarrow{\mathrm{FT}} \boldsymbol{\alpha}(\mathbf{r},\mathbf{r}',u). \tag{12}$$

The frequency-dependent polarizability $\boldsymbol{\alpha}(\mathbf{r},\mathbf{r}',u)$ is often called the dynamic polarizability. This transformation introduces a new level of complication by making the polarizability a complex quantity with real and imaginary components. However, these two components have a clear physical interpretation: the real part describes a non-lossy response of a material and the imaginary part represents dissipation.

4.2 Exact correlation energy from nonlocal dynamic polarizability

So far, we have not discussed the role that the nonlocal dynamic polarizability plays in the description of vdW interactions. This connection is formulated as an exact expression for the electron correlation energy that is usually referred to as the ACFD theorem. We will not repeat its elaborate derivation here, as it can be found elsewhere (Pines, 1999; Langreth and Perdew, 1977), but instead cover the physical ideas embodied in the derivation. The connection between the correlation energy and the polarizability starts with the realization that the delay in the response of a medium to an electromagnetic field, which is captured by the imaginary part of the dynamic polarizability, leads to dissipation of the field in the medium. The fluctuation–dissipation theorem then relates the behavior of this dissipation to the charge density fluctuations that are present in every quantum-mechanical system even at equilibrium. In essence, this theorem claims that the relaxation of a system from a perturbed state behaves according to the same laws both in the case when the perturbation was caused by an external field (such as when probing a molecule spectroscopically) or when it is an internal spontaneous fluctuation (Callen and Welton, 1951). This enables one to describe the density fluctuations in terms of dynamic response functions, such as the polarizability, $\boldsymbol{\alpha}(\mathbf{r},\mathbf{r}',u)$. Once we have the description of these fluctuations, the electron correlation energy then follows directly from their Coulomb interaction. In this way, one obtains the full electron correlation energy, of which the long-range part is responsible for vdW interactions. The reason why the ACFD framework is especially relevant for the problem of vdW interactions is that it is possible to construct good approximations to both $\boldsymbol{\alpha}(\mathbf{r},\mathbf{r}',u)$ and the ACFD expression itself when one is concerned only with the long-range part of the correlation energy.

In the literature, the ACFD is typically written in terms of

the density response function $\chi(\mathbf{r},\mathbf{r}',u)$ (see Eqs. (8) and (12)),

$$E_\mathrm{c} = -\int_0^\infty \frac{\mathrm{d}u}{2\pi}\int_0^1 \mathrm{d}\lambda \iint \mathrm{d}\mathbf{r}\mathrm{d}\mathbf{r}' \times \left(\chi_\lambda(\mathbf{r},\mathbf{r}',\mathrm{i}u) - \chi_0(\mathbf{r},\mathbf{r}',\mathrm{i}u)\right) v(\mathbf{r},\mathbf{r}'), \quad (13)$$

where $\mathbf{r}, \mathbf{r}'$ are spatial coordinates, u is the frequency, $v(\mathbf{r},\mathbf{r}') = 1/|\mathbf{r}-\mathbf{r}'|$ is the Coulomb potential, λ is a coupling strength that connects the Kohn–Sham (KS) electronic system ($\lambda = 0$) to the real system ($\lambda = 1$), χ_λ is the density response function of the system at coupling strength λ, and χ_0 is simply χ_λ for $\lambda = 0$, that is, the density response function of the noninteracting KS system. The integral over λ from 0 to 1 is the adiabatic connection that gives the other half of the name to the ACFD formula and originates from the Hellmann–Feynman theorem applied to the full electronic Hamiltonian with the electronic term scaled by λ. The integral of χ over imaginary frequencies is simply a mathematical trick, and is in fact equivalent to the integral over real frequencies of the imaginary part of χ (Landau and Lifschitz, 1980),

$$\int_0^\infty \mathrm{d}u\,\chi(\mathbf{r},\mathbf{r}',\mathrm{i}u) = \int_0^\infty \mathrm{d}u\,\mathrm{Im}\,\chi(\mathbf{r},\mathbf{r}',u). \quad (14)$$

It is the form on the right-hand side which comes directly from the fluctuation–dissipation theorem, because the imaginary part of the response function, Im χ, accounts for dissipation.

The KS response, χ_0, is directly given by the Adler–Wiser sum over the KS orbitals $\phi_\mu(\mathbf{r})$ (Adler, 1962; Wiser, 1963),

$$\chi_0(\mathbf{r},\mathbf{r}',\mathrm{i}u) = \sum_{\mu\nu}(f_\mu - f_\nu)\frac{\phi_\mu^*(\mathbf{r})\phi_\mu(\mathbf{r}')\phi_\nu^*(\mathbf{r})\phi_\nu(\mathbf{r}')}{\epsilon_\mu - \epsilon_\nu + \mathrm{i}u}, \quad (15)$$

where ϵ_μ are the orbital energies and f_μ are the occupation numbers.

For the purposes of this review, we will express the ACFD formula in an equivalent (Nimalakirthi and Hunt, 1993) form in terms of the polarizability $\boldsymbol{\alpha}(\mathbf{r},\mathbf{r}',u)$ and the dipole potential $\mathbf{T}(\mathbf{r},\mathbf{r}')$,

$$\begin{aligned}\mathbf{T}(\mathbf{r},\mathbf{r}') &= -\boldsymbol{\nabla}_\mathbf{r}\boldsymbol{\nabla}_{\mathbf{r}'} v(\mathbf{r},\mathbf{r}') \\ &= \frac{3(\mathbf{r}-\mathbf{r}')(\mathbf{r}-\mathbf{r}') - |\mathbf{r}-\mathbf{r}'|^2\mathbf{I}}{|\mathbf{r}-\mathbf{r}'|^5}\end{aligned}$$

Using the relationship between $\boldsymbol{\alpha}$ and χ in Eq. (9), the divergence theorem (not, a), and the limit $\chi(\mathbf{r},\mathbf{r}')v(\mathbf{r},\mathbf{r}') \to 0$ for $|\mathbf{r}-\mathbf{r}'| \to \infty$, one can transform

$$\begin{aligned}\iint \mathrm{d}\mathbf{r}\mathrm{d}\mathbf{r}'\,\chi v &= \iint \mathrm{d}\mathbf{r}\mathrm{d}\mathbf{r}' \left(\sum_{ij}\frac{\partial}{\partial r_i}\frac{\partial}{\partial r_j'}\alpha_{ij}\right) v \\ &= -\iint \mathrm{d}\mathbf{r}\mathrm{d}\mathbf{r}' \sum_{ij}\left(\frac{\partial}{\partial r_i}\alpha_{ij}\right)\frac{\partial}{\partial r_j'} v \\ &= \iint \mathrm{d}\mathbf{r}\mathrm{d}\mathbf{r}' \sum_{ij}\alpha_{ij}\frac{\partial}{\partial r_i}\frac{\partial}{\partial r_j'} v \\ &= -\iint \mathrm{d}\mathbf{r}\mathrm{d}\mathbf{r}' \sum_{ij}\alpha_{ij}T_{ij} \\ &= -\iint \mathrm{d}\mathbf{r}\mathrm{d}\mathbf{r}'\,\mathrm{Tr}[\boldsymbol{\alpha}\mathbf{T}], \end{aligned} \quad (16)$$

where the trace is over Cartesian components of $\boldsymbol{\alpha}\mathbf{T}$. The ACFD formula can then be rewritten as

$$E_\mathrm{c} = \int_0^\infty \frac{\mathrm{d}u}{2\pi}\int_0^1 \mathrm{d}\lambda \iint \mathrm{d}\mathbf{r}\mathrm{d}\mathbf{r}' \times \mathrm{Tr}\left[\left(\boldsymbol{\alpha}_\lambda(\mathbf{r},\mathbf{r}',\mathrm{i}u) - \boldsymbol{\alpha}_0(\mathbf{r},\mathbf{r}',\mathrm{i}u)\right)\mathbf{T}(\mathbf{r},\mathbf{r}')\right]. \quad (17)$$

Both the interacting $\boldsymbol{\alpha}_\lambda$ and noninteracting $\boldsymbol{\alpha}_0$ are in general nonlocal functions, but only the former contains information about the electron correlation. To explain this point, we note that the statement above that $\boldsymbol{\alpha}_0$ is the response of the KS system of noninteracting electrons does not mean that it is the response one would get from a KS calculation in the presence of an electric field. Indeed, in such a calculation the density and hence the mean field for the electrons would change under the influence of the perturbing electric field, so that all correlation effects described by the exchange-correlation potential would be propagated into the obtained response. In fact, with the exact exchange-correlation functional, one would obtain the exact $\boldsymbol{\alpha}_1$ from such a calculation. On the other hand, the response described by $\boldsymbol{\alpha}_0$ assumes that the mean field for the electrons (comprising the Hartree and exchange-correlation potential) is not changed by the perturbing field. That is, $\boldsymbol{\alpha}_0$ describes a process where each electron responds individually to the perturbing field while moving within the mean field of the unperturbed electrons. This is a crude approximation that neglects the essential mechanism in which the response of an electron is influenced by the response of all the other electrons. In the aforementioned KS calculation in the presence of an electric field, this mechanism is actually ensured by the self-consistent adaptation of the mean field, whereas in the Dyson approach introduced below, it is achieved by direct coupling of the electrons. In both cases, the response of an electron takes into account all the other electrons as it must. An indirect consequence of the approximations made in $\boldsymbol{\alpha}_0$ is that its spatial extent and nonlocal character are determined only by single-electron behaviour. As a result, $\boldsymbol{\alpha}_0$ is exponentially localized in materials with a finite gap (Ge and Lu, 2015), that is, $\boldsymbol{\alpha}_0(\mathbf{r},\mathbf{r}')$ goes exponentially quickly to zero as $|\mathbf{r}-\mathbf{r}'|$ increases. We note that this may not be the case for $\boldsymbol{\alpha}_1$ even in such materials, because the long-range correlation between electrons can induce long-ranged character in $\boldsymbol{\alpha}_1$. It is this difference between $\boldsymbol{\alpha}_\lambda$ and $\boldsymbol{\alpha}_0$ that is exploited by the adiabatic-connection formula in Eq. (17) to obtain the correlation energy.

The interacting polarizability $\boldsymbol{\alpha}_\lambda(\mathbf{r},\mathbf{r}',u)$ can be expressed in terms of $\boldsymbol{\alpha}_0$ by means of the self-consistent Dyson equation,

$$\begin{aligned}\boldsymbol{\alpha}_\lambda(\mathbf{r},\mathbf{r}') &= \boldsymbol{\alpha}_0(\mathbf{r},\mathbf{r}') \\ &\quad - \iint \mathrm{d}\mathbf{r}''\mathrm{d}\mathbf{r}'''\boldsymbol{\alpha}_0(\mathbf{r},\mathbf{r}'')\lambda\mathbf{T}_{\mathrm{xc},\lambda}(\mathbf{r}'',\mathbf{r}''')\boldsymbol{\alpha}_\lambda(\mathbf{r}''',\mathbf{r}') \\ &\equiv \boldsymbol{\alpha}_0(\mathbf{r},\mathbf{r}') - \{\!\!\{\boldsymbol{\alpha}_0\lambda\mathbf{T}_{\mathrm{xc},\lambda}\boldsymbol{\alpha}_\lambda\}\!\!\}(\mathbf{r},\mathbf{r}') \\ &= \boldsymbol{\alpha}_0(\mathbf{r},\mathbf{r}') - \lambda\{\!\!\{\boldsymbol{\alpha}_0\mathbf{T}_{\mathrm{xc},\lambda}\boldsymbol{\alpha}_0\}\!\!\}(\mathbf{r},\mathbf{r}') \\ &\quad + \lambda^2\{\!\!\{\boldsymbol{\alpha}_0\mathbf{T}_{\mathrm{xc},\lambda}\boldsymbol{\alpha}_0\mathbf{T}_{\mathrm{xc},\lambda}\boldsymbol{\alpha}_0\}\!\!\}(\mathbf{r},\mathbf{r}') - \ldots \\ &= \sum_{n=0}^{\infty}\left\{\!\!\left\{\boldsymbol{\alpha}_0\left(-\lambda\mathbf{T}_{\mathrm{xc},\lambda}\boldsymbol{\alpha}_0\right)^n\right\}\!\!\right\}(\mathbf{r},\mathbf{r}'), \end{aligned} \quad (18)$$

where $\mathbf{T}_{\mathrm{xc},\lambda}(\mathbf{r},\mathbf{r}',u) = \mathbf{T}(\mathbf{r},\mathbf{r}') - \lambda^{-1}\boldsymbol{\nabla}_{\mathbf{r}}\boldsymbol{\nabla}_{\mathbf{r}'} f_{\mathrm{xc},\lambda}(\mathbf{r},\mathbf{r}',u)$ is the dipole potential accompanied by the exchange-correlation kernel $f_{\mathrm{xc},\lambda}(\mathbf{r},\mathbf{r}',u) = \delta v_{\mathrm{xc},\lambda}(\mathbf{r},u)/\delta n(\mathbf{r}',u)$, $\{\!|\cdot|\!\}$ denotes the use of the shorthand implicit notation for the spatial integrals, and the dependence on the frequency has been omitted for clarity. The polarizability of the real system is expressed here as an infinite sum over progressively more coupled terms built from the polarizability of the noninteracting Kohn–Sham system. Straightforward use of the ACFD formula together with the Dyson equation to calculate the correlation energy from $\boldsymbol{\alpha}_0$ is impossible due to the lack of knowledge of the *exact* exchange-correlation kernel f_{xc}. This quantity is notoriously more difficult to approximate than the exchange-correlation functional itself.

The ACFD formula in Eq. (17) and the Dyson equation in Eq. (18) are the two basic building blocks for the first-principles description of vdW interactions. The latter is essentially the exact expression for the response of a material, while the former uses this response to give the exact correlation energy. So far, we have discussed an exact theoretical framework without any approximations. Now, we connect the ACFD framework to DFT by introducing new effective quantities. In a typical DFT calculation, the short-range part of the electron correlation is obtained from a semi-local or hybrid density functional (Fiolhais et al., 2003; Koch and Holthausen, 2015). However, the ACFD formula gives the total correlation energy, including the short-range part, and if it was used in its full form, the short-range part would be double-counted. To solve this issue, the ACFD expression can be range-separated, that is, the double integral over all space in Eq. (17) can be split into two parts,

$$\begin{aligned}\iint \mathrm{d}\mathbf{r}\mathrm{d}\mathbf{r}' = &\iint \mathrm{d}\mathbf{r}\mathrm{d}\mathbf{r}' \left(1 - f(|\mathbf{r}-\mathbf{r}'|)\right) \\ &+ \iint \mathrm{d}\mathbf{r}\mathrm{d}\mathbf{r}' f(|\mathbf{r}-\mathbf{r}'|),\end{aligned} \tag{19}$$

where $f(R)$ is some range-separating function for which $f(0) = 0$ and $f(R) \to 1$ as $R \to \infty$. The first and second terms on the right-hand side correspond to the short- and long-range parts, respectively. Such a range separation usually leads to approximate approaches as described below; however, despite being arbitrary, it is in principle exact if the treatment of the two parts is done consistently. For a more rigorous introduction of the range separation, see refs. (Toulouse et al., 2004, 2009). The partition splits the electron correlation energy into two parts,

$$E_{\mathrm{c}} = E_{\mathrm{c,sr}} + E_{\mathrm{c,lr}}. \tag{20}$$

The short-range part, $E_{\mathrm{c,sr}}$, can then be approximated with a KS calculation, while the long-range correlation energy, $E_{\mathrm{c,lr}}$, is given by the long-range part of the ACFD formula, that is, by Eq. (17) with $\iint \mathrm{d}\mathbf{r}\mathrm{d}\mathbf{r}'$ replaced with $\iint \mathrm{d}\mathbf{r}\mathrm{d}\mathbf{r}'\, f(|\mathbf{r}-\mathbf{r}|)$.

We note at this point that we do not identically equate the long-range correlation energy with vdW dispersion interactions. Whereas the former is uniquely defined by specifying a particular range separation, the latter has no formal non-perturbational definition. With that said, however, the overlap of the two phenomena is large and it is safe to say that the long-range electron correlation provides the microscopic explanation of vdW interactions. It is in this context that we present vdW methods as methods for calculating the long-range correlation energy. We also stress that at large enough distances, the contribution of long-range electron correlation to the electronic energy can be understood fully in terms of vdW interactions (or corresponding retarded Casimir interactions). In particular, although static (left-right, on-shell) electron correlation is manifest at large separations and is only partially captured by semi-local density functionals, it is nevertheless caused by the short-range part of the Coulomb potential, namely by a short-range repulsion of electrons being present at the same atomic sites although they should not be. In other words, issues with static correlation would persist in a hypothetical world in which the long-ranged Coulomb potential would be replaced with a short-ranged Yukawa potential.

The range-separating function f must depend on the underlying density functional that is used for the short-range correlation; more precisely, f must depend on the range to which the functional is able to capture the electron correlation. In addition, the range separation must certainly be also system-dependent as can be seen from the following examples. First, consider the case of the homogeneous electron gas, for which all LDA-based semi-local functionals give the exact energy, that is, the long-range part as defined here should be zero. In contrast, in the case of nonoverlapping fragments, no such functional can capture the electron correlation between these entities. However, neither the functional nor the system dependence are completely known or understood theoretically, and the particular form of the range-separating function is thus a matter of a long and unsettled debate in the literature. We will discuss the various approaches to this range separation in the respective sections below.

In analogy to the ACFD formula, the Dyson screening equation (18) can also be split into short- and long-range parts, albeit in a less straightforward manner. First, the coupling potential, $\mathbf{T}_{\mathrm{xc},\lambda}$, can be split as follows:

$$\begin{aligned}\mathbf{T}_{\mathrm{xc},\lambda}(\mathbf{r},\mathbf{r}') &\approx \left(1 - f(|\mathbf{r}-\mathbf{r}'|)\right)\mathbf{T}_{\mathrm{xc},\lambda}(\mathbf{r},\mathbf{r}') \\ &\quad + f(|\mathbf{r}-\mathbf{r}'|)\mathbf{T}(\mathbf{r},\mathbf{r}') \\ &\equiv \mathbf{T}_{\mathrm{sr},\lambda}(\mathbf{r},\mathbf{r}') + \mathbf{T}_{\mathrm{lr}}(\mathbf{r},\mathbf{r}'),\end{aligned} \tag{21}$$

where f is again some (in general different) range-separating function, and we replaced the screened dipole potential in the long-range part with the bare dipole potential, since it is assumed that the range of the exchange-correlation kernel is shorter than that of the range-separating function f. This separation splits the n-th term in the Dyson equation into 2^n terms, each of which is formed by some particular combination of $\mathbf{T}_{\mathrm{sr}}$ and $\mathbf{T}_{\mathrm{lr}}$.

Now we contract all the short-range segments $\cdots \boldsymbol{\alpha}_0\mathbf{T}_{\mathrm{sr}}\boldsymbol{\alpha}_0 \cdots$ contained in these terms and introduce an effective short-range screened polarizability $\boldsymbol{\alpha}_{\mathrm{sr}}(\mathbf{r},\mathbf{r}')$ such that the Dyson equation becomes

$$\alpha_\lambda(\mathbf{r},\mathbf{r}') = \sum_{n=0}^{\infty} \left\{\!\!\left|\, \boldsymbol{\alpha}_{\mathrm{sr}} \left(-\lambda \mathbf{T}_{\mathrm{lr}}\boldsymbol{\alpha}_{\mathrm{sr}}\right)^n \right|\!\!\right\}(\mathbf{r},\mathbf{r}'). \tag{22}$$

Here, only the long-range coupling is considered explicitly via

$\mathbf{T}_{\rm lr}$, whereas the short-range coupling enters implicitly in the effective short-range screened polarizability $\boldsymbol{\alpha}_{\rm sr}$.

The range separation of both the energy in the ACFD expression and $\boldsymbol{\alpha}$ in the Dyson equation enables us to combine these two equations, after performing one final simplification. The functions used for range separating both of these quantities should in principle be different. In the case of the energy, the separation should be governed by the underlying semi-local or hybrid density functional. In the case of the polarizability, the separation should be constructed based on the model for $\boldsymbol{\alpha}_{\rm sr}(\mathbf{r},\mathbf{r}')$. However, we will invoke a final approximation here, done by all vdW approaches known to us, by equating these two range-separating functions. In principle, one can always construct a model for $\boldsymbol{\alpha}_{\rm sr}(\mathbf{r},\mathbf{r}')$ such that these two functions match. Inserting Eq. (22) into the long-range part of Eq. (17) and integrating over λ, we arrive at

$$E_{\rm c} = -\sum_{n=2}^{\infty} \frac{(-1)^n}{n} \int_0^\infty \frac{\mathrm{d}u}{2\pi} \iint \mathrm{d}\mathbf{r}\mathrm{d}\mathbf{r}' \times \mathrm{Tr}\left[\left\{\left(\boldsymbol{\alpha}_{\rm sr}\mathbf{T}_{\rm lr}\right)^n\right\}(\mathbf{r},\mathbf{r}',\mathrm{i}u)\right]. \quad (23)$$

Starting at second order, Eq. (23) expresses the long-range electron correlation energy as an infinite sum over all orders of the long-range coupling of the short-range screened polarizability. To clarify the various shorthands, the lowest order contribution $E_{\rm c}^{(2)}$, written out in full form, is

$$E_{\rm c}^{(2)} = -\frac{1}{2}\int_0^\infty \frac{\mathrm{d}u}{2\pi} \iiiint \mathrm{d}\mathbf{r}\mathrm{d}\mathbf{r}'\mathrm{d}\mathbf{r}''\mathrm{d}\mathbf{r}''' \times \sum_{ijkl} \alpha_{ij}^{\rm sr}(\mathbf{r},\mathbf{r}',\mathrm{i}u) T_{jk}^{\rm lr}(\mathbf{r}',\mathbf{r}'') \alpha_{kl}^{\rm sr}(\mathbf{r}'',\mathbf{r}''',\mathrm{i}u) T_{li}^{\rm lr}(\mathbf{r}''',\mathbf{r}). \quad (24)$$

The structure of the individual terms in Eq. (23) is illustrated in Figure 6b for the case of the benzene dimer. These terms can be viewed as closed chains (loops) of quantum-mechanical events, in which a spontaneous fluctuation at some point generates a perturbation at another, which produces a response at yet another, which again generates a perturbation, etc., until some fluctuation interacts with the initial one. The closed form of these terms corresponds to the fact that these events are not triggered by an external perturbing field, but are spontaneous internal fluctuations.

Eq. (23) represents a general framework in which one can discuss all major vdW-inclusive methods in terms of the various realizations and approximations of this expression. When assessing a given vdW model, one can start with a discussion of how $\boldsymbol{\alpha}_{\rm sr}$ and $\mathbf{T}_{\rm lr}$ are constructed, followed by a discussion of how are they coupled. The fundamental motivation for the separation of the whole problem into short- and long-range components is that the explicit coupling $\mathbf{T}$ is relatively easy to handle at long-range and the properties of a material captured by $\boldsymbol{\alpha}$ can be reasonably modeled from the electron density at short range, as we show in the next section.

4.3 Local effective polarizability from the electron density

In this section, we argue that it is reasonable to approximate $\boldsymbol{\alpha}_{\rm sr}(\mathbf{r},\mathbf{r}')$ by its local counterpart $\boldsymbol{\alpha}_{\rm eff}(\mathbf{r})$. We already introduced a local polarizability, $\boldsymbol{\alpha}_{\rm loc}(\mathbf{r}) = \int \mathrm{d}\mathbf{r}'\boldsymbol{\alpha}(\mathbf{r},\mathbf{r}')$, which captures the local response to a homogeneous perturbation at all points. The main difference between $\boldsymbol{\alpha}_{\rm loc}(\mathbf{r})$ and $\boldsymbol{\alpha}_{\rm eff}(\mathbf{r})$ is that the former is obtained from the full $\boldsymbol{\alpha}(\mathbf{r},\mathbf{r}')$, whereas the latter comes from $\boldsymbol{\alpha}_{\rm sr}(\mathbf{r},\mathbf{r}')$, which is $\boldsymbol{\alpha}_0(\mathbf{r},\mathbf{r}')$ that was screened at short range only. As argued above, $\boldsymbol{\alpha}_0$ has mostly local character in finite-gap systems, which implies that $\boldsymbol{\alpha}_{\rm sr}(\mathbf{r},\mathbf{r}')$ is also mostly short-ranged. That is, $\boldsymbol{\alpha}_{\rm sr}(\mathbf{r},\mathbf{r}')$ describes only the response at points $\mathbf{r}$ that are near the perturbing field at point $\mathbf{r}'$. It is then reasonable to assume that the electric field is approximately homogeneous in this local neighborhood $M(\mathbf{r})$ surrounding $\mathbf{r}$, and hence the response can be well described with a local effective polarizability given by

$$\boldsymbol{\alpha}_{\rm eff}(\mathbf{r}) = \int_{\mathbf{r}'\in M(\mathbf{r})} \mathrm{d}\mathbf{r}'\boldsymbol{\alpha}_{\rm sr}(\mathbf{r},\mathbf{r}'). \quad (25)$$

This integration can be limited to the local neighborhood because $\boldsymbol{\alpha}_{\rm sr}(\mathbf{r},\mathbf{r}')$ goes quickly to zero for large $|\mathbf{r}-\mathbf{r}'|$. Since $\boldsymbol{\alpha}_{\rm eff}$ only depends on the local properties of a material, it turns out that reasonably good approximations for this quantity can be constructed using the electron density, its derivatives, or other density-derived quantities, which essentially was the motivation for range-separating the Dyson equation in the first place. In addition, the effective local polarizability also significantly simplifies the Dyson equation and hence our central correlation energy expression, Eq. (23). Here, $\boldsymbol{\alpha}_{\rm eff}(\mathbf{r})$ must enter these equations as $\delta(\mathbf{r}-\mathbf{r}')\boldsymbol{\alpha}_{\rm eff}(\mathbf{r}')$, where δ is the Dirac delta function. For example, the second-order contribution in Eq. (24) reduces in the following way after the substitution of $\boldsymbol{\alpha}_{\rm eff}(\mathbf{r})$:

$$E_{\rm c} = -\frac{1}{2}\int_0^\infty \frac{\mathrm{d}u}{2\pi} \iint \mathrm{d}\mathbf{r}\mathrm{d}\mathbf{r}' \times \mathrm{Tr}\left[\boldsymbol{\alpha}_{\rm eff}(\mathbf{r},\mathrm{i}u)\mathbf{T}_{\rm lr}(\mathbf{r},\mathbf{r}')\boldsymbol{\alpha}_{\rm eff}(\mathbf{r}',\mathrm{i}u)\mathbf{T}_{\rm lr}(\mathbf{r}',\mathbf{r})\right]. \quad (26)$$

Several distinct regions of the electron density can be considered when constructing a density model for $\boldsymbol{\alpha}_{\rm eff}(\mathbf{r})$, which may influence different types of materials as discussed in Section 2. The inner-shell electrons are relatively unresponsive, yet they cannot be safely neglected in all circumstances, especially for heavier atoms. Most of the response comes from the valence electrons, and hence a good model must capture the changes in the response associated with the formation of covalent bonds. In this regard, the tails of the electron density contain indirect information about the unoccupied electronic states, and hence are useful in models of $\boldsymbol{\alpha}_{\rm eff}$. Ionic (charge-transfer) states are reflected in the depletion and accumulation of the electron density and its derivatives with respect to neutral atoms. In all these examples, the response can be in principle captured well by a semi-local model for $\boldsymbol{\alpha}_{\rm eff}$ and the difficulties lie mostly in constructing a model that is general enough to describe all the cases as well as the continuous transitions between them on the same footing.

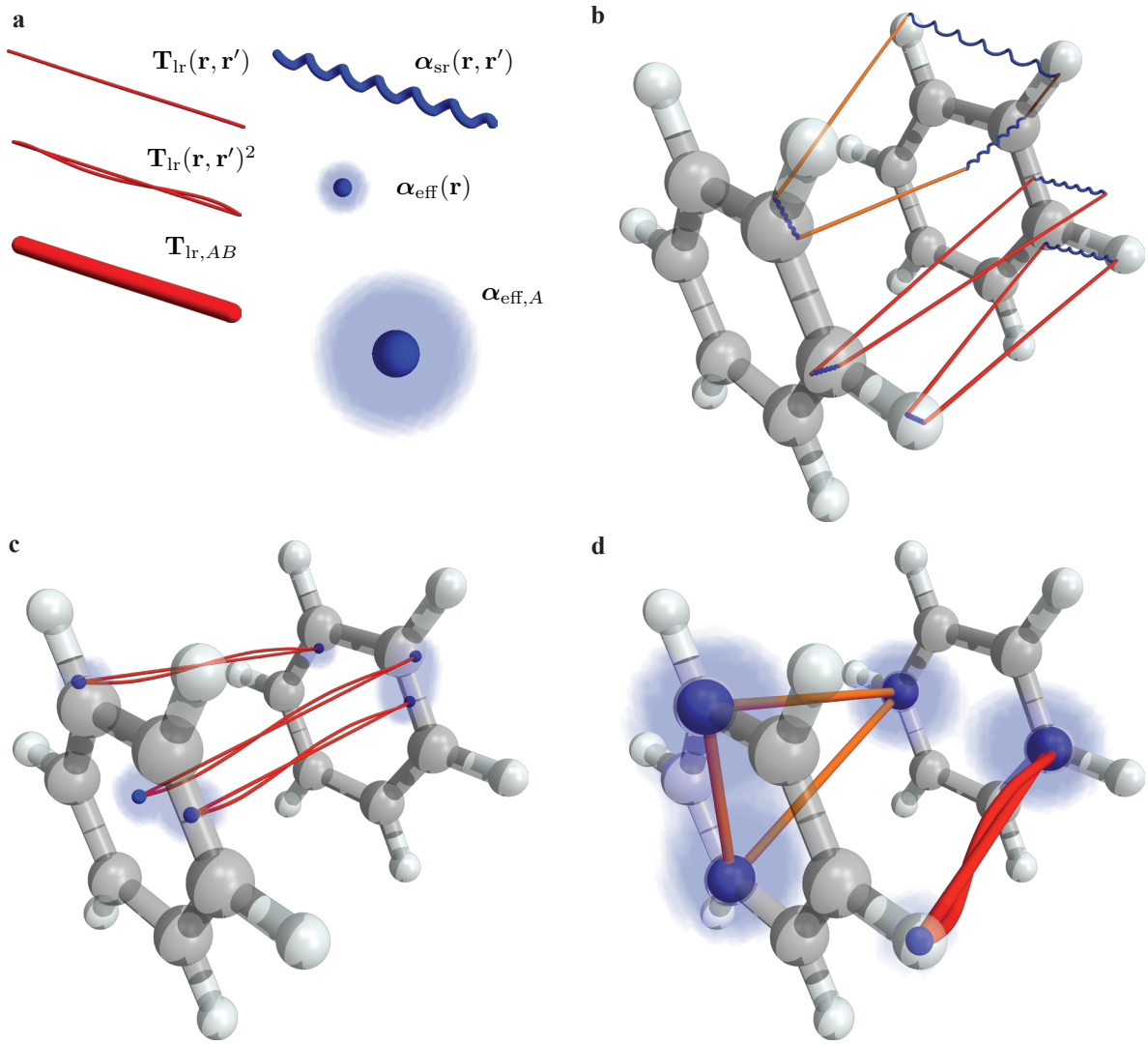

Figure 6. Schematic representation of different types of interaction terms present in exact and approximate models for van der Waals interactions as shown for the benzene dimer. (**a**) The legend for the individual quantities that are present in the different interaction terms. In the left column from top, the long-range dipole potential $\mathbf{T}_{\mathrm{lr}}(\mathbf{r},\mathbf{r}')$ (Eq. 21), its square, and the coarse-grained long-range dipole potential $\mathbf{T}_{\mathrm{lr},AB}$ (Section 4.4.1). In the right from top, the short-range screened nonlocal polarizability $\boldsymbol{\alpha}_{\mathrm{sr}}(\mathbf{r},\mathbf{r}')$ (Eq. 22), the local effective polarizability $\boldsymbol{\alpha}_{\mathrm{eff}}(\mathbf{r})$ (Eq. 25), and the coarse-grained local effective polarizability $\boldsymbol{\alpha}_{\mathrm{eff},A}$ (Section 4.7.2). The clouds around $\boldsymbol{\alpha}_{\mathrm{eff}}$ hint at the effective spatial extent of the local polarizability. (**b**) Examples of terms in the formally exact many-body expansion of the long-range correlation energy in Eq. (23). Points in space interact *via* chained short-range polarizabilities and long-range dipolar interactions. The red and orange colors distinguish examples of the second- and third-order terms, respectively. $\boldsymbol{\alpha}_{\mathrm{sr}}(\mathbf{r},\mathbf{r}')$ is largest when spatially localized on atoms and decays exponentially (in nonzero gap materials) with distance (see Figure 4c). On the other hand, $\boldsymbol{\alpha}_{\mathrm{lr}}$ is damped at short distances, but decays only polynomially with distance. The terms in the figure illustrate contributions not only from atoms, but also from bonds and even the tails of atomic densities (Section 4.3). (**c**) Examples of long-range correlation energy terms captured by nonlocal density functionals (Section 4.6). In this case, only second-order terms are accounted for and the short-range nonlocal polarizability is approximated by a density-derived effective local polarizability $\boldsymbol{\alpha}_{\mathrm{eff}}(\mathbf{r})$ (Section 4.3). (**d**) Examples of terms in a coarse-grained version of the full many-body expansion of the long-range correlation energy (Section 4.8). In this case, the second- (red) and third-order (orange) terms are depicted. Here, the interactions terms occur only between whole atoms.

4.3.1 Anisotropy of $\boldsymbol{\alpha}_{\mathrm{eff}}(\mathbf{r})$

The (point) polarizability of a molecule is in general an anisotropic quantity. A well-known example is the benzene molecule, in which the in-plane components of the polarizability are approximately two times larger than the out-of-plane component (see Figure 5a). Because this quantity is coupled with the highly anisotropic dipole potential $\mathbf{T}_{\mathrm{lr}}$, a proper account of the anisotropy in the polarizability is crucial for an accurate estimate of the long-range correlation energy $E_{\mathrm{c,lr}}$. In the context of Eq. (23), the contribution from the anisotropy

emerges in two distinct ways.

First, $\boldsymbol{\alpha}_{\mathrm{sr}}(\mathbf{r},\mathbf{r}')$ (or $\boldsymbol{\alpha}_{\mathrm{eff}}(\mathbf{r})$) introduces the anisotropy directly into the expression for $E_{\mathrm{c,lr}}$. This aspect of the anisotropy is neglected in most vdW models. This approximation enables one to write the polarizability as a scalar, $\boldsymbol{\alpha}_{\mathrm{eff}}(\mathbf{r}) \approx \alpha_{\mathrm{eff}}(\mathbf{r})$, which simplifies the equations by making α_{eff} and $\mathbf{T}_{\mathrm{lr}}$ commute. For example, the second-order contribution to $E_{\mathrm{c,lr}}$ in Eq. (24), reduces to the familiar $1/R^6$ dependence on the distance $R = |\mathbf{r}-\mathbf{r}'|$:

$$\begin{aligned} E_{\mathrm{c}}^{(2)} &= -\frac{1}{2}\int_0^\infty \frac{\mathrm{d}u}{2\pi} \iint \mathrm{d}\mathbf{r}\mathrm{d}\mathbf{r}' \\ &\quad \times \mathrm{Tr}\left[\alpha_{\mathrm{eff}}(\mathbf{r},\mathrm{i}u)\mathbf{T}_{\mathrm{lr}}(\mathbf{r},\mathbf{r}')\alpha_{\mathrm{eff}}(\mathbf{r}',\mathrm{i}u)\mathbf{T}_{\mathrm{lr}}(\mathbf{r}',\mathbf{r})\right] \\ &= -\frac{1}{2}\iint \mathrm{d}\mathbf{r}\mathrm{d}\mathbf{r}' \\ &\quad \times \left(\frac{3}{\pi}\int_0^\infty \mathrm{d}u\alpha_{\mathrm{eff}}(\mathbf{r},\mathrm{i}u)\alpha_{\mathrm{eff}}(\mathbf{r}',\mathrm{i}u)\right)\mathrm{Tr}\left[\frac{1}{6}\mathbf{T}_{\mathrm{lr}}(\mathbf{r},\mathbf{r}')^2\right] \\ &= -\frac{1}{2}\iint \mathrm{d}\mathbf{r}\mathrm{d}\mathbf{r}' C_6(\mathbf{r},\mathbf{r}')\frac{f(|\mathbf{r}-\mathbf{r}'|)^2}{|\mathbf{r}-\mathbf{r}'|^6}, \end{aligned} \tag{27}$$

where we introduced $C_6(\mathbf{r},\mathbf{r}') = \frac{3}{\pi}\int_0^\infty \mathrm{d}u\alpha(\mathbf{r},\mathrm{i}u)\alpha(\mathbf{r}',\mathrm{i}u)$, which is a generalization of the Casimir–Polder integral, and f is the damping function used for range-separating $\mathbf{T}_{\mathrm{lr}} = f(R)\mathbf{T}$ (see Eq. 21). $C_6(\mathbf{r},\mathbf{r}')$ defined in this way is just a more general form of the familiar atomic $C_{6,AB}$ coefficients.

Second, the anisotropy is also accounted for automatically by the long-range coupling in Eq. (23). This follows from the Dyson screening equation (18), which was incorporated into the ACFDT formula (17). In this regard, $\boldsymbol{\alpha}_\lambda$ obtained from the Dyson equation can be strongly anisotropic even if $\boldsymbol{\alpha}_0$ was isotropic.

4.3.2 Harmonic oscillator model of dynamic response

The exact dependence of the polarizability on the frequency is in general unknown. Here, we briefly introduce the model system of a quantum harmonic oscillator (QHO), which is used to a different degree by many vdW approaches in modeling the frequency dependence of the local effective polarizability. Because of the harmonic force and associated quadratic potential, the QHO is the simplest model for studying small perturbations of a system in equilibrium. In our case, the equilibrium system is the electronic ground state, or the ground-state electron density, and the small perturbations are the quantum-mechanical charge fluctuations. The QHO also happens to be a quantum system with equidistant energy levels, which makes it a perfect tool for "counting" electronic excitations, which in turn describe all response properties of molecules and materials. It is for both these intertwined reasons that the QHOs are such a useful model for modeling vdW interactions, among others.

Many properties of a QHO can be derived analytically. In particular, the dynamic (point) polarizability of a QHO is

$$\alpha^{\mathrm{QHO}}(u) = \frac{q^2}{m(\omega^2 - u^2 - \mathrm{i}\delta u)}, \tag{28}$$

where q is the charge of the oscillator, m is its mass, ω is its excitation (characteristic) frequency, and δ is an infinitesimally small number. The oscillator may be considered also infinitesimal, in which case m and q would be infinitesimals $\mathrm{d}m$ and $\mathrm{d}q$, respectively. The infinitesimal imaginary part in the denominator is necessary to satisfy the Kramers–Kronig causal identities for response functions, and its physical meaning is simply that the absorption spectrum (imaginary part of α^{QHO}) is a Dirac delta function located at ω. In other words, the QHO only absorbs electromagnetic radiation corresponding to its own excitation frequency. Furthermore, this infinitesimal imaginary part disappears in the integral over the imaginary frequency $\mathrm{i}u$, as can be seen for example in the form of Eq. (14) for α^{QHO}

$$\int_0^\infty \mathrm{d}u\,\alpha^{\mathrm{QHO}}(\mathrm{i}u) = \int_0^\infty \mathrm{d}u \frac{q^2}{m(\omega^2+u^2)} = \frac{\pi}{2}\frac{q^2}{m\omega} \tag{29}$$

$$\int_0^\infty \mathrm{d}u\,\mathrm{Im}\,\alpha^{\mathrm{QHO}}(u) = \int_0^\infty \mathrm{d}u \frac{\pi}{2}\frac{q^2}{mu}\delta(u-\omega) = \frac{\pi}{2}\frac{q^2}{m\omega}. \tag{30}$$

The QHO model, with its single-frequency absorption spectrum, is insufficient to describe the full spectrum of a real atom. However, a frequency integral of such a complicated spectrum (imaginary part of α) is a single number, and as such can be effectively captured by an integral of a simple spectrum characterized by a single frequency. The choice of such an effective frequency necessarily depends on the particular form of the integrand, and the use of a single effective frequency for all cases constitutes the so-called Unsöld approximation (Unsöld, 1927). For instance, consider the generalization of the Casimir–Polder integral for the C_6 coefficient in Eq. (27). This expression demonstrates that the second-order correlation energy between two atoms (with complicated absorption spectra) can be captured exactly by the interaction between two QHOs (with single-frequency spectra) as long as the pairs of atoms and QHOs have the same C_6 coefficient. The C_6 coefficient for two identical QHOs depends only on the static dipole polarizability and the characteristic excitation frequency:

$$C_6^{\mathrm{QHO}} = \frac{3}{\pi}\int_0^\infty \mathrm{d}u\,\alpha^{\mathrm{QHO}}(\mathrm{i}u)\alpha^{\mathrm{QHO}}(\mathrm{i}u) = \frac{3}{4}\left(\alpha^{\mathrm{QHO}}(0)\right)^2\omega. \tag{31}$$

A useful combination rule holds for the C_6 coefficient of two QHOs A and B (with different sets of parameters q, ω and m):

$$\begin{aligned} C_{6,AB} &= \frac{3}{\pi}\int_0^\infty \mathrm{d}u\,\alpha_A(\mathrm{i}u)\alpha_B(\mathrm{i}u) \\ &= \frac{2C_{6,AA}C_{6,BB}}{C_{6,AA}\frac{\alpha_B(0)}{\alpha_A(0)} + C_{6,BB}\frac{\alpha_A(0)}{\alpha_B(0)}}, \end{aligned} \tag{32}$$

where $C_{6,AA}$ are the C_6 coefficients between two identical oscillators A from Eq. (31) and $\alpha_A(0)$ are the corresponding static dipole polarizabilities. However, using Eq. (32) for combining the C_6 coefficients of real atoms is precisely an example of the Unsöld approximation, as the effective frequencies needed to exactly capture the integrals in Eqs. (31) and (32) would in general be different. On the other hand, it has been shown that this approximation leads to a mean absolute relative error of only 3% in the C_6 coefficients for heteronuclear atomic pairs (Tkatchenko and Scheffler, 2009).

4.4 Classification of approximate van der Waals methods

Here, we introduce a general classification of vdW methods based on two independent approximations to the general expression for $E_{\mathrm{c,lr}}$ in Eq. (23). The first one involves coarse-graining spatial quantities such as $\boldsymbol{\alpha}(\mathbf{r},\mathbf{r}')$, $\boldsymbol{\alpha}_{\mathrm{eff}}(\mathbf{r})$, or $\mathbf{T}(\mathbf{r},\mathbf{r}')$. The second approximation involves truncating the infinite series, or the many-body expansion, in Eq. (23) to some finite order. Methods that do not use either of these two approximations (but use other instead) comprises the class of models based on the random-phase approximation (see Section 4.5). Nonlocal density functionals, which will be discussed in Section 4.6, constitute a class of truncated, but non–coarse-grained methods. The many-body dispersion (MBD) framework of coupled harmonic oscillators represents a class of coarse-grained, but nontruncated models (see Section 4.8). Finally, both the coarse-graining and truncation approximations are used in the popular class of pairwise methods (see Section 4.7).

4.4.1 Coarse-graining the ACFD formula and Dyson equation

Each of the spatial integrals (over $\mathbf{r}$ and $\mathbf{r}'$) in the ACFD expression in Eq. (17) can be partitioned into N parts with the use of a set of functions, $w_A(\mathbf{r})$, which satisfy $\sum_{A=1}^{N} w_A(\mathbf{r}) = 1$ at each point $\mathbf{r}$. When these functions are spatially localized, they naturally define a set of N fragments. Using such a partitioning scheme breaks the ACFD formula into N^2 terms,

$$E_{\mathrm{c}} = \sum_{AB} \int_0^\infty \frac{\mathrm{d}u}{2\pi} \int_0^1 \mathrm{d}\lambda \iint \mathrm{d}\mathbf{r}\mathrm{d}\mathbf{r}' \times \mathrm{Tr}\left[\left(\boldsymbol{\alpha}_\lambda(\mathbf{r},\mathbf{r}',\mathrm{i}u) - \boldsymbol{\alpha}_0(\mathbf{r},\mathbf{r}',\mathrm{i}u)\right)\mathbf{T}(\mathbf{r},\mathbf{r}')\right] w_A(\mathbf{r}) w_B(\mathbf{r}') \tag{33}$$

One may now coarse-grain the two-point dipole potential, $\mathbf{T}(\mathbf{r},\mathbf{r}')$, via

$$w_A(\mathbf{r}) w_B(\mathbf{r}') \mathbf{T}(\mathbf{r},\mathbf{r}') \approx w_A(\mathbf{r}) w_B(\mathbf{r}') \mathbf{T}(\mathbf{R}_A,\mathbf{R}_B) \tag{34}$$

in which $\mathbf{T}(\mathbf{R}_A,\mathbf{R}_B)$ is the dipole potential between the centers $\mathbf{R}_A$ and $\mathbf{R}_B$ of fragments A and B. Such an approximation then enables one to reduce the spatial integrals in the ACFD formula,

$$\begin{aligned} E_{\mathrm{c}} &= \sum_{AB} \int_0^\infty \frac{\mathrm{d}u}{2\pi} \int_0^1 \mathrm{d}\lambda \\ &\times \mathrm{Tr}\left[\left[\iint \mathrm{d}\mathbf{r}\mathrm{d}\mathbf{r}' \left(\boldsymbol{\alpha}_\lambda(\mathbf{r},\mathbf{r}',\mathrm{i}u) - \boldsymbol{\alpha}_0(\mathbf{r},\mathbf{r}',\mathrm{i}u)\right) w_A(\mathbf{r}) w_B(\mathbf{r}')\right] \times \mathbf{T}(\mathbf{R}_A,\mathbf{R}_B)\right] \\ &\equiv \int_0^\infty \frac{\mathrm{d}u}{2\pi} \int_0^1 \mathrm{d}\lambda \sum_{AB} \mathrm{Tr}\left[\left(\boldsymbol{\alpha}_{\lambda,AB}(\mathrm{i}u) - \boldsymbol{\alpha}_{0,AB}(\mathrm{i}u)\right)\mathbf{T}_{AB}\right] \end{aligned} \tag{35}$$

where we defined $\boldsymbol{\alpha}_{AB} = \iint \mathrm{d}\mathbf{r}\mathrm{d}\mathbf{r}' \boldsymbol{\alpha}(\mathbf{r},\mathbf{r}') w_A(\mathbf{r}) w_B(\mathbf{r}')$ and $\mathbf{T}_{AB} = \mathbf{T}(\mathbf{R}_A,\mathbf{R}_B)$, which are now coarse-grained versions of $\boldsymbol{\alpha}(\mathbf{r},\mathbf{r}')$ and $\mathbf{T}(\mathbf{r},\mathbf{r}')$, respectively. A simple, yet illustrative example of such a coarse-graining procedure is any numerical, real-space grid implementation of the ACFD formula, in which $\mathbf{R}_A$ are simply the grid points. In this case, the error associated with approximating $\mathbf{T}(\mathbf{r},\mathbf{r}')$ with $\mathbf{T}_{AB}$ would be considered a numerical error arising from the use of a grid that is too coarse. In the case of vdW models, however, one is only concerned with the long-range part of $\mathbf{T}$, $\mathbf{T}_{\mathrm{lr}}$, and hence the fragments A can be much larger than grid points, while still maintaining a reasonable level of accuracy. Here, the fragments are typically chosen to be atoms, whereby an effective atoms-in-molecules partitioning scheme $w_A(\mathbf{r})$ is used; however, other fragmentation schemes can also be used with good results. Using an analogy from electrostatics, we now connect the coarse-graining to the standard multipole expansion procedure.. The electrostatic interaction energy of two charge distributions, $n_A(\mathbf{r})$, is given by $E_{n\text{–}n} = \frac{1}{2}\iint \mathrm{d}\mathbf{r}\mathrm{d}\mathbf{r}' n_1(\mathbf{r}) v(\mathbf{r},\mathbf{r}') n_2(\mathbf{r}')$. The same quantity for two dipole distributions, $\mathbf{P}_A(\mathbf{r})$, is $E_{\mathbf{P}\text{–}\mathbf{P}} = \frac{1}{2}\iint \mathrm{d}\mathbf{r}\mathrm{d}\mathbf{r}' \mathbf{P}_1(\mathbf{r}) \mathbf{T}(\mathbf{r},\mathbf{r}') \mathbf{P}_2(\mathbf{r}')$. $E_{n\text{–}n}$ can be expanded into the multipole series q–q, q–$\mathbf{p}$, $\mathbf{p}$–$\mathbf{p}$, $\mathbf{p}$–$\mathbf{Q}$, etc., where q, $\mathbf{p}$, and $\mathbf{Q}$ denote monopole (charge), dipole, and quadrupole moments, respectively. Likewise, the dipole distribution interaction energy $E_{\mathbf{P}\text{–}\mathbf{P}}$ can also be expanded into an analogous series starting with the $\mathbf{p}$–$\mathbf{p}$ term. Here, we consider only charge distributions $n_A(\mathbf{r})$ that arise from dipole distributions $\mathbf{P}_A(\mathbf{r})$ via $n_A(\mathbf{r}) = -\boldsymbol{\nabla}\cdot\mathbf{P}_A(\mathbf{r})$, and are therefore characterized by zero monopole (charge) moments. It then follows that the energies $E_{n\text{–}n}$ and $E_{\mathbf{P}\text{–}\mathbf{P}}$, as well as their multipole expansions, would in fact be identical. Within this context, the coarse-graining of Eq. (34) simply corresponds to considering only the $\mathbf{p}$–$\mathbf{p}$ term in the multipole expansion of $E_{\mathbf{P}\text{–}\mathbf{P}}$.

The feasibility of such an approximation is determined by the spatial extent of each $w_A(\mathbf{r})$ around R_A relative to the distances between the fragments.

When the fragments are atoms, the issue of considering only the dipole–dipole term is a well-known and well-analyzed approximation. Some models improve upon this approximation by including higher-order terms from the multipole expansion, such as the dipole–quadrupole or quadrupole–quadrupole terms. However, the multipole expansion of $\mathbf{T}_{\mathrm{lr}}(\mathbf{r},\mathbf{r}') = f(|\mathbf{r}-\mathbf{r}'|)\mathbf{T}(\mathbf{r},\mathbf{r}')$ is not simply the multipole expansion of $\mathbf{T}(\mathbf{r},\mathbf{r}')$ multiplied by the damping function $f(|\mathbf{r}-\mathbf{r}'|)$. Therefore, the coupling of the higher-order moments is not separable from the damping function itself; rather, it can be partially and effectively captured in f, as this function often contains some empiricism anyway. An alternative path to mitigate this error would be simply to use a finer graining for $\boldsymbol{\alpha}(\mathbf{r},\mathbf{r}')$. This returns to the fact that the fully nonlocal dipole polarizability is sufficient for an exact description of the long-range electron correlation.

As was done for the ACFD formula, one can also coarse-grain the Dyson Eq. (18):

$$\begin{aligned} \boldsymbol{\alpha}_{\lambda,AB} &= \boldsymbol{\alpha}_{0,AB} - \sum_{CD} \boldsymbol{\alpha}_{0,AC} \lambda \mathbf{T}_{\mathrm{xc},\lambda,CD} \boldsymbol{\alpha}_{\lambda,DB} \\ &\equiv \boldsymbol{\alpha}_{0,AB} - [\![\boldsymbol{\alpha}_0 \lambda \mathbf{T}_{\mathrm{xc},\lambda} \boldsymbol{\alpha}_\lambda]\!]_{AB} \end{aligned} \tag{36}$$

where $[\![\cdot]\!]$ denotes implicit summations over fragments, in analogy to $\{\!\{\cdot\}\!\}$ which denotes implicit integrations over space. As

a result, the many-body expansion of $E_{\mathrm{c,lr}}$ in Eq. (23) can be also coarse-grained,

$$E_{\mathrm{c}} = \int_0^\infty \frac{\mathrm{d}u}{2\pi} \int_0^1 \mathrm{d}\lambda \sum_{AB} \mathrm{Tr}\left[\sum_{n=1}^{\infty} \left[\!\left[\boldsymbol{\alpha}_{\mathrm{sr}} \left(-\lambda \mathbf{T}_{\mathrm{lr}} \boldsymbol{\alpha}_{\mathrm{sr}}\right)^n\right]\!\right]_{AB} \mathbf{T}_{\mathrm{lr},AB}\right]$$
$$= -\sum_{n=2}^{\infty} \frac{(-1)^n}{n} \int_0^\infty \frac{\mathrm{d}u}{2\pi} \sum_{AB} \mathrm{Tr}\left[\left[\!\left[\left(\boldsymbol{\alpha}_{\mathrm{sr}} \mathbf{T}_{\mathrm{lr}}\right)^n\right]\!\right]_{AB} (\mathrm{i}u)\right] \quad (37)$$

The coarse-grained versions of these equations will serve as a basis for discussing the pairwise and many-body dispersion vdW methods. We note that the only approximation made so far is the replacement of the full multipole expansion with the dipole–dipole term. As long as all short-range correlation effects are properly accounted for in $\boldsymbol{\alpha}_{\mathrm{sr},AB}$, there is no reduction in generality in this regard.

4.4.2 Truncating the many-body expansion of the long-range correlation energy

In Eq. (23), $E_{\mathrm{c,lr}}$ is expanded in the number of interactions of $\boldsymbol{\alpha}_{\mathrm{sr}}$ via the coupling potential $\mathbf{T}_{\mathrm{lr}}$. The second-order (*i.e.*, the lowest-order) contribution corresponds to two interactions, the third-order contribution to three interactions, etc. These interactions occur between bodies (atoms, molecules, points in space), which motivates the terminology of two-, three-, four-body, contributions to the interaction energy. We point out that the correspondence between the m-body and n-th order contributions is not straightforward. Starting at $n = 4$, terms at n-th order describe interactions between $m < n$ bodies and hence contribute to the m-body interaction energy. For instance, the term at fourth order contains four $\mathbf{T}_{\mathrm{lr}}$ between two bodies, and so contributes to the 2-body interaction energy (at fourth order). On the other hand, the lowest-order contribution to a given n-body interaction energy is typically the largest, which justifies the colloquial equivalence of these two distinct expansions.

The lowest-order contribution to $E_{\mathrm{c,lr}}$ corresponds to two $\mathbf{T}_{\mathrm{lr}}$ (*e.g.*, red lines in Figure 6b). The higher-order contributions in Eq. (23) tend to cancel out in weakly polarizable systems or for symmetrical geometries, which is the basis for pairwise schemes and nonlocal density functionals. In general, the quality of this second-order approximation is difficult to assess; however, three universal factors can be distinguished. First, the increasing number of the interactions $\mathbf{T}_{\mathrm{lr}}$ decreases the magnitude of the higher-order terms. This effect dominates at long range, where $\mathbf{T}_{\mathrm{lr}}$ is small, and indeed the asymptotic interaction between finite bodies corresponds to the second order. But this requires that the correlation is treated to infinite order within the interacting bodies to obtain their respective nonlocal polarizabilities. Second, the increasing number of terms within each order may increase the total magnitude of the higher-order contributions. This effect is important in larger molecular systems and materials. (The number of terms at n-th order in a coarse-grained model with N fragments grows as $O(N^n)$, and hence the relative number of terms in subsequent orders grows as $O(N)$.) The third universal factor is the symmetry and dimensionality of the system. Whereas the second-order terms always lower the total energy of the system (*i.e.*, stabilize), the signs of the individual higher-order terms have an angular dependence. In high-symmetry crystals with simple unit cells and lattices, the higher-order terms tend to cancel out, leading to higher-order contributions that may be collectively negligible. In contrast, this is not the case in low-dimensional materials in which, as a result, nontrivial behavior $E_{\mathrm{c,lr}}$ and response properties can be observed.

In the present context, the often used Axilrod–Teller–Muto (ATM) three-body potential constitutes a third-order contribution to $E_{\mathrm{c,lr}}$. The previous discussion makes it clear that while such a correction may extend the applicability of a second-order model, it does not provide a universal description of vdW interactions.

A more detailed discussion of these terms can be found below in Section 4.8 which deals with the many-body dispersion framework.

4.5 Methods based on random-phase approximation

Here, we discuss electronic structure methods formulated in the ACFD formalism that do not coarse-grain nor truncate the expression for the correlation energy, but work with $\boldsymbol{\alpha}_0$ in the molecular orbital basis as obtained directly from a KS calculation via Eq. (15). These methods construct a model for the nonlocal polarizability in a way that is also applicable for the short-range correlation energy, which distinguishes them from the explicit models for $E_{\mathrm{c,lr}}$ discussed in the next three sections. For the purpose of this review, we discuss the methods only from the point of view of long-range electron correlation and refer the reader elsewhere for a more general exposition (Ren et al., 2012; Eshuis et al., 2012).

A starting point for the methods of this section is the random-phase approximation (RPA), in which the exchange-correlation kernel $f_{\mathrm{xc}}(\mathbf{r}, \mathbf{r}', u) = \delta v_{\mathrm{xc}}(\mathbf{r}, u)/\delta n(\mathbf{r}', u)$ in the Dyson equation (18) is set to zero. Its name comes from the original derivation of the approximation, in which the fluctuations of electrons are assumed to be influenced only by in-phase Coulomb contributions, whereas out-of-phase terms are considered to be random and hence cancel out.. This was later shown to be equivalent to the $f_{\mathrm{xc}} = 0$ definition in DFT. The application of RPA to the Dyson equation leads to a conceptually simple method for the electron correlation energy, which amounts to evaluating the expression Eq. (23) with $\boldsymbol{\alpha}_{\mathrm{sr}}$ and $\mathbf{T}_{\mathrm{lr}}$ replaced by $\boldsymbol{\alpha}_0$ and $\mathbf{T}$, respectively, that is

$$E_{\mathrm{c}} = -\sum_{n=2}^{\infty} \frac{(-1)^n}{n} \int_0^\infty \frac{\mathrm{d}u}{2\pi} \iint \mathrm{d}\mathbf{r}\mathrm{d}\mathbf{r}' \times \mathrm{Tr}\left[\left\{\!\!\left\{\left(\boldsymbol{\alpha}_0 \mathbf{T}\right)^n\right\}\!\!\right\} (\mathbf{r}, \mathbf{r}', \mathrm{i}u)\right] \quad (38)$$

Using the explicit Adler–Wiser expression in Eq. (15) for the bare response in the χ-representation, this expression can be evaluated numerically in a straightforward manner, yielding the total electron correlation energy (Furche, 2001). In DFT, $\boldsymbol{\alpha}_0$ is obtained from a KS calculation carried out with some approximate density functional, and hence is only an approximation to the true $\boldsymbol{\alpha}_0$ that would be obtained with the exact functional. The remainder of the total electronic energy is usually taken as

the sum of the kinetic, nuclear-electron attraction, Hartree, and exact-exchange terms, which are themselves approximate due to the fact that they were obtained from KS orbitals based on an approximate density functional.

RPA treats not only the long-range but also the short-range electron correlation explicitly via the coupling potential, both on the level of the energy, E_{sr}, in the ACFD formula, and the level of the response, $\boldsymbol{\alpha}_{\mathrm{sr}}$, in the Dyson equation. This raises two questions:. First, the short-range correlation energy may be inadequate, leading to incorrect description of vdW systems in equilibrium geometries, where this quantity plays a significant role. Second, the fully coupled $\boldsymbol{\alpha}_\lambda$ may lack contributions from f_{xc} at short range, leading to inaccurate molecular polarizabilities and hence incorrect long-range vdW coefficients. Below, we discuss three different approaches to mitigate these issues.

4.5.1 Range-separated random-phase approximation

The first attempt at correcting the behavior of RPA at short range was given by Kurth and Perdew (Kurth and Perdew, 1999). They suggested a correction to RPA, termed RPA+, given by

$$E_{\mathrm{c}}^{\mathrm{RPA+}} = E_{\mathrm{c}}^{\mathrm{RPA}} - E_{\mathrm{c}}^{\mathrm{GGA@RPA}} + E_{\mathrm{c}}^{\mathrm{GGA}} \tag{39}$$

where $E_{\mathrm{c}}^{\mathrm{RPA}}$ is the RPA correlation energy, $E_{\mathrm{c}}^{\mathrm{GGA@RPA}}$ is the correlation energy calculated with a special GGA designed for capturing $E_{\mathrm{c}}^{\mathrm{RPA}}$, and $E_{\mathrm{c}}^{\mathrm{GGA}}$ is the correlation energy from a standard GGA. The idea of the RPA+ approach is to remove the incorrect short-range part of the correlation energy from RPA with the use of a special GGA, and then reintroduce a better approximation to it using a standard GGA, such as PBE (Perdew et al., 1996). The special GGA designed for this purpose was constructed by replacing the LDA part of the PBE correlation functional with an LDA parametrized to reproduce the RPA correlation energy of the homogeneous electron gas. This was later refined by specially constructing also the density-gradient dependent part using additional properties of the short-range behavior of RPA (Yan et al., 2000). Here, the short-range correlation energy, E_{sr}, comes from a GGA density functional, while the RPA is used only for the long-range part, E_{lr}. But the range separation is accomplished only approximately using $E_{\mathrm{c}}^{\mathrm{GGA@RPA}}$ and depends on how well this GGA functional describes the short-range part of RPA. The issue of explicit range separation of RPA was later attacked by Toulouse *et al.* (Toulouse et al., 2009). In their work, a range-separated version of the KS scheme was used, in which only the short-range part of the electron correlation was included in the exchange-correlation potential for the electrons, while the long-range part was treated explicitly via the long-range version of the ACFD formula. In such a scheme, the long-range Dyson equation in Eq. (22) is essentially solved with $\boldsymbol{\alpha}_0$ instead of $\boldsymbol{\alpha}_{\mathrm{sr}}$, that is, the long range is treated as in RPA, but at short range, it is assumed that $v(\mathbf{r}, \mathbf{r}')$ and $f_{\mathrm{xc}}(\mathbf{r}, \mathbf{r}')$ partially cancel each other.

4.5.2 Approximate exchange-correlation kernels

In a different approach, the ACFD framework is used in full without range separation, but a suitable approximation to f_{xc} is constructed. A straightforward nontrivial approximation can be obtained from any density functional $E_{\mathrm{xc}}[n]$ via

$$f_{\mathrm{xc}}(\mathbf{r}, \mathbf{r}', u) \approx \delta(\mathbf{r} - \mathbf{r}') \frac{\delta^2 E_{\mathrm{xc}}[n]}{\delta n(\mathbf{r})^2} \tag{40}$$

where the kernel is approximated as local and independent of frequency. This so-called adiabatic local density approximation (ALDA) violates several known limits of f_{xc}, which make it unsuitable for use in the ACFD formula. Olsen and Thygesen analysed the ALDA in the homogeneous electron gas in reciprocal space and noticed that whereas ALDA provides a good description of the small-q (large-wavelength) behavior of the electron correlation hole, it decays too slowly to zero for large q compared to the exact behaviour. This observation lead them to introduce the renormalized ALDA (rALDA) by modifying the dependence of f_{xc} in ALDA on large q (Olsen and Thygesen, 2012, 2013a, 2014). By transforming back to real space and generalizing to inhomogeneous densities, this defines a universal approximation to f_{xc} and hence a method for obtaining the electron correlation energy via the ACFD formula. Compared to RPA, the short-range part of the coupling in the Dyson equation is described more realistically here, which propagates into a better description of both the short-range correlation energy and the short-range effects in the polarizability.

A more straightforward, but computationally more demanding approach is to approximate f_{xc} with the exact exchange kernel, f_{x}, leading to the so-called tdEXX method (Görling, 1998; Heßelmann and Görling, 2010). The development of more accurate and sophisticated kernels is the domain of TD-DFT and the associated study of response properties, which is beyond the scope of this review. For a way to make these approaches faster and hence more easily applicable to studying vdW interactions, as well as for an overview of this rich field, see *e.g.* ref. 99 and the refs. therein.

4.5.3 Renormalized perturbation theory to second order

Yet a different path to fixing the issues of RPA comes from the standard many-body perturbation theory for electrons. The Møller–Plesset correlation energy at second order (MP2) consists of the Coulomb and exchange terms, of which only the former is significant at all ranges (decays polynomially with distance) whereas the latter is significant only at short range (decays exponentially). In this context, RPA can be described as an infinite-order sum of the so-called ring excitations, of which the Coulomb term of MP2 is the first one (the higher orders are combinations of the single Coulomb term).. This renormalization of the Coulomb term resolves many of the deficiencies of MP2, such as its inapplicability to zero-gap systems and its tendency to overestimate $E_{\mathrm{c,lr}}$. In the same breath, RPA neglects exchange effects which are partially captured at the MP2 level, which can lead to issues at short range where these effects become important. The second-order screened exchange (SOSEX) is constructed in a similar way as RPA by

renormalizing the exchange part of MP2, that is, by summing the corresponding type of the perturbation term to infinite order. Together, RPA and SOSEX form a method that extends well beyond MP2 via renormalization of both the Coulomb and exchange terms, resulting for instance in a description of one-electron systems free of self-correlation.

A renormalized form of the full second-order perturbation theory (rPT2) can be obtained by adding the first-order perturbation term, the so-called single-excitation (SE) correction (Ren et al., 2011). This term is trivially zero in the standard MPn scheme, because the Brillouin's theorem guarantees that single excitations of the HF orbitals do not contribute to the correlation energy. In a KS-based calculation, however, this term is required because the KS orbitals are not stationary with respect to the RPA and SOSEX energy expression. In addition, the SE correction was found to approximately compensate for the difference between the exact exchange energies evaluated with HF and KS orbitals. In analogy to RPA and SOSEX, the SE term can be summed to infinite order, leading to the renormalized SE (rSE) correction. The resulting rPT2 method combines the rSE, RPA, and SOSEX schemes (Ren et al., 2013). Klimeš et al. derived an alternative formulation of rSE, in which the singles excitation energies are taken from the GW approximation (Klimeš et al., 2015). A detailed discussion of many different flavors of RPA-like approximations can be found in other publications (Scuseria et al., 2008; Jansen et al., 2010; Ángyán et al., 2011).

4.6 Nonlocal density functionals

Nonlocal density functionals derive their name from their two-point semi-local dependence on the electron density via

$$E_c = \frac{1}{2}\iint \mathrm{d}\mathbf{r}\mathrm{d}\mathbf{r}' n(\mathbf{r})n(\mathbf{r}')\Phi[n](\mathbf{r},\mathbf{r}') \tag{41}$$

where Φ is a so-called nonlocal kernel, constructed to capture the long-range part of the correlation energy. The first universal functional of this type, called vdW-DF, was derived by Dion *et al.* (Dion et al., 2004) as a culmination of the body of work established by Langreth and Lundqvist throughout the course of three decades (for a detailed discussion of the vdW-DF class of nonlocal functionals, see (Langreth et al., 2005; Hyldgaard et al., 2014; Berland et al., 2015)). We start this section with a review of the general approximations to the ACFD formula leading to nonlocal functionalsand continue with a detailed description of particular functionals including the vdW-DF family. The section concludes with a discussion of relationships between nonlocal functionals and other vdW methods.

Nonlocal density functionals represent the class of non–coarse-grained and second-order truncated approximations to the ACFD formula. In addition, they use an isotropic density-dependent model for the effective polarizability α_{eff} which was defined in Section 4.3.1. We start the discussion by rewriting the second-order contribution to $E_{c,\mathrm{lr}}$ from Eq. (27) in a different form:

$$E_c^{(2)} = -\frac{1}{2}\iint \mathrm{d}\mathbf{r}\mathrm{d}\mathbf{r}'\frac{3}{\pi}\int_0^\infty \mathrm{d}u \times \alpha_{\mathrm{eff}}[n](\mathbf{r},\mathrm{i}u)\,\alpha_{\mathrm{eff}}[n](\mathbf{r}',\mathrm{i}u)\frac{f[n](|\mathbf{r}-\mathbf{r}'|,u)^2}{|\mathbf{r}-\mathbf{r}'|^6} \tag{42}$$

where the functional dependence on the electron density is explicitly denoted in all relevant quantities and the range-separating function f is generalized to depend on the frequency. Examples of the interaction terms under the spatial integral sign are depicted in Figure 6c. Here, pairs of infinitesimal fluctuations with properties described by α_{eff} are correlated via the coupling potential f^2/R^6.

The use of α_{eff} is the first of two local approximations used by all nonlocal functionals. As described in Section 4.3, $\alpha_{\mathrm{eff}}(\mathbf{r})$ is the local counterpart of the short-range nonlocal polarizability $\boldsymbol{\alpha}_{\mathrm{sr}}(\mathbf{r},\mathbf{r}')$ and in general can be constructed as an integral over the local neighborhood surrounding $\mathbf{r}$ as in Eq. (25). We note that Eq. (42) does not specify the explicit functional form for the dependence of α_{eff} on the electron density. In this sense, the second local approximation commonly enters via the models used for $\alpha_{\mathrm{eff}}(\mathbf{r})$, which depend only on the electron density and its gradient,

$$\alpha_{\mathrm{eff}}[n](\mathbf{r}) \approx \alpha_{\mathrm{eff}}(n(\mathbf{r}),\boldsymbol{\nabla}n(\mathbf{r})) \tag{43}$$

Because the polarizability in these methods is also approximated as isotropic, the directional information in the density gradient is not used; this leads to the further simplification that only the norm of the density gradient enters the formulas: $\alpha_{\mathrm{eff}}[n](\mathbf{r}) \approx \alpha_{\mathrm{eff}}(n(\mathbf{r}),|\boldsymbol{\nabla}n(\mathbf{r})|)$. This leaves potential room for further improvement, as the density gradient in fact does contain information about the directionality of bonds, for example, and hence the differential response of the electron density parallel and perpendicular to them (see Figure 5 in Section 2 and the discussion there).

The density gradient is the key ingredient for a successful density-functional model of the local effective polarizability. Although early nonlocal functionals did not depend explicitly on the density gradient, even these approaches used this quantity to determine hard cutoffs for the spatial integrals in Eq. (42) when treating nonoverlapping fragments (Andersson et al., 1996). The usefulness of the gradient is apparent from the fact that the ratio of the density gradient to the density in the density tail region of an atom or a molecule determines their ionization potential. The ionization potential is approximately proportional to the average excitation energy in the Unsöld approximation, which is in turn inversely proportional to the polarizability, thus establishing the connection. The dependence on the density gradient enables $\alpha_{\mathrm{eff}}[n]$ to capture electron correlation effects in the neighborhood of a given point, similar to how GGA functionals achieve the same compared to LDA. From this analogy, a natural idea is to extend the current functionals for α_{eff} to depend on the kinetic energy density in the spirit of meta-GGA density functionals; such functionals have not been suggested so far.

The dependence of $\alpha_{\mathrm{eff}}(\mathbf{r},\mathrm{i}u)$ on the frequency in all nonlocal functionals is approximated with that of an infinitesimal

harmonic oscillator:

$$\alpha^{\mathrm{QHO}}(\mathrm{i}u) = \frac{q^2}{m(\omega^2+u^2)} = \frac{q}{\omega^2+u^2} \xrightarrow{q\to \mathrm{d}q} \frac{n(\mathbf{r})\mathrm{d}\mathbf{r}}{\omega[n](\mathbf{r})^2+u^2} = \alpha_{\mathrm{eff}}(\mathbf{r},\mathrm{i}u)\mathrm{d}\mathbf{r} \quad (44)$$

where $\mathrm{d}q = n\mathrm{d}\mathbf{r}$ and it is assumed that the ratio q/m corresponds to that of an electron, that is, it is equal to 1 (in atomic units). Here, the characteristic frequency ω corresponds to the plasma frequency, the frequency of the macroscopic oscillations in a homogeneous electron gas of the same density. Using this form for $\alpha_{\mathrm{eff}}[n]$, the correlation energy expression in Eq. (42) can be recast into the standard form for a nonlocal functional in Eq. (41) with the nonlocal kernel

$$\Phi(\mathbf{r},\mathbf{r}') = -\frac{3}{\pi}\int_0^\infty \mathrm{d}u \times \frac{1}{\omega[n](\mathbf{r})^2+u^2}\frac{1}{\omega[n](\mathbf{r}')^2+u^2}\frac{f[n](|\mathbf{r}-\mathbf{r}'|,u)^2}{|\mathbf{r}-\mathbf{r}'|^6} \quad (45)$$

where the differences between distinct nonlocal functionals reside in the specific functional forms of $\omega[n]$ and $f[n]$.

4.6.1 A simple nonlocal functional

Vydrov and van Voorhis designed a simple model for the local effective frequency $\omega[n]$ and the range-separating function $f[n]$, which together form the VV10 nonlocal functional. Here, we provide an alternative derivation of the VV10 nonlocal functional equivalent to the original one. In VV10, $\omega[n](\mathbf{r})$ is approximated with (Vydrov and Van Voorhis, 2010c)

$$\omega[n](\mathbf{r})^2 = \frac{4\pi}{3}n + C\left|\frac{\boldsymbol{\nabla} n}{n}\right|^4 \quad (46)$$

where C is an empirical parameter fitted to a reference set of C_6 coefficients. There are three distinct ideas used in this expression. First, the $4\pi n$ term is motivated by the homogeneous electron gas. Second, the factor $1/3$ comes from the Clausius–Mossotti equation and makes the expression exact for the limiting case of a jellium sphere in vacuum. Third, the gradient term is constructed as a local effective correction to the characteristic frequency due to the nonzero gap between occupied and unoccupied orbitals. In the density tails of atoms, the gradient term goes to a constant which smoothly damps the polarizability expression and avoids the need for hard cut-offs.

The specification of $\omega[n]$ already fully describes the asymptotic behavior of the functional, leaving out only the short-range behavior. The construction of the range-separating function f in VV10 is motivated by considering the overlap of the two oscillators at short distances, which effectively attenuates their mutual interaction. This is modeled with a second pair of oscillators in which ω depends on the distance between them and increases in such a way that they in fact never overlap. The damping mechanism can be then written as a range-separating function of the form

$$f(\mathbf{r},\mathbf{r}',u)^2 = \frac{\tilde{\alpha}_{\mathrm{eff}}(\mathbf{r},\mathrm{i}u,R)\tilde{\alpha}_{\mathrm{eff}}(\mathbf{r}',\mathrm{i}u,R)}{\alpha_{\mathrm{eff}}(\mathbf{r},\mathrm{i}u)\alpha_{\mathrm{eff}}(\mathbf{r}',\mathrm{i}u)} \quad (47)$$

where $\tilde{\alpha}_{\mathrm{eff}}(\mathbf{r},\mathrm{i}u,R)$ is the polarizability of an oscillator modified by the presence of the other oscillator at distance R. The R-dependent term in ω contains the second empirical parameter of VV10, b, which effectively controls the onset of the range separation. This parameter is fitted to reference interaction energies and is specific for each semi-local functional, with which the VV10 functional is combined (Hujo and Grimme, 2011). The two empirical parameters, C and b, control two distinct properties of VV10: C controls the local effective response and b controls the range separation. The VV10 nonlocal kernel was later slightly modified by Sabatini *et al* to enable efficient evaluation in a plane-wave basis (Sabatini et al., 2013). Two reparametrizations of VV10 targeted at binding in layered materials were presented by Björkman (Björkman, 2012, 2014).

4.6.2 vdW-DF functional

We start the discussion of the vdW-DF functional with the model it uses for $\omega[n]$:

$$\omega[n](\mathbf{r})^2 = 4\pi^2\epsilon_{\mathrm{xc}}[n]^4 \approx 4\pi^2\left(\epsilon_{\mathrm{xc}}^{\mathrm{LDA}}(n) + Z\left|\frac{\boldsymbol{\nabla} n}{n^{\frac{7}{6}}}\right|^2\right)^4 \quad (48)$$

where ϵ_{xc} is the exchange-correlation energy density and Z is a constant (not, b). The first equality is obtained by using $\omega[n]$ for a calculation of the total exchange-correlation energy of a slowly varying electron gas. In vdW-DF, ϵ_{xc} is then approximated with a GGA functional. The GGA functional is used here only for the parametrization of $\omega[n]$ and its choice is completely independent from the functional used for calculating the short-range exchange-correlation energy. Despite $\omega[n]$ in vdW-DF having a completely different form from that of VV10, both functionals feature a single parameter which controls the essential density gradient term. In vdW-DF, however, the value of this parameter is determined from first-principles arguments. We find it remarkable that the functional forms of $\omega[n]$ in vdW-DF and VV10 differ even in powers of n and $|\boldsymbol{\nabla} n|$, yet both functionals provide relatively accurate polarizabilities. This agreement might deteriorate for heavier elements, where the ratio of the density and the density gradient changes significantly compared to the lighter elements.

The range-separation mechanism in vdW-DF is more elaborate than in VV10, partly because it is constructed in reciprocal space. There are two distinct mechanisms that saturate the vdW-DF functional at short range. The first one is analogous to that in VV10: the local frequency ω is made to increase as q^2 for large q (short wavelengths), akin to ω increasing with R^{-2} in VV10. This leads to a contraction of the infinitesimal oscillators and a decrease of the local effective polarizability α_{eff}. The second mechanism comes from the requirement that the vdW-DF functional evaluates to zero for the homogeneous electron gas. This requirement forces the nonlocal kernel to positive values at short distances R when transformed back to real space. In VV10, this condition is trivially satisfied by an *a posteriori* addition of a constant energy term for a given number of electrons, wheras in vdW-DF, this requirement is built directly into the nonlocal kernel. As a result, the range-separating

function $f[n](|\mathbf{r}-\mathbf{r}'|,u)$ in vdW-DF has a complicated form and we do not present it here; however, this function still serves merely to damp the nonlocal functional at short range and goes to unity at long range.

The original vdW-DF functional used a particular value of the parameter Z that was derived earlier in the context of semi-local functionals. This choice provides relatively accurate polarizabilities when used in conjunction with the GGA functional for $\omega[n]$ in Eq. (48). By construction, Z controls not only $\omega[n]$ and hence the long-range asymptotic behavior, but also the onset of the short-range damping mechanism. This seemingly elegant property introduces complications when one wants to couple $E_{\rm lr}$ from vdW-DF with the short-range part $E_{\rm sr}$ from some semi-local density functional. Essentially, there is no way to adapt the range separation of vdW-DF without modifying its asymptotic behavior at the same time. Hence, instead of adapting a single parameter for a given semi-local functional as is done in VV10, vdW-DF (with Z fixed by enforcing the correct long-range behavior) requires some *a priori* unknown semi-local functional that would complement it in the short range. The original work suggests that the revised PBE (revPBE) functional (Zhang and Yang, 1998) is such a complement, but other alternatives were found later, as discussed in the next section. In any case, vdW-DF cannot be easily paired with a given density functional that might be the best choice for the short-range part of the electron correlation energy. Attempts at changing the value of Z were also made, but this in general leads to incorrect long-range behavior (Lee et al., 2010).

The vdW-DF functional was implemented self-consistently (Thonhauser et al., 2007; Vydrov et al., 2008; Gulans et al., 2009), which enables calculations of the electron density polarization stemming from vdW interactions. Román-Pérez and Soler used the fast Fourier transformation to efficiently evaluate the nonlocal functional in periodic systems (Román-Pérez and Soler, 2009), avoiding the otherwise costly evaluation of the double integral in Eq. (41).

4.6.3 Variations of vdW-DF

There are two popular ways to modify nonlocal density functionals: first, by changing the nonlocal functional itself, and second, by using a different semi-local or hybrid functional for the short-range part of the electron correlation energy. A simple modification of vdW-DF can be done by changing its single parameter Z, which controls the density gradient contribution to the local frequency $\omega[n]$. The value used in the original formulation (vdW-DF) predicts good C_6 coefficients and was combined with the semi-local revPBE functional. In the second version, vdW-DF2, Z is more than twice as large, leading to larger values of $\omega[n]$ and hence smaller polarizabilities and C_6 coefficients, which turn out to be severely underestimated. This is compensated at short range with a change of the underlying semi-local functional: here, PW86 (Perdew and Yue, 1986) was suggested as a good candidate. The combination of Z and the GGA functional used in vdW-DF2 gives more accurate results for the binding energies of small vdW complexes, where the short-range behavior dominates over the long range.

More significant modifications of vdW-DF were presented by Vydrov and van Voorhis. In vdW-DF-09, a different form for $\omega[n]$ was used as well as a slightly different range-separation mechanism (Vydrov and Van Voorhis, 2009a). This modification makes the damping independent of the magnitude of the gradient term in $\omega[n]$, in contrast to the original vdW-DF; this allows one to determine the short- and long-range behavior of the functional separately by fitting to reference binding energies and C_6 coefficients, respectively. This makes the nonlocal functional usable in conjunction with any semi-local or hybrid functional. The idea of having two distinct parameters in the nonlocal functional that control the short- and long-range behavior turned out to be decisive for achieving better accuracy. The follow-up to vdW-DF-09, called VV09, can be considered a transition between vdW-DF and VV10 (Vydrov and Van Voorhis, 2009b; Langreth and Lundqvist, 2010; Vydrov and Van Voorhis, 2010d). Whereas the damping mechanism was still constructed in reciprocal space as in vdW-DF, the functional form for $\omega[n]$ in VV09 was already the same as that used later in VV10.

Several attempts were made to find semi-local or hybrid density functionals that would be more compatible with vdW-DF than the original suggestion of revPBE (Murray et al., 2009). Cooper designed a new GGA exchange functional, termed C09, whose gradient behaviour interpolates between that of a simple gradient expansion of LDA to that of revPBE (Cooper, 2010). Pernal *et al*. devised a "dispersion-less" GGA functional by using the symmetry-adapted perturbation theory without the dispersion component as a reference (Pernal et al., 2009). A different approach to the same problem was suggested by Rajchel *et al*., in which electronic motion is treated by full DFT within interacting fragments, but the interfragment degrees of freedom are described by Coulomb and exchange terms, resulting in an effective dispersionless description ready to be supplemented by a vdW model (Rajchel et al., 2010). Klimeš *et al*. reparametrized the PBE and B88 (Becke, 1988b) functionals (termed optPBE and optB88) by fitting their parameters to reference binding energies of a set of small vdW complexes (Klimeš et al., 2010, 2011). These reparametrizations break some of the exact constraints used in the construction of PBE and B88 with unclear consequences. Wellendorf *et al*. used statistical methods, several reference sets, and a relatively general form of a GGA exchange functional to find an optimal short-range complement to vdW-DF2, called BEEF (Wellendorff et al., 2012). They found that the optimal exchange functional significantly depends on the particular system under study. As the original vdW-DF functional has better long-range behaviour than vdW-DF2, better results might have been obtained if BEEF used vdW-DF. Hamada reparametrized B86b (Becke, 1986) to better suit vdW-DF2 (Hamada, 2014), while Berland and Hyldgaard devised a new exchange functional that interpolates between the Langreth–Vosko functional and revised PW86, and combined it with vdW-DF (Berland and Hyldgaard, 2014). Several authors identified that vdW-DF is not compatible with exact exchange and the use of hybrid functionals leads to considerable overbinding when coupled with the vdW-DF family.

4.7 Fragment-based pairwise methods

The simplest pairwise models of vdW interactions are constructed using the following formula,

$$E_{\mathrm{c}} = -\frac{1}{2}\sum_{AB} C_{6,AB}\frac{g(|\mathbf{R}_A - \mathbf{R}_B|)}{|\mathbf{R}_A - \mathbf{R}_B|^6} \tag{49}$$

where the sum is over pairs of fragments A and B (*e.g.*, atoms), $\mathbf{R}_A$ is the position of fragment A, g is some short-range damping function, and the C_6 coefficient was defined via the Casimir–Polder integral in Eq. (27). We use the term "fragment" when referring to A and B to cover all vdW methods; the fragments are atoms in most cases, but not in all.

The R^{-6} potential, which describes the asymptotic attraction between two fragments at distance R, was derived for the first time from quantum mechanics by Wang in 1927 (Wang, 1927) for the case of two hydrogen atoms and later generalized by London (London, 1930; Eisenschitz and London, 1930; London, 1937). This potential served as a basis for vdW corrections to theories ranging from the HF mean-field approximation (Hepburn et al., 1975), to the Lennard–Jones potential, to semi-empirical quantum-chemical methods, long before having been used in DFT (Wu and Yang, 2002; Elstner et al., 2001; Zimmerli et al., 2004). . In 2004, Grimme popularized this approach in DFT by illustrating that even a simple empirical scheme of this kind improves the performance of standard semi-local exchange-correlation functionals for vdW-bound systems (Grimme, 2004). This was then followed by the development of several models for C_6 coefficients that explicitly take into account the electronic structure of a given molecule or material, which are discussed here.

Eq. (49) is a nontrivial generalization of the textbook R^{-6} potential between a single pair of fragments to a pairwise sum. In this section, we show which approximations to the expression for $E_{\mathrm{c,lr}}$ in Eq. (23) lead to this pairwise sum and then present an overview of several particular pairwise models.

4.7.1 Fragment-based pairwise models from the ACFD formula

Like the nonlocal functionals, the pairwise methods use a second-order truncation of $E_{\mathrm{c,lr}}$ and an isotropic local effective model for the short-range polarizability. Unlike the nonlocal functionals, however, these methods also use coarse-graining of the spatial quantities: α_{eff}, $\mathbf{T}_{\mathrm{lr}}$, and the damping function g. It then follows that the pairwise formula in Eq. (49) is obtained from the second-order long-range correlation energy in Eq. (27) by using the coarse-graining presented in Section 4.4.1:

$$\begin{aligned} E_{\mathrm{c}}^{(2)} &= -\frac{1}{2}\iint \mathrm{d}\mathbf{r}\mathrm{d}\mathbf{r}' C_6(\mathbf{r},\mathbf{r}')\frac{f(|\mathbf{r}-\mathbf{r}'|)^2}{|\mathbf{r}-\mathbf{r}'|^6} \\ &= -\frac{1}{2}\sum_{AB}\iint \mathrm{d}\mathbf{r}\mathrm{d}\mathbf{r}' C_6(\mathbf{r},\mathbf{r}')\frac{f(|\mathbf{r}-\mathbf{r}'|)^2}{|\mathbf{r}-\mathbf{r}'|^6} w_A(\mathbf{r}) w_B(\mathbf{r}') \\ &\approx -\frac{1}{2}\sum_{AB} C_{6,AB}\frac{f(|\mathbf{R}_A-\mathbf{R}_B|)^2}{|\mathbf{R}_A-\mathbf{R}_B|^6} \end{aligned} \tag{50}$$

This formula is identical to Eq. (49) after identifying $f^2 \equiv g$ and $C_{6,AB} = \iint \mathrm{d}\mathbf{r}\mathrm{d}\mathbf{r}' C_6(\mathbf{r},\mathbf{r}') w_A(\mathbf{r}) w_B(\mathbf{r}')$. Formally, this expression could be obtained by replacing the double spatial integral in the nonlocal functional formula (in Eq. (41)) with a double sum over pairs of fragments. In this view, the role of the model for the local frequency ω in nonlocal functionals is played by the models for the C_6 coefficients in pairwise methods, and the square of the range-separating function f corresponds to the damping function g.

As discussed in Section 4.4.1, the coarse-graining is equivalent to considering only the (lowest) dipole–dipole term from the multipole expansion of the polarizability $\alpha_{\mathrm{eff}}(\mathbf{r})w_A(\mathbf{r})$ and the coupling potential $\mathbf{T}(\mathbf{r},\mathbf{r}')$. In pairwise schemes, including the higher multipole terms is straightforward and leads to the well-known series starting with C_8/R^8 and C_{10}/R^{10}. We have also argued that these higher-order contributions can be at least partially captured in the empiricism of the damping function. This is further supported by the existence of simple approximate recursive formulas for the higher-order C_n coefficients based on the C_6 coefficients and various integral moments of the fragment densities (Starkschall and Gordon, 1972; Thakkar, 1988).

The accuracy and reliability of a given pairwise method is influenced both by the particular model for C_6 coefficients and the choice of the damping function g. The quality of these two components can be evaluated separately, because only the C_6 coefficients determine the asymptotic behaviour. Such a distinction is useful, because the C_6 coefficients and damping function g influence the performance of a method in different ways. For one, the relative importance of C_6 and g for the resulting vdW energies changes with system size. The C_6 coefficients become more important in larger molecular or crystal systems, whereas the damping function plays a substantial role in small vdW complexes.

Another difference comes from the fact that the models for C_6 coefficients discussed here are typically based on some underlying first-principles arguments and assumptions, whereas the damping functions are mostly empirical. For the most part, this is caused by the lack of general knowledge about the behavior of the short-range part of the electron correlation energy as described by the underlying exchange-correlation density functionals in the range of typical vdW equilibrium distances. Furthermore, all other noncovalent interactions (electrostatics, induction, Pauli repulsion) also in general contribute to the binding energies in this regime. When damping functions are fitted to reference binding energies, which is a common technique, any errors in the non-vdW part of the energies propagate into the fitted parameters, making the resulting vdW model less transferable. This complicates the discussion of the vdW methods separate from the underlying functionals. We note that this issue is in fact common to all methods that use a density-functional approximation for the short-range correlation energy, including the range-separated RPA methods, nonlocal functionals, as well as the many-body dispersion framework that will be discussed in the next section.

4.7.2 Models for C_6 dispersion coefficients and other vdW parameters

Although we set out to cover strictly vdW methods that explicitly take into account the electronic structure of a system, we open this section with a particular family of methods that do not leverage any information about a molecule or a solid besides its geometry. The DFT-D1 (Grimme, 2004), DFT-D2 (Grimme, 2006), and DFT-D3 (Grimme et al., 2010) methods largely popularized the approach of correcting DFT calculations for vdW interactions, providing a context for further development of less empirical models that use electronic structure as an input. As discussed in Section 2, the spectrum of behaviours of vdW interactions in real materials is vast, reflecting the intricacies of electronic structure theory, and an effort to capture all this complexity purely from geometry is a formidable task, akin to classical force fields attempting to calculate electronic energy without explicitly considering electrons. This is reflected in more elaborate constructions of the DFT-D*n* methods with increasing *n*, as they tried to cover wider array of systems.

DFT-D1 used fixed atomic C_6 coefficients that did not depend on any molecular environment. The heteronuclear coefficients were calculated using an expression that is equivalent to Eq. (32) with polarizabilities of all atoms considered equal. The damping function was constructed using vdW radii in such a way that it did not go to unity for $R \to \infty$, leading to incorrect asymptotic behaviour. DFT-D2 followed the same protocol (with some numerical reparametrizations) except for the C_6 combination rule, which used an expression equivalent to Eq. (32) with $\alpha_{0,A}/\alpha_{0,B} = \sqrt{C_{6,AA}/C_{6,BB}}$, arguably a more reasonable model than in DFT-D1. DFT-D3 introduced several changes. First, the damping was modified to satisfy the expected asymptotic behaviour ($f(R) \to 1$ for $R \to \infty$). Second, fixed C_6 coefficients were estimated from reference hydride dimers by approximate decomposition of their long-range interaction into contributions from the corresponding heavy atoms and the hydrogen atoms. Third, the vdW radii were replaced with atomic radii calculated as a distance at which an interaction energy between the corresponding atoms calculated in a certain special way (Grimme et al., 2010) equals an arbitrary threshold. Fourth, an elementary dependence of the C_6 coefficients on the environment was included via empirical geometrical factors that estimate a coordination number of the atoms. The reference C_6 coefficients are then interpolated for a given estimated coordination number in a complicated but arbitrary way motivated by numerical results. However, the true dependence of the electronic structure on geometry is still much more complex than what this comparably simple geometrical interpolation captures, leading to unphysical bumps in the potential energy surface of many molecular systems besides simple organic compounds. Apart from these changes, C_8 coefficients were added to the model as a fixed part, and three-atom C_9 coefficients and the corresponding 3-atom potential as an optional part, which seems to improve the accuracy of DFT-D3 for large molecular systems, but worsens it for smaller systems, without a clear consensus of the crossover regime. In general, it is the absence of the dependence of C_6 coefficients on the environment in DFT-D1/2 and the difficulty with which it was modeled based purely on geometry in DFT-D3, which motivated development of methods based on electronic-structure information, described in the following.

Becke and Johnson devised a model for treating vdW interactions based on the dipole moment of the exchange hole, termed XDM. In a series of papers, they used this quantity to construct a heuristic model for the C_6 coefficients of isolated atoms and molecules (Becke and Johnson, 2005b). Later, the model was generalized to the case of atoms in molecules with the use of a partitioning scheme devised by Hirshfeld (Hirshfeld, 1977). In this scheme, a reference set of free-atom densities is used to construct the following stockholder model for the partition functions w_A,

$$w_A^{\mathrm{Hirsh}}(\mathbf{r}) = \frac{n_A^{\mathrm{free}}(|\mathbf{r}-\mathbf{R}_A|)}{\sum_B n_B^{\mathrm{free}}(|\mathbf{r}-\mathbf{R}_B|)} \tag{51}$$

where $n_A^{\mathrm{free}}(r)$ is the (radially-averaged) density of the atom A *in vacuo* (*i.e.*, a free atom) at a distance r from the nucleus and $0 < w_A^{\mathrm{Hirsh}}(\mathbf{r}) \leq 1$ at each point in space by construction. (The Hirshfeld-partitioned density of an atom A is then given by $n_A(\mathbf{r}) = n(\mathbf{r}) w_A^{\mathrm{Hirsh}}(\mathbf{r})$.) The partitioned atomic C_6 coefficients were then combined with a damping function to formulate a full vdW model in ref (Johnson and Becke, 2005). The approach was also extended to include higher-order C_n coefficients and modified so that the dependence on the static molecular polarizability as an external input was removed (Becke and Johnson, 2006). Finally, all of these incremental improvements were combined into a single general pairwise method for vdW interactions in ref (Johnson and Becke, 2006).

The dipole moment of the exchange hole used by the XDM model is calculated from occupied KS orbitals (Ángyán, 2007; **?**; Heßelmann, 2009). The exchange hole represents the electron density that is pushed away from an electron due to the Pauli exclusion principle. The combined charge of the exchange hole and the reference electron is always zero, but it possesses a nonzero dipole polarization density, $\mathbf{P}_{\mathrm{x}}(\mathbf{r})$, which was argued to correspond to instantaneous quantum-mechanical charge fluctuations. The C_6 coefficients are thus obtained from the square of the dipole moment of the exchange-hole polarization as

$$C_6 = \frac{1}{2}\alpha_{\mathrm{pt}}(0) \int \mathrm{d}\mathbf{r} |\mathbf{P}_{\mathrm{x}}(\mathbf{r})|^2 \tag{52}$$

where $\alpha_{\mathrm{pt}}(0)$ is an isotropic static point polarizability of the given atom or molecule.

(For an alternative density-functional explanation for vdW interactions based on the correlation hole, see (Alonso and Mañanes, 2007).) To obtain the atomic C_6 coefficients, the integral above can be coarse-grained with the Hirshfeld partitioning,

$$C_{6,AA} = \frac{1}{2}\alpha_{\mathrm{eff},A}(0) \int \mathrm{d}\mathbf{r} |\mathbf{P}_{\mathrm{x}}(\mathbf{r})|^2 w_A^{\mathrm{Hirsh}}(\mathbf{r}) \tag{53}$$

where the static atomic polarizabilities $\alpha_{\mathrm{eff},A}(0)$ are obtained by scaling the reference free-atom polarizabilities (Chu and

Dalgarno, 2004) via

$$\alpha_{\mathrm{eff},A}(0) = \alpha_A^{\mathrm{free}}(0)\frac{\int \mathrm{d}\mathbf{r} n(\mathbf{r}) w_A(\mathbf{r})|\mathbf{r}-\mathbf{R}_A|^3}{\int \mathrm{d}\mathbf{r} n_A^{\mathrm{free}}(\mathbf{r})|\mathbf{r}-\mathbf{R}_A|^3} \equiv \alpha_A^{\mathrm{free}}(0)\frac{V_{\mathrm{eff}}[n]}{V_{\mathrm{free}}} \tag{54}$$

The integrated quantities V_{eff} and V_{free} in the numerator and denominator are measures of the "volume" of the atom in a molecule and the free atom, respectively—quantities that correlate with atomic polarizabilities (Brinck et al., 1993). To get C_6 coefficients between different atoms, XDM uses the combination rule derived in Eq. (32) for two harmonic oscillators. Similar expressions can be used to calculate higher-order C_n coefficients from the higher multipole moments of the exchange-hole polarization density, $\mathbf{P}_{\mathrm{x}}$. The XDM model can be also used together with density functional approximations for the exchange hole (Becke and Roussel, 1989; Steinmann and Corminboeuf, 2011a), which removes the dependence on the occupied KS orbitals (Becke and Johnson, 2005a). The triple-dipole ATM-like term can be obtained from the exchange-hole dipole model as well (Otero-de-la-Roza and Johnson, 2013).

Two distinct damping functions were suggested for XDM (Becke and Johnson, 2005a; Johnson and Becke, 2006). The first one uses an approach based on correlation energy ratios,

$$g_{AB}^{\mathrm{XDM1}}(R) = \left(1 + c\left(\frac{C_{6,AB}/R^6}{E_{\mathrm{c},A}^{\mathrm{free}} + E_{\mathrm{c},B}^{\mathrm{free}}}\right)\right)^{-1} \tag{55}$$

where $E_{\mathrm{c},A}$ is the correlation energy of a free atom and c is a fitted empirical parameter. The second suggested damping function follows a more common approach, which is based on a ratio of length scales,

$$g_{AB}^{\mathrm{XDM2}}(R) = \left(1 + c_1\left(\frac{R_A^{\mathrm{vdW}} + R_B^{\mathrm{vdW}} + c_2}{R}\right)^6\right)^{-1} \tag{56}$$

where R_A^{vdW} is a vdW radius for atom A and c_1, c_2 are empirical constants.

Tkatchenko and Scheffler (TS) devised a pairwise method for vdW interactions in which the free-atom scaling approach is extended to all relevant vdW parameters, that is, the atomic polarizabilities, C_6 coefficients, and radii (Tkatchenko and Scheffler, 2009), hence making them all functionals of the electron density

$$\alpha_{\mathrm{eff},A}(0) = \alpha_A^{\mathrm{free}}(0)\frac{V_{\mathrm{eff}}[n]}{V_{\mathrm{free}}}, \quad C_{6,AA} = C_{6,AA}^{\mathrm{free}}\left(\frac{V_{\mathrm{eff}}[n]}{V_{\mathrm{free}}}\right)^2 \quad R_{\mathrm{vdW},A} = R_{\mathrm{vdW},A}^{\mathrm{free}}\left(\frac{V_{\mathrm{eff}}[n]}{V_{\mathrm{free}}}\right)^{\frac{1}{3}} \tag{57}$$

The TS approach effectively describes a larger portion of the short-range correlation effects based on accurate free-atom values, whereas the XDM model tries to recover them from the properties of the exchange hole. The strategy of using free-atom reference values could also be viewed as constructing the polarizability model in such a way that it satisfies the exactly known (free-atom) limits, an approach that has been successfully used for exchange-correlation density functionals, where it is known as satisfying exact norms. In the case of density functionals for polarizability, this normalization was so far used only in the atomic models ($\boldsymbol{\alpha}_{\mathrm{eff},A}$)—properly normed point functionals, $\boldsymbol{\alpha}_{\mathrm{eff}}(\mathbf{r})$, are yet to be developed. Finally, the TS model for the C_6 coefficients is combined with a logistic damping function,

$$g_{AB}^{\mathrm{TS}}(R) = \left(1 + \exp\left[-c_1\left(c_2\frac{R}{R_A^{\mathrm{vdW}} + R_B^{\mathrm{vdW}}} - 1\right)\right]\right)^{-1} \tag{58}$$

The TS method can be straightforwardly combined with a wide range of semi-local and hybrid functionals by adjusting a single range-separation parameter (Marom et al., 2011). The value of the range-separation parameter is close to 1 when TS is coupled with the nonempirical PBE, PBE0, or HSE functional. Values slightly larger are obtained for meta-GGA functionals (**?**Peverati and Truhlar, 2011; Sun et al., 2016), which confirms that these functionals can effectively describe electron correlation at intermediate interatomic distances.

In larger molecules and solids, many-body and screening effects become important, which motivated several improvements to the original TS approach. Bučko *et al.* applied electrodynamic screening from Eq. (18) to the atomic C_6 coefficients, leading to improvements in the description of layered materials (Bučko et al., 2013b). Zhang *et al.* and Ruiz *et al.* (Zhang et al., 2011b; Ruiz et al., 2012) used the dielectric function of bulk materials to define atomic polarizabilities in solids as an alternative to the free-atom reference data used in Eq. (57). Such renormalized bulk reference parameters can be used to investigate cohesion in solids (Zhang et al., 2011b; Liu et al., 2013) and adsorption of molecules on surfaces (Ruiz et al., 2012; Carrasco et al., 2014; Liu et al., 2014; Ruiz et al., 2016). Furthermore, the TS approach was also extended from DFT (Tkatchenko and Scheffler, 2009) to the density-functional tight-binding (DFTB) method (Stöhr et al., 2016), as well as classical force fields (Bereau and von Lilienfeld, 2014; Cole et al., 2016).

Sato and Nakai developed an atomic pairwise method that can be considered a direct bridge to the class of nonlocal functionals, by directly expanding an ALL-like density functional into a multipole series around the atomic centers (Sato and Nakai, 2009, 2010). They used the general formula for the dynamic polarizability of an infinitesimal harmonic oscillator in Eq. (44) (Dobson and Dinte, 1996), combined with the characteristic excitation frequency from the vdW-DF-09 nonlocal functional of Vydrov and van Voorhis (Vydrov and Van Voorhis, 2009a),

$$\omega[n](\mathbf{r})^2 = \frac{1}{9}(3\pi^2 n)^{\frac{4}{3}}\left(1 + \lambda\frac{1}{4(3\pi^2)^{\frac{2}{3}}}\left|\frac{\boldsymbol{\nabla} n}{n^{\frac{4}{3}}}\right|^2\right)^4 \tag{59}$$

where λ is an empirical parameter to be fitted to a set of C_6 coefficients. This formula shows yet another density functional for the effective local frequency which was the main topic in

the section about nonlocal functionals. A molecular system described by this local effective polarizability is then partitioned into atomic fragments by means of the Becke scheme (Becke, 1988a), which is otherwise often used in DFT calculations to construct real-space integration grids, but serves here as an alternative to the Hirshfeld partitioning used by the XDM and TS methods. By assuming that the contribution to the polarizability from areas of significant atomic density overlaps is small, one obtains a complete representation of $\alpha_{\text{eff}}(\mathbf{r})$ in terms of the effective atomic dipole polarizabilities $\alpha_{\text{eff},A}$ and higher moments. This then leads directly to C_6, C_8, and higher-order coefficients via the Casimir–Polder integral (the series is truncated after C_{10} in practice). This method, named local response dispersion (LRD), is then combined with the following damping function (shown here only for the C_6 coefficients)

$$g_{AB}^{\text{LRD}}(R) = \exp\left(-\left(\frac{R}{c_1\left(\sqrt[3]{\alpha_{\text{eff},A}}+\sqrt[3]{\alpha_{\text{eff},B}}\right)+c_2}\right)^6\right) \quad (60)$$

where c_1, c_2 are parameters to be determined for each underlying density functional by fitting to a set of accurate interaction energies, and the atomic polarizabilities serve here as measures of atomic radii. We note that essentially any nonlocal density functional for vdW interactions could be turned into a fragment-based pairwise method by the same multipole-expansion technique used in LRD. A related approach to LRD was presented by Heßelmann (Heßelmann, 2012), in which the polarizability model is replaced by a more rigorous form obtained by directly approximating the expression for an uncoupled response function.

Silvestrelli formulated a pairwise method, named vdW-WF (Silvestrelli, 2008), where the interacting fragments are not atoms, but maximally-localized Wannier functions (MLWFs) (Marzari et al., 2012). MLWFs are essentially a generalization of localized Boys molecular orbitals to periodic systems; as such, they are the counterparts to the periodically symmetrized Bloch functions, which are by definition fully delocalized. The vdW-WF model is constructed by approximating each occupied MLWF with a single Slater-type s-function of the same spread S (spatial extent). Here, the assumption of an exponential decay of the MLWF is appropriate in systems with a nonzero gap, while the omission of any angular structure is in general an approximation. Given an approximate s-orbital, its dynamic polarizability is then calculated using the ALL polarizability functional (Andersson et al., 1996), where the density gradient (of the approximate s-orbital) enters via the definition of a MLWF-specific integration domain Ω_A for the following spatial integral,

$$\alpha_{\text{eff},A}(\mathrm{i}u) = \int_{\mathbf{r}\in\Omega_A} \mathrm{d}\mathbf{r}\, \frac{n_A(\mathbf{r})}{4\pi n_A(\mathbf{r})+u^2}, \quad (61)$$

with

$$\Omega_A = \{\mathbf{r} : |\nabla n_A(\mathbf{r})| < k n_A(\mathbf{r})^{\frac{7}{6}}\} \quad (62)$$

where $n_A(\mathbf{r})$ is the electron density of the MLWF A as approximated by the square of the corresponding s-function and k is a non-empirical constant. The C_6 coefficients are then directly obtained via the Casimir–Polder integral and the damping function used in vdW-WF is the same as in the TS model with the following modification. The atomic vdW radii in g^{TS} in Eq. (58) are replaced by distances from the centers of the MLWFs at which $n_A(\mathbf{r})$ falls below a predetermined threshold; the choice for this distance was the subject of a later modification (Silvestrelli et al., 2009). The MLWF partitioning used in vdW-WF significantly differs from the atomic partitioning used in the XDM and TS models. Given that the ALL polarizability functional is nonlinear in the input density ($\alpha^{\text{ALL}}[n_1+n_2] \neq \alpha^{\text{ALL}}[n_1]+\alpha^{\text{ALL}}[n_2]$), using it with the individual fragment densities as the input constitutes a different scheme than evaluating the functional integrand with the total density and then partitioning the integral according to the MLWF fragments. Furthermore, the use of the approximate s-functions for the MLWFs results in a partitioning of the total density that is not exact, that is, $\sum_A n_A(\mathbf{r}) \neq n(\mathbf{r})$.

Tao *et al*. developed a density functional for the point dynamic polarizability (and hence the C_6 coefficient), which uses the static polarizability as an input (Tao et al., 2010),

$$\alpha_{\text{pt}}(\mathrm{i}u) = a^3 \int_{\mathbf{r}\in\Omega} \mathrm{d}\mathbf{r}\, \frac{n}{\frac{4\pi}{3}a^4 n + u^2}, \quad \Omega = \{\mathbf{r} : |\mathbf{r}|^3 < a\alpha(0)\} \quad (63)$$

where Ω is an integration domain, and a is a constant determined by satisfying the exact high-frequency limit of $\alpha_{\text{pt}}(\mathrm{i}u)$ and the limiting case of a classical metallic sphere (consisting of a uniform electron density). The choice of the integration domain in this functional guarantees that the input static polarizability $\alpha(0)$ is recovered for $u = 0$. This model was later extended to describe higher-multipole coefficients as well (Tao et al., 2012). In the context of general vdW methods, this model is not fully complete, as the C_6 coefficient model is not combined with a damping function, and still requires a prescription for the input static polarizability. However, such a generalization could be obtained in a straightforward manner, for example with the approach used in the XDM or TS methods, and hence we chose to present this model to illustrate the flexibility with which density-functional models for the local effective polarizability can be constructed.

Besides developing new functionals for the C_6 coefficients, novel pairwise methods can be constructed by using alternative partitioning schemes. For instance, Steinmann and Corminboeuf adapted the XDM model by using the self-consistent Hirshfeld partitioning scheme (Steinmann and Corminboeuf, 2010, 2011b), which provides a more robust description of ionic systems than the original Hirshfeld partitioning (Bultinck et al., 2007). Similarly, Bučko *et al*. introduced this scheme into the TS model (Bučko et al., 2013a, 2014), and demonstrated that it substantially improves the performance of DFA+TS for systems with strong local charge transfer. In these modified Hirshfeld schemes, the original free-atom reference densities n_A^{free} are modified into generalized reference densities $n_{0,A}$, which themselves depend on the partitioned fragment densities n_A. This makes Eq. (51) a self-consistent equation that needs to be solved in an iterative fashion. Several suggestions were made for the construction of $n_{0,A}$ in terms of the fragment densities

n_A (Verstraelen et al., 2012). The most common approach, used in the modified XDM and TS methods, is to consider $n_{0,A}$ as a linear combination of the free-atom and free-ion reference densities for a given species, where the coefficients are determined in such a way that the charges of the Hirshfeld density n_A and the reference density $n_{0,A}$ are equivalent.

4.8 Many-body dispersion framework

So far, we covered three of the four classes of methods which arise from the independent use of the second-order truncating and coarse-graining approximations. In this section, we conclude this overview by discussing the recent many-body dispersion (MBD) framework, which represents a class of nontruncated (akin to the RPA-based methods) and coarse-grained (akin to the fragment-based methods) approximations. The central idea of the MBD model is the approximation of the dynamic response of a molecule or a material by that of a fully coupled system of QHOs, where each oscillator corresponds to some fragment of the system of interest. Apart from the response properties of the QHO model discussed above, the motivation for this approach comes from the fact that the correlation energy of such a system can be evaluated exactly by diagonalizing the corresponding Hamiltonian, which is given by

$$H_{\mathrm{MBD}} = -\frac{1}{2}\sum_A \nabla^2_{\xi_A} + \frac{1}{2}\sum_A \omega_A^2 \xi_A^2 + \frac{1}{2}\sum_{AB} \omega_A \omega_B \sqrt{\alpha_A(0)\alpha_B(0)}\,\boldsymbol{\xi}_A \mathbf{T}_{AB} \boldsymbol{\xi}_B \quad (64)$$

where $\boldsymbol{\xi}_A = \sqrt{m_A}(\mathbf{r}_A - \mathbf{R}_A)$ is the mass-weighted displacement of the oscillator A from its equilibrium position $\mathbf{R}_A$ (*i.e.*, the fragment center), ω_A is the characteristic frequency of the QHO, and $\alpha_A(0)$ is its static polarizability. The first two terms in this Hamiltonian represent the kinetic and potential energy terms, respectively, while the third term corresponds to the inter-oscillator coupling. In the context of vdW interactions, this model Hamiltonian was first introduced by Bade (Bade, 1957; Bade and Kirkwood, 1957) in 1957 and used later by Mahan (Mahan, 1965), Lucas (Lucas, 1967), Renne and Nijboer (Renne and Nijboer, 1967), and Donchev (Donchev, 2006) in the investigation of various qualitative aspects of long-range interactions between particles. In recent years, a renewed interest in this approach was initiated by the introduction of a general scheme for parametrizing and range-separating this Hamiltonian to obtain a universal and quantitative model for treating the energetic (Tkatchenko et al., 2012; Ambrosetti et al., 2014b) and structural (Blood-Forsythe et al., 2016) effects of vdW interactions in molecules and materials. In this section, we briefly review how the MBD Hamiltonian emerges from the long-range correlation energy expression in Eq. (23), discuss several properties of this approach in the context of other vdW methods, and finally describe the range-separated MBD method in particular. We note that the term "MBD" may refer to the general framework (Section 4.8.1) as well as a specific *method* within this framework (Section 4.8.2).

4.8.1 Many-body dispersion framework from the ACFD formula

The starting point for obtaining the MBD Hamiltonian as a model for electron correlation is the coarse-grained version of the exact expression for the long-range correlation energy in Eq. (37). In addition to the coarse-graining, MBD also approximates the short-range polarizability in that formula by a local effective polarizability, which leads to the following expression:

$$E_{\mathrm{c}}^{\mathrm{MBD}} = -\sum_{n=2}^{\infty} \frac{(-1)^n}{n} \int_0^\infty \frac{\mathrm{d}u}{2\pi} \sum_{AB} \mathrm{Tr}\left[\left[\!\left[\left(\boldsymbol{\alpha}_{\mathrm{eff}} \mathbf{T}_{\mathrm{lr}}\right)^n \right]\!\right]_{AB} (\mathrm{i}u) \right] \quad (65)$$

Although the local approximation to $\boldsymbol{\alpha}_{\mathrm{sr}}(\mathbf{r}, \mathbf{r}')$ in the MBD framework is shared with both the nonlocal functionals and pairwise methods, it is in general not required here that $\boldsymbol{\alpha}_{\mathrm{eff}}(\mathbf{r})$ be isotropic. We note that here, the long-range correlation energy is expanded into an infinite series, and such an expansion could be converted to the class of pairwise methods discussed in the previous section if truncated at second order. To proceed further, the dynamic polarizability $\boldsymbol{\alpha}_{\mathrm{eff}}(\mathrm{i}u)$ is approximated by the corresponding expression for a QHO in Eq. (28). This set of approximations then enables one to perform the integration in the frequency domain in Eq. (65) analytically (Tkatchenko et al., 2013), leading to the so-called plasmon-pole formula for the correlation energy,

$$E_{\mathrm{c}} = \frac{1}{2}\sum_{p=1}^{3N} (\overline{\omega}_p - \omega_p) \quad (66)$$

where N is the number of fragments (depending on the system and the choice of partitioning), the sum is over all $3N$ characteristic frequencies of the system, $\overline{\omega}_p$ are the frequencies of the fully interacting system (corresponding to $\boldsymbol{\alpha}_1$), and ω_p are the frequencies of the noninteracting system (corresponding to $\boldsymbol{\alpha}_0$).

The plasmon-pole formulation of the correlation energy is a general approach that can be used for many nontruncated approximations to the ACFD formula, in particular the class of RPA-based methods discussed in Section 4.5. In this expression, the analytical integration in the frequency domain is essentially performed by transforming the integral over imaginary frequencies iu to the imaginary part of the integral over real-valued frequencies u. In the latter form of the integral, $\boldsymbol{\alpha}_{\mathrm{eff},A}(u)$ directly describes the absorption spectrum of a system which is characterized by delta functions located at the excitation frequencies for both the interacting and noninteracting cases. Therefore the integral over real-valued frequencies is reduced to a sum of the excitation frequency differences in Eq. (66) above. It can also be shown that the plasmon-pole expression can be obtained as a difference between the ground state energy of a system of coupled QHOs and the ground state energy of a system of uncoupled QHOs, thereby establishing the equivalence between the plasmon-pole formulation and the Hamiltonian formulation in Eq. (64) (Tkatchenko et al., 2013). In other words, whereas the plasmon-pole expression is only an approximation to the exact correlation energy of the full

electronic system, it is in fact exact for the correlation energy of a system of QHOs coupled within the dipole approximation.

The Hamiltonian formulation of the long-range correlation energy gives a useful insight into the nature of vdW interactions. In the noninteracting limit ($\lambda = 0$), the charge fluctuations are fully localized on the individual fragments; as λ is increased towards the interacting limit ($\lambda = 1$), these localized fluctuations couple to form plasmon-like delocalized charge oscillations. These delocalized fluctuations have lower characteristic frequencies on average than their localized counterparts, and hence the coupling decreases (stabilizes) the total energy of the system.

4.8.2 Range-separated many-body dispersion method

At first, Tkatchenko *et al*. developed a MBD method based on fully screened atomic polarizabilities (Tkatchenko et al., 2012), which lead to a double counting of the long-range correlation effects in some cases. Later, this was avoided by using a range-separating approach, in which the atomic polarizabilities are screened by the surrounding atoms only at short range (Ambrosetti et al., 2014b). Here, we describe only the latter approach, termed MBD@rsSCS, where "rsSCS" stands for range-separated self-consistent screening. To define a particular method within the MBD framework, one needs to specify the partitioning scheme, the models for the static polarizabilities $\boldsymbol{\alpha}_{\mathrm{eff},A}(0)$ and the noninteracting characteristic frequencies ω_A, and the range-separating function $f(R)$ which defines $\mathbf{T}_{\mathrm{lr}}$. The MBD@rsSCS method partitions the electronic system into atomic fragments by means of the Hirshfeld scheme, which is also used in the XDM and TS pairwise methods. The effective atomic polarizabilities $\boldsymbol{\alpha}_{\mathrm{eff},A}(0)$ are then obtained in a two-step manner. First, the volume-scaling approach of the TS method is applied to the reference free-atom polarizabilities, while the characteristic frequencies are kept unchanged. Second, the Dyson screening in Eq. (18) with only the short-range part of the dipole potential is applied to the atomic dynamic polarizabilities, which produces the short-range nonlocal polarizability $\boldsymbol{\alpha}_{\mathrm{sr},AB}(iu)$. The range separation used in this second step is the same that is later used to define $\mathbf{T}_{\mathrm{lr}}$, which is used to obtain the long-range correlation energy. In this regard, the short-range response and the long-range coupling are constructed consistently in the MBD@rsSCS method.

To obtain the local effective dynamic polarizabilities of the atomic fragments, $\boldsymbol{\alpha}_{\mathrm{sr},AB}(u)$ is then summed along one fragment coordinate, $\boldsymbol{\alpha}_{\mathrm{eff},A} = \sum_B \boldsymbol{\alpha}_{\mathrm{sr},AB}$, which is equivalent to Eq. (25) for the coarse-grained case when the neighborhood is taken to be the entire system. Finally, the fragment polarizabilities are spherically averaged, and in this regard, the MBD@rsSCS scheme does not use the full flexibility of the MBD framework, which in general supports anisotropic local effective polarizabilities. To fully specify MBD@rsSCS, the range-separating function $f(R)$ is of the same type as the damping function in Eq. (58) used in the TS method, and is parametrized on a reference set of small- and medium-sized vdW complexes at various binding distances. The range-separating functions $f(R)$ used to define $\mathbf{T}_{\mathrm{lr}}$ are in general much smoother than the damping functions $g(R)$ of the pairwise methods, as the latter are in fact the square of the corresponding $f(R)$. With all relevant quantities determined, the MBD@rsSCS long-range correlation energy is then obtained by diagonalizing the general MBD Hamiltonian in Eq. (64) and evaluating the plasmon-pole formula in Eq. (66). Bučko *et al*. derived and implemented a formulation of MBD@rsSCS for periodic boundary conditions in reciprocal space, which results in faster and more easily converged calculations (Bučko et al., 2016).

4.8.3 General remarks about MBD and n-body expansions

As briefly discussed in Section 4.4.2, the infinite n-th order expansion of the long-range correlation energy in the MBD framework is not equivalent to the general (and finite) n-body expansion, where the latter is often used to discuss beyond-pairwise corrections to the pairwise methods. Here, we discuss the correspondence between various higher-order terms of the $g_n(R)C_n/R^n$ type and the n-th order terms in MBD in more detail.

To go beyond the pairwise approximation, the three-body (triple-dipole) ATM term of the form $g_9(R)C_9/R^9$ is sometimes used in the class of pairwise models. For the $n = 3$ case, the n-body and n-th order expansions are equivalent and hence these triple-dipole terms are contained in the third order of MBD. However, the origins of the corresponding terms differ significantly in MBD and in the beyond-pairwise models and so does the effective contribution of these terms to the long-range correlation energy. In particular, the three-body term in the beyond-pairwise methods is constructed independently of the pairwise term, that is, the C_9 coefficients are not in exact correspondence with the C_6 coefficients (via the general Casimir–Polder integrals) and the damping function g_9 contains parameters that are independent of the parameters in g_6. Therefore, the contributions of all the higher n-body terms ($n \geq 3$) in such a scheme influence the parametrization of the three-body term. As such, the resulting three-body energetic contribution effectively captures the effects of these higher-order terms, thus raising the question of transferability. In contrast, the three-body triple-dipole term arises automatically in the MBD framework and is constructed with the same atomic polarizabilities and long-range potential as the second-order dipole–dipole term. In other words, the range-separating function f and the polarizability $\boldsymbol{\alpha}_{\mathrm{eff},A}$ are the same for the second, third, and higher orders. Furthermore, the higher-order contributions in MBD have typically an alternating sign as given by Eq. (65) and hence their sum, that is, the difference between the total long-range correlation energy and the second-order approximation to it, can be significantly smaller than the third-order contribution. Finally, the triple-dipole term is an example of an n-th order term acting between n bodies, yet there is also the other class of n-th order terms acting between $m < n$ bodies. For $m = 2$, these terms correspond to the higher-order contributions to the two-body energy and these are not accounted for explicitly in pairwise approximations; for example, the lowest 4-th order two-body term would correspond to the C_{12}/R^{12} term in the language of dispersion coefficients.

The other class of higher-order C_n/R^n terms that come from higher-order multipoles of the polarizability (dipole–quadrupole, quadrupole–quadrupole) can be in principle obtained in the MBD framework in three ways. First, the higher multipoles can be partially captured in the parametrization of the range-separating function, as was the case with pairwise methods. Second, additional oscillators and coupling potentials describing quadrupole oscillations could be added. The contributions of such oscillators would reduce to the higher-order C_n/R^n terms when evaluated at second order. Third, the higher multipole terms could be evaluated as a perturbation to the dipole-coupled Hamiltonian due to the full Coulomb coupling by means of the perturbation theory. We note that none of these approaches have been yet introduced in a working method.

5 Models for vdW interactions: Applications

In this section, we continue with an assessment of the numerical performance of vdW models in treating systems for which vdW interactions play a key role. First, we discuss benchmark databases that consist of small noncovalently bound dimers, molecular crystals, and supramolecular complexes. We then follow with a brief survey of other important results for select systems, focusing on structural and electronic properties beyond binding and cohesive energies. This section is then concluded with a concise review of recent *ab initio* molecular dynamics simulations that use approaches based on first principles for describing vdW interactions.

Critical evaluation of exchange-correlation functionals through benchmarking and extensive testing plays a central role in DFT. Such an approach is particularly crucial for density functionals with a higher degree of empiricism, but served also to identify the robustness of many first-principles functionals, for which theoretical reasons were often found only later. A similar situation can be found in the field of vdW methods, where critical assessment is essential for the more empirical approaches, but is of great value even for the first-principles based methods covered in this review. There are several reasons why a quantitative assessment is needed, as opposed to a qualitative evaluation. First, it provides evidence for the level of uncertainty in predicted quantities that one may expect when using a particular method for a particular class of systems. This becomes ever more important as computational chemistry and materials physics play increasingly a predictive, rather than supportive role to experiment. Second, quantitative evaluation can identify both specific and systematic issues of a given method and hence provide guidance for further improvement. This is particularly important as quantitative differences in the relative energies of molecular systems and materials—the primary results of electronic structure calculations—often translate into qualitative differences in derived quantities such as structural, thermodynamic, and response properties. In this regard, the systematic verification of a given vdW method is usually achieved through comparison against the results of higher-level (more costly and more accurate) theoretical methods or to experimental results with sufficient resolution.

The presented vdW methods consist of many ingredients (models for response, partitioning schemes, range separation approaches, treatments of higher-order contributions) which all contribute to their overall performance. As a result of this composition, evaluations of vdW methods are often interpreted in terms of these individual ingredients. However, it is not always clear to what degree the individual choices for the ingredients contribute to the overall difference in performance between different methods. Detailed analyses of the performance in this regard are rare and remain to be performed for many popular vdW methods, even on simple model systems. This presents one clear path forward for the development of more robust and transferable vdW models, in which such comparative analyses can be used to identify the best ingredients from individual models, which can then be combined to form new methods with better performance.

5.1 Benchmark databases

In this section, we briefly discuss four benchmark databases for noncovalent interactions that were used to test many of the methods reviewed here. The tradition of such high-quality noncovalent databases started with the S22 test set of Jurečka *et al*. (Jurečka et al., 2006), which contains 22 binary complexes with a median number of atoms of 19, molar mass of 131 g/mol, and binding energy of 4.7 kcal/mol. The S22 set constitutes a representative sample of hydrogen-bonded, vdW bound, and mixed complexes. A similarly designed but more extensive set of 66 dimers (the S66 test set) with a median number of atoms of 20, molar mass of 126 g/mol, and binding energy of 4.1 kcal/mol, was published several years later (Řezáč et al., 2011). The reference energies in both these databases were obtained using high-level coupled-cluster calculations with single, double, and perturbative triple excitations (CCSD(T)) extrapolated to the complete basis set (CBS) limit, which represents the gold-standard electronic structure method in quantum chemistry. The benchmark C21 database (Otero-de-la-Roza and Johnson, 2012a) extends the analysis to condensed-phase systems via 21 molecular crystals with reference binding energies obtained from experimental sublimation enthalpies. This work was later extended and refined to cover 23 molecular crystals in the X23 database (Reilly and Tkatchenko, 2013a), with a median number of atoms per molecule of 10, molar mass of 89 g/mol, and binding energy of 7.3 kcal/mol. The final database considered in this section, the S12L set, deals with large molecules and consists of 12 supramolecular complexes with a median number of atoms of 134, molar mass of 1060 g/mol, and binding energy of 28 kcal/mol, with reference binding energies obtained from experimental Gibbs free energies of association, or alternatively from quantum Monte Carlo calculations (Grimme, 2012; Ambrosetti et al., 2014a). Although the available data in the literature are far from complete (*i.e.*, binding energies of every method discussed in this review on every one of these databases have not been calculated to date), Figure 7 still illustrates the following general trend: the differences in the predictions among the individual vdW methods increase as

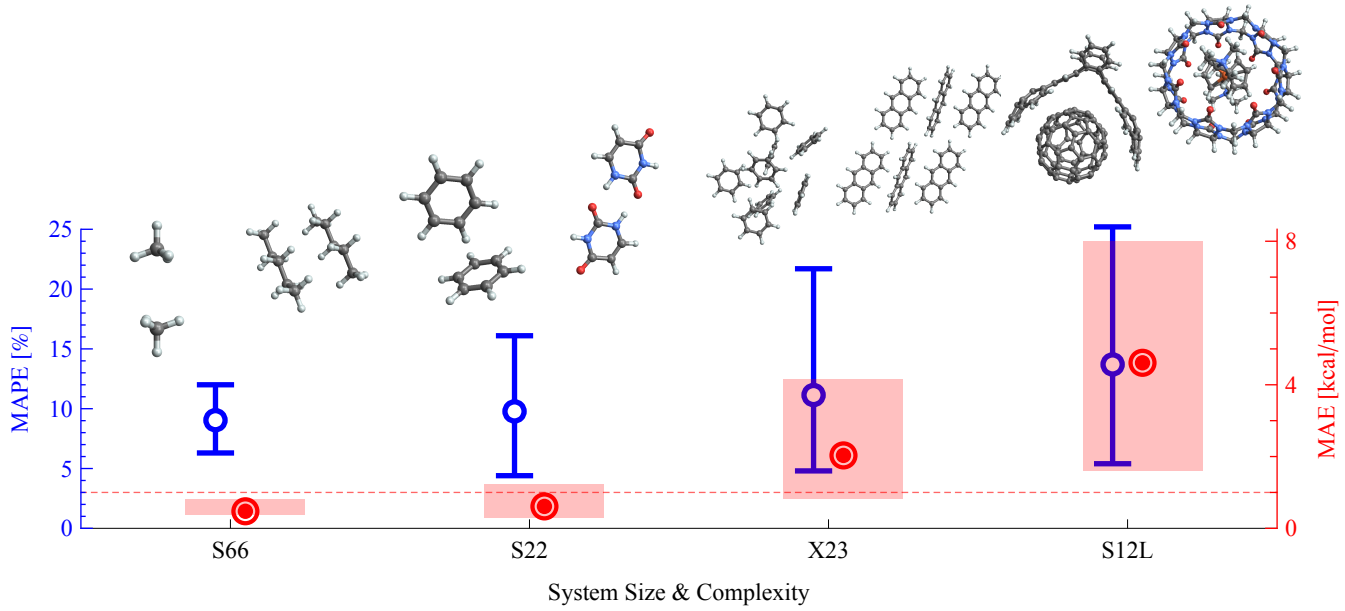

Figure 7. Overall performance of vdW methods on four benchmark datasets. The selection includes the methods XDM, MBD, TS, VV10, RPA, rPT2, vdW-DF and vdW-DF2. When a vdW method specifies a particular exchange-correlation functional, results with that functional were taken; otherwise, the PBE functional was considered. The blue and red data points reflect the mean and range of mean absolute percentage errors (MAPE) and mean absolute errors (MAE), respectively, on a given dataset. The dotted line denotes 1 kcal/mol. The displayed structures are illustrative examples of systems of a given size and complexity. Data are collected from refs. 122; 323; 232; 7; 225; 162; 83; 173; 179; 139; 204; 203; 343; 319; 205; 57; 67; 320; 177; 237; 54; 199; 250; 251; 206.

the size and complexity of the systems in question grow. In other words, the reliability of the vdW methods seems to decrease with increasing system size and complexity. However, this trend is also accompanied by a corresponding decrease in the accuracy and reliability of the underlying benchmark energies. In the following, we elaborate on various reasons for this observation, accompanied by an illustrative analysis of the differences between particular methods on select systems from these databases.

The S22 and S66 databases are relatively similar in design and will be discussed together. Figure 7 shows that the error ranges corresponding to the S22 and S66 databases are narrowest among the four benchmark sets. (We note that the error distribution is narrower for the S66 set due to its increased size with respect to the S22 set—a larger "sample" leads to a smaller variance between methods.) The consistent performance observed for these datasets illustrates that after intense development throughout the last decade, the majority of popular vdW methods managed to capture this first-rung level of complexity of nonbonded interaction energies. In the same breath, however, this does not mean that these simple systems cannot provide further insight into the performance of a given vdW model. On the contrary, a detailed analysis of a particular system can reveal valuable information about the relative contributions of different physical phenomena to the total binding energy as well as the degree to which those phenomena are accounted for in a given model. We will focus on two systems from these datasets, namely the benzene dimer and the adenine–thymine complex, each of which will serve to illustrate different potential complications that may occur when describing vdW interactions.

The benzene dimer has been the primary model system for noncovalent interactions over the past 40 years (Jaffe and Smith, 1996; Hobza et al., 1996; Tsuzuki et al., 2000, 2002; Sinnokrot et al., 2002; Sinnokrot and Sherrill, 2004; Park and Lee, 2006; DiStasio et al., 2007). In particular, the fine balance between the Pauli repulsion, electrostatic (quadrupole–quadrupole) interactions, and vdW dispersion results in an intricate potential energy surface (PES) with many local minima (Bludský et al., 2008). The nearly degenerate T-shaped and parallel-displaced (PD) conformations of the benzene dimer are contained in both S22 and S66 sets, but whether a particular method reproduces this degeneracy is naturally not reflected in the corresponding statistical errors. Another reason why these two geometries are particularly interesting is precisely the fact that they are two probes of the same PES and hence the number of potential sources of error in their description is limited. In this system, a physically sound description of the anisotropy in the vdW interactions becomes crucial for quantitative prediction of the finer details of the PES. As discussed in Sec. 2, the PD conformation exhibits alignment among the distinct in-plane charge fluctuations, whereas such fluctuations are orthogonal in the T-shaped conformation (see Figure 5). To capture these effects, a given vdW model has to correctly describe both the

monomer screening and polarizability as well as the intermolecular coupling of these anisotropic fluctuations (see the short-range $\alpha_{\text{sr}}(\mathbf{r}, \mathbf{r}')$ and its long-range coupling in Eq. (22)). This difficult task may be one of the underlying reasons why many second-order vdW methods, which neglect such effects, and even RPA-based methods fail to predict this degeneracy—both versions of vdW-DF either predict a difference of 0.6 kcal/mol (20%) at the true equilibrium geometries (Lee et al., 2010) or overestimate the binding distances by as much as 0.5 Å (Puzder et al., 2006), the error of the pairwise TS method on the PD conformation is 0.8 kcal/mol (DiStasio et al., 2014b), all RPA-derived methods reviewed in Section 4.5 overbind the PD conformation by ∼0.7 kcal/mol (Ren et al., 2013). In contrast, the MBD method, which explicitly accounts for the intra- and intermolecular many-body effects, reduces the error of the TS description to only 0.2 kcal/mol. Exceptions to this clear distinction are some parametrizations of the XDM model (Kannemann and Becke, 2010) and the VV10 functional (Vydrov and Van Voorhis, 2010b), which predict the degeneracy within a 10% margin, while being only second-order approximations. However, the XDM predictions substantially depend on a particular choice of the exchange-hole model, which suggests that other effects may effectively cancel out with the higher-order contributions in this particular system.

The adenine-thymine complex can be considered as a prototypical biological system and is represented twice in the S22 set: first, as a vdW bound stacked conformation; second, as a classical Watson–Crick nucleobase pair. While the first case is similar in character to the PD benzene dimer, the latter case contains strong directional hydrogen bonds in which several types of noncovalent binding contribute (electrostatic interactions, induction, and dispersion), posing a difficult challenge (Cooper et al., 2008; Silvestrelli, 2009a; Santra et al., 2008). Of all these interactions, only dispersion is described by vdW models whereas the other components are treated at the level of the underlying exchange-correlation functional. In this regard, an accurate description of electrostatic interactions relies predominantly on the correct assignment of permanent moments to the individual interacting molecules. For the case of induction, this must also be accompanied by a consistent treatment of the molecular polarizabilities. In DFT, all these quantities are predicted only approximately, yet these inaccuracies are rarely decoupled or even discussed separately from the errors introduced by the vdW models. A similar conclusion can also be made for the Pauli repulsion, the magnitude of which can be relatively large compared to the total binding energy, yet its description via different exchange functionals can vary greatly. The decomposition of the total binding energy of hydrogen-bonded complexes into the individual components varies greatly with distance (Hoja et al., 2014), which may potentially lead to decreased transferability between different system sizes if some of the errors mentioned above are effectively incorporated into the short-range behaviour or mutually compensate at a certain size range. Indeed, while the Watson–Crick pair is described relatively well by most vdW methods, with differences within 1.5 kcal/mol (10%), the relative errors across a range of hydrogen-bonded complexes of different sizes vary significantly (Boese, 2015). These observations suggest that at least a part of the remaining errors in the predicted binding energies cannot only be attributed to the vdW methods themselves, but rather to the underlying density functionals.

The fact that certain pairwise dispersion corrections are seemingly able to achieve good accuracy for molecular crystals stems from their more empirical nature and parametrization on large molecular systems. Essentially all pairwise methods (D3, XDM, TS) can be made accurate enough for the X23 database by adjusting two empirical parameters (Reilly and Tkatchenko, 2013a). However, such adjustments just serve the purpose of mimicking some of the dielectric screening effects and can only be successful for relatively symmetric systems. The true nature of dielectric screening in arbitrary systems and geometries can only be captured with explicit many-body approaches.

One large class of complex molecular environments consists of molecular crystals. The X23 database contains 23 such systems with a similar profile of the local intermolecular bonding as in the S22 and S66 sets (ranging from hydrogen-bonded to vdW bound and mixed complexes). While this might lead one to expect a comparable range of errors for the different vdW methods, Figure 7 reveals that there is in fact a significant decrease in the reliability among the methods when treating molecular crystals as opposed to gas-phase molecular dimers. As a model case for discussion, consider the benzene crystal which is a natural extension of the benzene dimer from the molecular databases, yet it is significantly more complicated (Podeszwa et al., 2008; Lilienfeld and Tkatchenko, 2010; Wen and Beran, 2011; Kennedy et al., 2014). For instance, the second-order, pairwise TS method overestimates the lattice energy by 3 kcal/mol, while treatment of the electron correlation to all orders within the MBD method results in a prediction within the 1 kcal/mol (though a slightly better result is obtained with PBE0 compared to PBE, suggesting small error cancellation in play). Similarly, considering only individual pairs of benzene molecules in the crystal within SAPT(DFT) or only doubles excitations within the coupled-cluster method leads to overestimation of the energy by 2 kcal/mol, while increasing the degree of correlation decreases the error under 1 kcal/mol. In contrast, the DFT-D3 method achieves 1 kcal/mol without considering any many-body effects, and their addition worsens the results by approximately 1 kcal/mol (Moellmann and Grimme, 2014). There are several possible reasons for the increased complexity and less predictable behaviour of a crystal compared to the molecular dimer. First, the benzene crystal contains individual pairs of benzene molecules in many different orientations, each of which needs to be described with the same level of accuracy; as such, the molecular crystal serves as another indirect probe into the quality of the dimer PES. Second, the solid state introduces stronger intermolecular polarization in addition to the intramolecular polarization that was already present in the isolated molecular complex; this coupling of short- and long-range many-body effects further increases the polarizability of a molecule within the crystal. Third, the presence of the three-dimensional crystal lattice effectively screens the long-range dipole correlations, resulting in an overall decrease in the lattice energies. The total contribution of the latter two competing long-range effects can range from negative to positive in the prediction of lattice energies,

and hence adds to the mixed conclusions regarding the applicability of pairwise schemes and three-body corrections for the description of molecular crystals.

To put these numerical differences into perspective, consider that a correct ordering of crystal polymorphs necessary for successful crystal structure prediction requires an accuracy of only fractions of a kcal/mol (Price, 2014; Reilly and Tkatchenko, 2015; Marom et al., 2013; Beran, 2016). More than half of the compounds in a pharmaceutically relevant data set show polymorphism (Cruz-Cabeza et al., 2015), and the energy differences between polymorphs are usually less than 1 kcal/mol and often even less than 1 kJ/mol (0.24 kcal/mol). The X23 database contains two polymorphs of oxalic acid, for which the experimental energy difference between the α and β forms amounts to only 0.05 kcal/mol (Otero-de-la-Roza and Johnson, 2012a; Reilly and Tkatchenko, 2013a; de Wit et al., 1983). Yet current vdW-inclusive first-principle approaches yield energy differences between about -1 and 1 kcal/mol. PBE+MBD has an absolute error in the difference of only 0.12 kcal/mol, but predicts the wrong ordering (Reilly and Tkatchenko, 2015), whereas PBE0+MBD correctly predicts the ordering with an absolute error of 0.22 kcal/mol, illustrating how subtle the differences in the two polymorphs are. The three polymorphs of glycine have also been studied with a variety of methods, of which only PBE0+MBD was able to correctly predict the relative stability ordering as observed in experiment (Marom et al., 2013). Molecular crystals are usually studied experimentally at finite temperature and pressure, requiring that free energies are considered instead of bare lattice energies. For instance, form I of the aspirin crystal is much more abundant in nature than form II, yet both forms have almost degenerate bare lattice energies. The higher stability of form I could only be explained by considering harmonic free energies at room temperature (Reilly and Tkatchenko, 2014a). Thermal and pressure effects are not only crucial for the stability under thermodynamic conditions, but are also essential for the unit-cell structure itself and a variety of response properties, such as vibrational spectra and elastic constants (Hoja et al., 2017). The most recent structure prediction blind test for organic crystals (Reilly et al., 2016) featured a practically relevant and highly polymorphic system involving a quite flexible molecule. This flexibility leads to a much larger number of local minima within a narrow energy window compared to crystals containing only rigid molecules. While most polymorphs have been found by at least one participant within the top 100 predicted structures, the relative ordering of the polymorphs is still challenging. That said, inclusion of many-body effects in the description of vdW interactions and accounting for free energies clearly improves the relative stability prediction.

A related class of solid-state systems, which shares similar features to the vdW binding motifs in molecular crystals, consists of layered materials. To date, there is no systematic benchmark database for such systems, however, we can still learn from particular representative systems. We will consider graphite, one of the prototypical layered materials for which there is an abundant number of both experimental and theoretical results (Graziano et al., 2012; Lebègue et al., 2010; Marini et al., 2006; Spanu et al., 2009; Björkman et al., 2012; Brandenburg et al., 2013), regarding both its energetic and structural properties (Rêgo et al., 2015). Graphite features the same set of many-body effects as found in molecular crystals, but these effects are amplified by the extreme difference in response properties between the in-plane and out-of-plane directions in the graphene layers. The correlation of the long-range fluctuating dipole waves within each layer decays very slowly with distance, as demonstrated by the slow convergence of the binding energy of multilayer graphene (Tkatchenko, 2015; Gobre and Tkatchenko, 2013; Ambrosetti et al., 2016). On the other hand, these correlations are nontrivially screened by the inner layers, resulting in a competition between these two effects as captured by the various correlation orders in Eq. (23). Although approximate, RPA describes these effects at least on a semi-quantitative basis, and so can serve as a first-order reference with the predicted binding energy of 1.11 kcal/mol per carbon atom. Many vdW methods, including all nonlocal density functionals and most atom-based pairwise methods, fall short from this result, with predictions ranging from 0.46 to 1.86 kcal/mol per carbon atom. When structural data such as lattice constants and bulk moduli are considered as well, only methods that treat the dipole correlations to all orders are capable of matching the experimental reference results. For instance, while both the XDM and MBD methods provide good estimates of the interlayer lattice parameter and the binding energy, XDM underestimates the curvature of the energy minimum more than twofold, whereas MBD predicts a value within 15% of experiment (Gao and Tkatchenko, 2015; Rêgo et al., 2015).

As a final benchmark dataset, we consider the S12L (S30L) set of 12 (30) supramolecular complexes (Risthaus and Grimme, 2013; Sure and Grimme, 2015). In these systems, the total binding energies are mostly dominated by vdW interactions and hence the choice of a particular underlying density functional is of less importance than in the previous datasets, which makes this database an ideal playground for analyzing vdW methods. As a prototypical example, we will discuss the so-called buckyball catcher complex, as it was studied most extensively both theoretically and experimentally. A prominent feature of this system is the strong anisotropy in the polarizability of the pincers of the catcher, which results in nonlocal dipole fluctuations spanning the whole complex. This situation is partially analogous to the mechanisms occurring in graphite and graphene, but the screening of the dipole correlations is much weaker in this case (in contrast to graphite) and there is no cancellation of the higher-order effects due to symmetry (in contrast to graphene). This results in the nonlocal fluctuations having a large destabilizing contribution to the binding energy, which can reduce this quantity by as much as 10 kcal/mol with respect to a pairwise-additive decomposition of the long-range correlation energy in the TS, VV10 and bare XDM model, resulting in two- to fourfold reduction in the mean relative error (Risthaus and Grimme, 2013; Ambrosetti et al., 2014b). By accounting for the effect of such fluctuations (either inherently as in MBD or by higher-order corrections in the XDM, VV10 or DFT-D3 model), the reference binding energies can be predicted within 2 kcal/mol (5%), leading to many-body effects playing a crucial role in the binding of supramolecular complexes.

Apart from the established datasets discussed above, we briefly list other that have not seen broader adoption. All datasets mentioned below were benchmarked using the CCSD(T)/CBS method. The X40 set comprises complexes of small halogenated organic molecules and provides a good test of how well a method handles strongly ionic and charge-transfer compounds (Řezáč et al., 2012). The L7 set consists of larger organic complexes than those included in the S22 and S66 sets, but smaller than the supramolecular complexes in the S12L set. (Sedlak et al., 2013). The 3B-69 dataset is of particular interest to the discussion here as it benchmarks molecular three-body contributions to interactions energies (Řezáč et al., 2015). An interesting approach was used by Faver et al. (Faver et al., 2011), who dissected a protein-ligand complex 1HSG into 21 smaller fragment dimers bound by noncovalent interactions.

A final point in the discussion of the benchmark datasets concerns the reliability of the underlying reference data. For the S22 and S66 sets, well-converged state-of-the-art electronic structure theory methods were used by several groups to obtain the benchmark data. These efforts leave very little room for potential improvement, with the possible exception of almost degenerate structures such as the aforementioned benzene dimer conformations, where an accuracy of less than 0.1 kcal/mol is needed to decisively determine the most stable geometry. The X23 set presents a more difficult challenge not only for the approximate vdW methods, but also for the computational techniques used for obtaining the benchmark energetics. The common method of deriving these energies from experimental sublimation enthalpies involves several approximations, the particular choice of which can lead to differences as large as 1 kcal/mol (Otero-de-la-Roza and Johnson, 2012a; Reilly and Tkatchenko, 2013a). In contrast, Yang *et al*. recently calculated the lattice energy of a benzene crystal at the CCSD(T) level with an estimated uncertainty of only ∼0.1 kcal/mol (Yang et al., 2014), which may mark a future path towards obtaining suitably accurate benchmark energetics for molecular crystals. Finally, the S12L dataset is a difficult problem due to the sheer size of the complexes in question and the fact that they have not been isolated experimentally in the gas phase. The original reference binding energies were obtained by subtracting the vibrational and solvation contributions from the experimental Gibbs free energies of association (Grimme, 2012). The largest uncertainty in this approach comes from the solvation contributions that are obtained by using semi-empirical models with uncertainties that can exceed ±5 kcal/mol. Indeed, the differences between the experimentally derived binding energies and those obtained by the diffusion quantum Monte Carlo (DQMC) method (statistically converged to 1 kcal/mol) are similar in magnitude to the uncertainties in the solvation contributions.

Besides systematic benchmark databases, much work has also been done on select systems bound by vdW interactions, which are in some ways representative of a wider class of molecules or materials. The vdW-WF method was tested on small dimers and adsorption of small molecules on various surfaces in several studies (Ambrosetti and Silvestrelli, 2011; Andrinopoulos et al., 2011; Silvestrelli, 2009b; Silvestrelli et al., 2012). Sorescu *et al*. performed an extensive study of many different methods on a set of 26 nitrogen containing molecular crystals (Sorescu et al., 2014). With the benzene dimer being such a well studied complex, its natural extension is the adsorption of a single benzene molecule on a surface. Such a system has an appeal both from an experimental point of view as a model for heterogeneous catalysis, as well as from a theoretical stance as it combines contributions coming from electrostatic interactions (benzene quadrupole moment) and long-range polarization induced in the surface. Typical choices for the surface are a single graphene sheet (Chakarova-Käck et al., 2006; Berland and Hyldgaard, 2013) and metallic surfaces (Toyoda et al., 2009; Liu et al., 2013, 2015; Chwee and Sullivan, 2012; Reckien et al., 2014). In the latter case, the surface charge fluctuations of the metallic electrons have a large effect on the polarizability of the adsorbed molecule and substantially change its response compared to the gas-phase case, thus influencing the resulting binding energy. However, the metallic response has an intricate many-body character and a general first-principles approximate method for description of vdW interactions in hybrid interfaces is yet to be seen. A further step in complexity can be taken by studying the interaction of a single graphene sheet with a metallic surface (Vanin et al., 2010; Hamada and Otani, 2010; Olsen et al., 2011; Mittendorfer et al., 2011; Olsen and Thygesen, 2013b, 2014). Here, the long-range response of a covalent two-dimensional zero-gap semiconductor is coupled with the response of surface plasmons of the metal, presenting a severe test for vdW models. Maurer *et al.* summarized the performance of different methods for graphene/Ag(111) binding energy, with results ranging from 0.77 to 1.67 kcal/mol per carbon atom (Maurer et al., 2015). This work demonstrates the sheer complexity of describing vdW interactions in complex nanostructured materials.

To fully assess the complicated nature of realistic systems when testing approximate models, they need to be probed in many different ways, either by using different configurations and conformations, or by investigating other properties besides binding energies, such as polarizabilities, stress tensors, work functions or dynamical properties. Such studies are the topic of the following sections.

5.2 Structural and electronic properties

Up to this point, we have been concerned primarily with the binding energy effects of long-range electron correlation as those are typically large in relative magnitude. In this section, we discuss the effects of vdW interactions on structural and electronic properties. While the energy ordering of different conformers of the benzene dimer poses a significant challenge to all vdW models, an even more sensitive probe into the robustness of a given model and a gateway to obtaining equilibrium structures as well as dynamical properties of systems at nonzero temperatures, is provided by derivatives of the energy with respect to the nuclear coordinates, $-\mathrm{d}E/\mathrm{d}\mathbf{R}_A$. Furthermore, the vdW models discussed here all directly depend on the electron density and therefore, via the functional derivative of the energy, $\delta E/\delta n$, and the Hohenberg–Kohn variational principle, necessarily influence the electron density and hence all electronic properties. Whereas the structural effects have been recognized since the beginning of the empirical treatment of

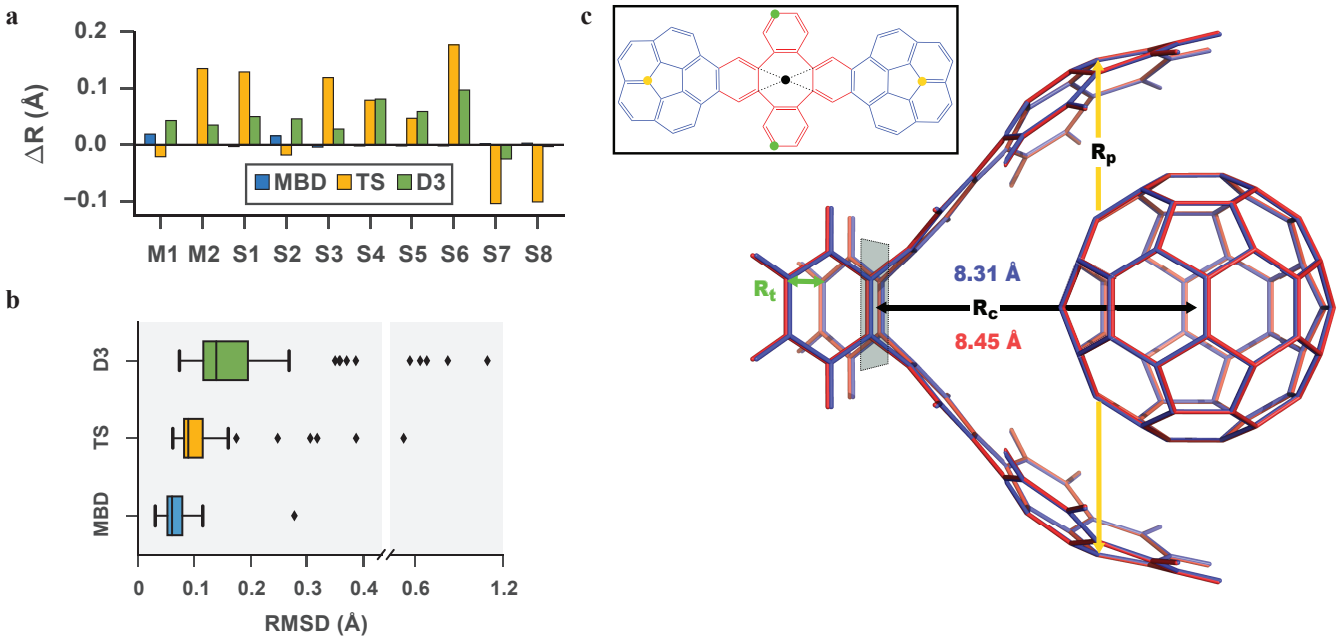

Figure 8. Structural changes induced by vdW interactions as predicted by several methods. D3 is the semi-empirical DFT-D3 model of Grimme et al. (Grimme et al., 2010). (**a**) Errors in monomer distances of ten locally stable conformations of the benzene dimer with respect to reference DFT/CCSD(T) results (Bludský et al., 2008). (**b**) Predicted structures of 76 conformers of 5 isolated small peptides using different methods are aligned with reference MP2 structures by minimizing the root-mean-square deviation (RMSD) of the atomic coordinates. The minimized RMSDs are represented using their mean, quartiles, and whiskers covering data within 1.5-fold quartile range. The outliers are plotted as individual points. (**c**) The equilibrium geometries of the buckycatcher–C60 complex as predicted by PBE+MBD (blue) and PBE+D3 (red). [Adapted with permission from Blood-Forsythe et al. (2016)]

vdW interactions, the electronic effects have been largely neglected and it is only in recent years that they have become the topic of investigation.

Although searching for local minima on PES forms the basis of most computational chemistry studies, it is used to systematically evaluate the accuracy of vdW methods to a much smaller degree than the corresponding binding energies. Recently, several researchers attempted to close this gap. Witte et al. investigated the performance of may electronic structure methods in predicting the equilibrium geometries of small to large molecular complexes (Witte et al., 2015). They found that the nonlocal density functionals vdW-DF2 and VV10 perform reasonably well on small systems with respect to CCSD(T); however, the relative errors associated with vdW-DF2 increase with system size, whereas the accuracy associated with VV10 was more transferable to larger systems. This issue can be possibly traced back to the way that the vdW-DF2 functional is constructed as explained in Section 4.6. Compared to the original vdW-DF functional, the second version uses a larger density gradient contribution, leading to more rapid cutoff of the tail densities in the polarizability density functional and hence decreased C_6 coefficients. When coupled with a more attractive semi-local functional than the original revPBE, this approach may reach better accuracy than vdW-DF on small systems, but as the system size grows, the part of the binding that comes from the short range diminishes, while the underestimation of the long-range contribution begins to manifest itself.

Blood-Forsythe et al. investigated the performance of the MBD and TS methods together with the DFT-D3 model in the description of the PES of the benzene dimer, a set of small peptides, and a large supramolecular complex (Blood-Forsythe et al., 2016). For the benzene dimer, they found an almost perfect agreement between MBD and the reference structures of CCSD(T) quality (RMS error of 0.01 Å), whereas both the pairwise TS and D3 methods yield errors that are several times larger in magnitude (Figure 8a). Comparing the differences between MBD and TS for the individual conformations, it can be seen that the pairwise approximation shortens the binding distances in stacked conformations, whereas they are increased in the T-shaped structures. This can be explained by the anisotropy in the polarizability of the benzene molecule, which is neglected in the pairwise approximation. Because the destabilizing many-body effects are pronounced in cases where the larger components of the polarizability are aligned, the binding distances are shortened when these effects are neglected, consistent with the observed behavior. Similar trends were also observed in the prediction of the secondary structures of select small peptides (Figure 8b), governed by subtle intramolecular nonbonded interactions. The fragment separation in the supramolecular buckycatcher complex was found to decrease by 0.2 Å with the MBD model (Figure 8c), demonstrating a distinct effect of many-body vdW interactions on the structure of larger and more realistic molecular systems of interest.

After discussing the nuclear degrees of freedom of the total molecular Hamiltonian, we turn to the electronic degrees of

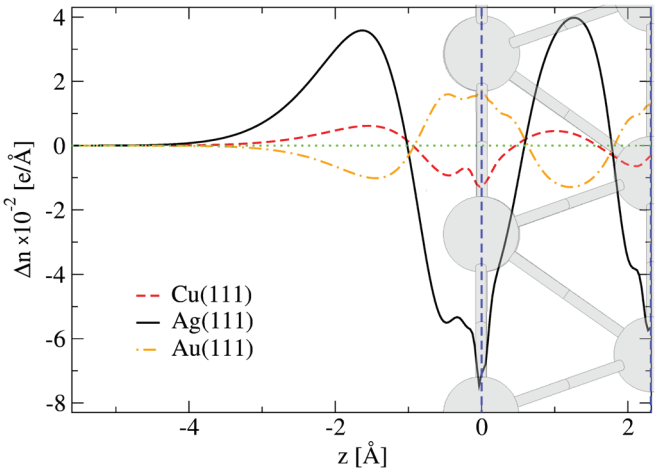

Figure 9. Charge density polarization of metallic surfaces due to long-range electron correlation. Δn is the integrated difference between the total electron densities obtained by the PBE functional and the self-consistent PBE+vdW$^{\text{surf}}$ method. [Reprinted with permission from ref. 86. Copyright 2015 American Physical Society.]

freedom. The long-range electron correlation energy is typically around five orders of magnitude smaller than the total electronic energy, and accordingly the electron density changes associated with vdW interactions are of a similar relative magnitude with respect to the total electron density. This is the reason why vdW methods can be applied in a perturbative fashion as an *a posteriori* correction to the total energy, without affecting the electron density, which is obtained *a priori* from the self-consistent Kohn–Sham equations. On the other hand, for any method that is formulated as a functional of the density, $E_c[n]$, one can derive the corresponding contribution to the exchange-correlation potential, $\delta E_c/\delta n$, and include it in the Kohn–Sham equations, resulting in subtle changes in the electron density. In fact, the Hellman–Feynman theorem shows that it is this charge polarization induced by the long-range correlation of quantum electron fluctuations that acts as the origin of the vdW forces on the nuclei (Feynman, 1939; Hunt, 1990). Self-consistent implementations have been recently provided for several vdW methods discussed throughout Section 4, including RPA (Bleiziffer et al., 2013), nonlocal density functionals (Thonhauser et al., 2007; Vydrov et al., 2008; Gulans et al., 2009), the TS (Ferri et al., 2015) and XDM (Kong et al., 2009) pairwise methods. In many of these works, the effect of self-consistency on the binding energies are reported as negligible and in general, the electron density is polarized in such a way that it shifts slightly away from the atoms towards the intermolecular regions. However, these conclusions were reached on small, typically organic gas-phase molecular dimers. In contrast, Figure 9 shows that the charge polarization induced by vdW interactions on a metallic surface depends significantly on the particular metal: whereas the charge density is accumulated above the surface in the case of copper and silver, it is depleted in the case of gold. The effects of this charge redistribution can be directly compared to experiment via the surface work function. This quantity is the energy associated with extracting an electron from the surface and is directly influenced by the dipole density of the surface, which is in turn connected to the charge distribution along the direction normal to the surface. As a result of the charge polarization shown in Figure 9, the work functions of the coinage metals can be changed by as much as 0.3 eV due to long-range electron correlation (Ferri et al., 2015). These work functions can then be additionally tuned by noncovalent adsorption of organic molecules on the metallic surface in hybrid organic-inorganic interfaces (Toyoda et al., 2009; Sony et al., 2007; Ferri et al., 2015).

5.3 Molecular dynamics

After considering the effects of vdW interactions on microscopic structural and electronic properties, we turn to how these forces influence the macroscopic properties of materials. As argued previously, a first-principles description of vdW interactions is required to accurately treat the variety of structural, electronic, and environmental features that influence the properties of systems found throughout biology, chemistry, physics, and materials science (see Figure 1). *Ab initio* molecular dynamics (AIMD), in which PES is generated "on the fly" from the electronic ground state without the need for empirical input, provides such a framework. The AIMD technique has been applied to many problems (Zipoli et al., 2010; Ikeshoji et al., 2011; Geissler et al., 2001) and allows for a quantum-mechanical treatment of the structure and dynamics of a given molecular system as well as its electronic and dielectric properties, and potential chemical reactions. In this section, we consider several examples of studies which demonstrate that the predictive power of AIMD simulations depends crucially upon the accuracy of the underlying potential, and in particular, the inclusion of and choice for the respective vdW description.

As a first example, we consider the effects of vdW interactions on the structure and properties of liquid water (Gillan et al., 2016). Many AIMD studies demonstrated that vdW interactions significantly influence the microscopic structure and macroscopic equilibrium density (Schmidt et al., 2009; Ma et al., 2012; Del Ben et al., 2013b) of ambient liquid water. However, the influence of vdW forces on its properties largely depends on the particular vdW approach. For instance, the semi-empirical pairwise DFT-D approach of Grimme (Grimme, 2004) tends to reduce the intensity of the first maximum in the oxygen-oxygen radial distribution function ($g_{\text{OO}}(r)$) of liquid water over a wide range depending on the underlying functional (Lin et al., 2009; Jonchiere et al., 2011; Schmidt et al., 2009). With the use of the nonlocal density functionals from the vdW-DF family, one can obtain mixed results in reproducing the second coordination shell in ambient liquid water depending on the choice of the underlying exchange-correlation functional (Wang et al., 2011; Møgelhøj et al., 2011; Zhang et al., 2011a). On the other hand, AIMD simulations using a self-consistent (SC) exchange-correlation potential that accounts for both exact exchange (via the PBE0 functional) and vdW interactions (via the pairwise TS model) are able to quantitatively reproduce the experimentally derived $g_{\text{OO}}(r)$ of liquid water (DiStasio et al., 2014a) (see Figure 10a). In this case, the PBE0 hybrid functional reduces the amount of self-

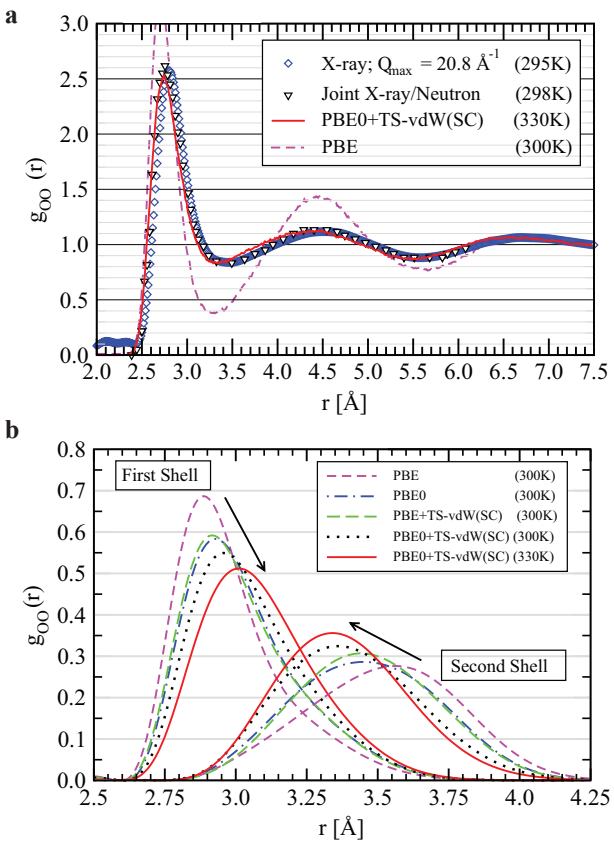

Figure 10. Individual and collective effects of vdW interactions and exact exchange on the structure of liquid water. (**a**) The oxygen-oxygen radial distribution functions, $g_{OO}(r)$, of liquid water obtained from theory (via DFT-based AIMD simulations) and various scattering experiments (Soper and Benmore, 2008; Skinner et al., 2013). (**b**) Contributions from the first and second shells of neighboring water molecules to the $g_{OO}(r)$ of liquid water. The arrows indicate systematic shifts in the main peak positions and intensities of the computed distributions with the addition of self-consistent vdW interactions and exact exchange in the underlying exchange-correlation functional. [Adapted with permission from ref. 71. Copyright 2014 AIP Publishing LLC.]

interaction error in the underlying exchange-correlation potential and thereby weakens the hydrogen-bond strength in liquid water relative to a GGA such as PBE; in doing so, hydrogen-bonded molecules in the first shell move outward, resulting in a marked increase in the population of molecules located in the interstitial region, i. e., the region between the first and second coordination shells (see Figure 10b). On the other hand, vdW forces, as described by the TS method, are non-directional and strengthen the interactions between a given water molecule and the molecules in its first and second coordination shells (and stabilize broken hydrogen-bond configurations in general), which causes the molecules in the second shell to move inward and populate the interstitial region (see Figure 10b). In terms of dynamical properties, one also observes a significant increase in the predicted diffusion coefficient of liquid water when going from PBE ($D = 0.02\,\text{Å}^2 \cdot \text{ps}^{-1}$) to PBE0+TS-vdW(SC) ($D = 0.15\,\text{Å}^2 \cdot \text{ps}^{-1}$), which makes it much closer to the experimental value of $0.23\,\text{Å}^2 \cdot \text{ps}^{-1}$ (Hardy et al., 2001). As such, both these effects work collectively to yield a microscopic description of liquid water that is less structured, more fluidic, and significantly closer to experiment.

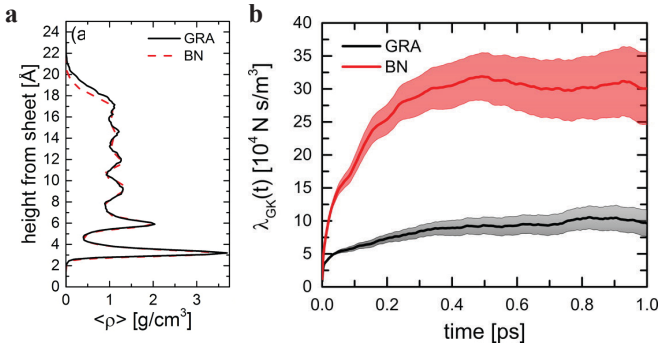

Figure 11. Similar structure but different friction of water on graphene and hexagonal boron nitride surfaces. (**a**) Average density profile of a liquid water film computed at the optB88-vdW level as a function of the height from a graphene (GRA) and hexagonal boron nitride (BN) sheet. (**b**) Comparison between the Green–Kubo estimate of the friction coefficient of liquid water on GRA and BN (with shaded areas representing the uncertainties in the coefficients). [Reprinted with permission from ref. 304. Copyright 2014 American Chemical Society.]

As a second example, we consider the use of vdW-inclusive AIMD (via the optB88-vdW nonlocal functional) to map the molecular structure and energetics of liquid water films on layered materials, such as graphene and hexagonal boron nitride (BN), to the complex transport of water at the nanoscale (Tocci et al., 2014). Here, AIMD simulations reveal that the structures of the liquid water films, substantially influenced by vdW interactions, are in fact very similar for both graphene and BN; however, slight differences in the contact layer (that are not related to the wetting properties of these interfaces) give rise to a remarkably different water slippage of these sheets (see Figure 11). This threefold increase in the friction on BN with respect to graphene is not captured by force-field based molecular dynamics simulations, thus stressing the importance of a first-principles based description in predicting transport properties at complex interfaces.

As a third and final case, we consider the role played by vdW interactions in stabilizing key helical domains in the secondary structure of gas-phase polypeptides (Schubert et al., 2015; Rossi et al., 2010; Baldauf and Rossi, 2015; Rossi et al., 2015, 2014). In a recent AIMD study (Tkatchenko et al., 2011), it was shown that the inclusion of vdW forces can explain the notable stability of polyalanine (Ac-Ala$_n$-LysH$^+$) helices up to a temperature of 725 K (Kohtani et al., 2004). Figure 12 illustrates the fact that AIMD simulations at the PBE and PBE+TS levels of theory paint very different pictures of the dynamical helix structure over a wide range of temperatures. For instance, AIMD simulations at 700 K with PBE+TS give a structure that is comprised

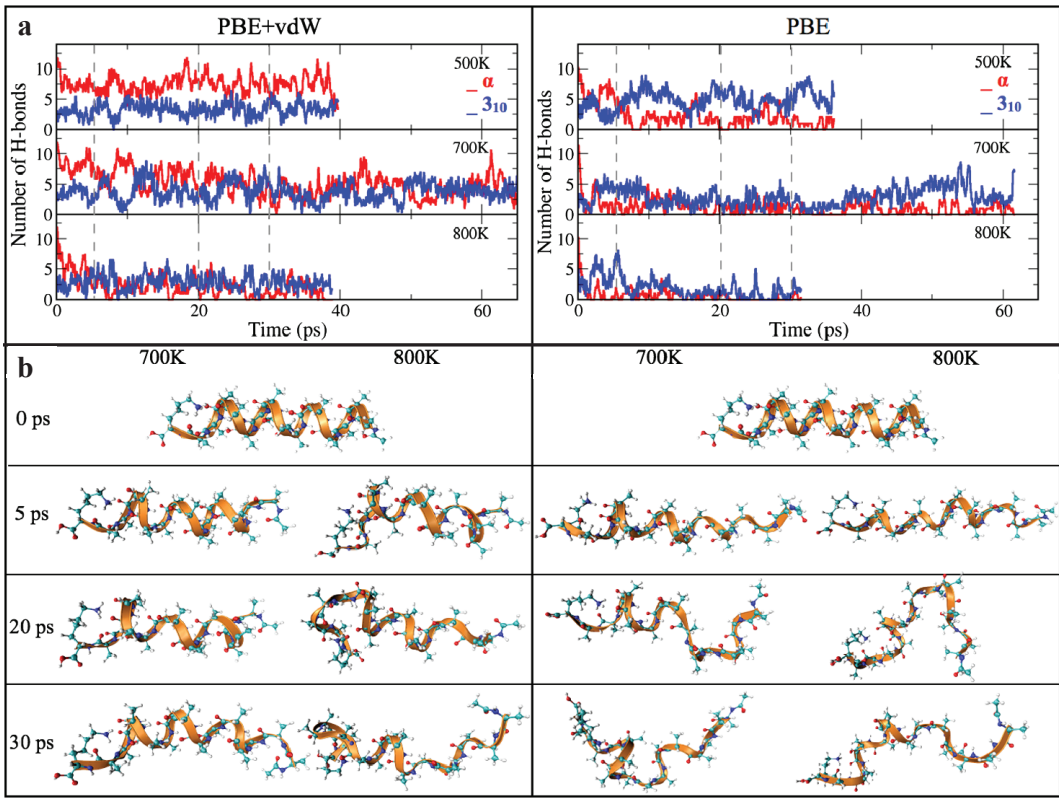

Figure 12. Importance of vdW interactions in determining the thermodynamic stability of polypeptide helices. (**a**) Overall number of hydrogen bonds recorded throughout AIMD simulations at the PBE+TS-vdW and PBE levels of theory, with the α-helical bonds (red) and 3_{10}-helical bonds (blue) counted separately. (**b**) Snapshots of the helical conformations from the corresponding AIMD simulations. [Reprinted in part with permission from ref. 301. Copyright 2011 American Physical Society.]

of both α and 3_{10}-helical motifs with an overall helical structure that is preserved after 65 ps of simulation, whereas PBE predicts that the α-helical motifs quickly disappear within 5–7 ps, in contradiction of the experimental evidence.

6 Challenges and outlook

Recent developments of sophisticated methods for modeling vdW interactions brought unprecedented insights into the nature of noncovalent interactions in complex molecules and materials. The development of vdW methods based on first principles vastly extended the applicability of density-functional calculations in chemistry, biology, and materials science. The continuing efforts to increase the accuracy and reliability of these methods will further improve our understanding and capacity to model the noncovalent interactions in large molecular systems.

Despite all the advances, a unified method that could accurately model noncovalent interactions in a wide range of molecular and extended systems is yet to become available. All existing vdW-inclusive methods have their advantages and limitations. Recognizing the limitations is perhaps the most important area of current research, which will eventually enable systematic developments towards the universally applicable method. Aiming towards this goal, we present here a set of challenges which we deem as particularly important to address to enable progress in the field of modeling vdW interactions:

- Is it possible to develop an efficient density-based method for vdW interactions which would allow reliable description of a wide range of phenomena and systems illustrated in Figure 1? Could such a unified method treat neutral small and large molecules, salts, ions, metals, and interfaces between these systems, on equal footing? Besides developing improved methods, this goal also requires creating systematic datasets of validated structures, binding and cohesive energies, and response properties for a wide range of noncovalently bound systems.
- It has been convincingly demonstrated that the many-body effects in the vdW energy are crucial both for qualitatively correct and quantitatively accurate modeling of large molecular systems.
  Can simple rules of thumb be developed that would allow design of molecular systems that exhibit desirable properties stemming from collective many-body effects? While explicitly correlated quantum-chemical methods allow achieving quantitative accuracy, insights are more easily obtained from coarse-grained models (Ambrosetti et al., 2016).
- As the molecular size grows, eventually quantum electrodynamic or Casimir-like effects, not considered by existing vdW-inclusive methods, become important: retardation due to the finite speed of light or thermal field fluctuations

among others. Can we develop methods that seamlessly cross from the vdW into the Casimir regime? Can we devise rules based on system sizes and topologies for when such crossover becomes necessary?

- Can we develop efficient density-based methods for modeling vdW interactions in systems subject to both homogeneous and inhomogeneous electric fields, between excited-state (and ground-state) molecules, or in general molecules embedded in complex static or fluctuating environments? How can we properly include the effect of a generalized frequency-dependent bath on vdW interactions in complex molecular systems?
- How do nuclear (classical or quantum) fluctuations at finite temperature affect vdW interactions between molecules? Do they compensate or accentuate many-body effects? Are there novel phenomena resulting from the coupling between quantum nuclear fluctuations and long-range electronic correlations?
- The crucial role of vdW interactions in the structure and stability of molecular systems is convincingly established by now. What about the role of vdW interactions in vibrational, mechanical, electronic, optical, and other response properties of molecular systems?
- What is the role of solvents on intermolecular interactions? This question combines both the contribution of thermal effects and electrodynamic fluctuations (Yang et al., 2013).

We proceed by raising methodological questions relevant for the development of improved methods for vdW interactions and for better understanding of long-range electronic correlation in general:

- Is there a systematic way to combine semi-local density functionals with long-range models for vdW interactions? As density functionals become more farsighted and vdW models become more nearsighted, what is the optimal crossover between semi-local and nonlocal approaches to electron correlation? How to balance between many-body electronic effects in the semi-local functional and the nonlocal electron correlation (Tkatchenko and von Lilienfeld, 2008)?
- Is there a systematic way to combine classical force fields that approximately model bonding and electrostatics with methods for long-range vdW interactions? For example, recent work by Martyna *et al.* lays the foundation for quantum-mechanical force fields based on quantum Drude oscillators (Jones et al., 2013b,a; Sokhan et al., 2015). How much quantum mechanics can (should) an empirical force field capture?
- Some of the vdW methods discussed in this review provide a link between DFT, semi-empirical density-functional approaches and classical force fields. For example, the TS method was extended from DFT (Tkatchenko and Scheffler, 2009) to the tightbinding method (Stöhr et al., 2016) and force fields (Bereau and von Lilienfeld, 2014; Cole et al., 2016). Can such flexibility be transferred to other vdW methods?
- What is the nature of nonlocal fluctuations contained in $\chi_0(\mathbf{r},\mathbf{r}')$ and $\boldsymbol{\alpha}_0(\mathbf{r},\mathbf{r}')$? How well can they be represented locally? Could the freedom in the gauge of the $\boldsymbol{\alpha}$ vector field be used to some advantage?
- Can narrow-gap or zero-gap materials be described with a local α_0? Is the atom-dipole description, which is an efficient approximation for finite-gap materials, efficient also for metals?
- Is there a clear-cut theoretical distinction between dipole and charge fluctuations? Can charge fluctuations be modelled efficiently with semi-local dipole fluctuations even in metallic systems?
- How good is the single-oscillator Unsöld approximation in general? Can we systematically generalize this model to a many-body approach with multiple frequencies per site?
- How much can be achieved with finer coarse-graining of the response? Apart from mitigating the dipole-approximation error, can more complex electronic effects be encoded in finely-grained local response functions?
- Is the equivalence of electronic χ and $\boldsymbol{\alpha}$ transferable to the coarse-grained (oscillator) descriptions?
- How can anisotropic local polarizability be constructed in both the atomic case and density-functional case? Can we use the directionality of the density gradient?
- Can we have truly nonlocal functionals for $\boldsymbol{\alpha}_{\text{eff}}(\mathbf{r}) = \int_{\mathbf{r}'\in M(\mathbf{r})} \mathrm{d}\mathbf{r}' F(\mathbf{r},\mathbf{r}')$?
- Can we have more exact constraints and limits on $\alpha[n]$? Can we go to meta-GGA functionals for $\alpha[n]$? Can we have point functionals that are exact for isolated atoms?
- When information from the density is used to construct the local effective $\alpha[n]$, what is the "range" of such models?

Finally, we mention a range of possible applications that should enable better understanding of strengths and weaknesses of existing vdW-inclusive methods and guide the development of the next generation of unified methods:

- Databases of high-quality binding or cohesive energies of molecular systems at equilibrium geometries (S22/S66, S12, C21/X23) have substantially contributed to the development of better vdW-inclusive methods during the last decade. Some of these methods are now able to consistently achieve relative accuracy of 5–10% and absolute accuracy of 1 kcal/mol on these datasets. However, the performance seems to deteriorate once the methods are applied outside the domain of those databases. Substantially more reference data should become available in the next years for increasingly heterogeneous and complex molecular systems, including non-equilibrium geometries and transition states. It remains to be seen how well existing vdW-inclusive methods perform for such more complex benchmarks, representing molecules in more realistic non-equilibrium situations.
- The performance of the methods strongly varies with the complexity and size of a system (Figure 7). For small molecular dimers in the S22/S66 datasets, all methods perform well, but this changes as the systems become increasingly nontrivial. Can we better understand the scaling of vdW interactions with size and complexity? When do many-body or higher-multipole effects become more important? Answering such questions would require development of an efficient method that includes

both multipolar and many-body effects to infinite order in perturbation theory.

- How well do current vdW-inclusive methods model different phases of solids? The nature of bonding strongly depends on the solid structure, and different phases of the same building block (atom, molecule, or cluster) can exhibit very different polarization response. Substantial understanding can be gained by analyzing the performance of vdW-inclusive methods for cohesive and elastic properties of different solid phases. This applies to both hard solids (semiconductors, ionic solids, metals) (Zhang et al., 2011b; Moellmann et al., 2012) and molecular crystals when studying polymorphism (Marom et al., 2013; Reilly and Tkatchenko, 2015; Kronik and Tkatchenko, 2014).
- Is the performance of vdW-inclusive methods uniform across the periodic table? There is some evidence that performance deteriorates for heavier elements and materials with nontrivial electronic states, such as narrow-gap semiconductors, metals, polarizable 2D materials, and topological insulators. Many more benchmarks are required to gain better understanding of the performance for different elements in the periodic table.
- Hybrid interfaces between organic and inorganic systems play an important role in fundamental science and technological applications. The structure and binding of such hybrid interfaces is often determined by vdW interactions (Liu et al., 2014). Considerable experimental data is available for structures and energetics of such interfaces. Continuous assessment of vdW methods for such interface properties is necessary to enable predictive simulations of hybrid systems.
- Do existing vdW-inclusive methods perform consistently for dimers, clusters, and solids of polarizable elements, such as semiconductors and metals? When going from a dimer through larger clusters to a solid, the polarizability scales nonlinearly, and this can have a strong influence on vdW interactions (Tkatchenko et al., 2012; Ruzsinszky et al., 2012; Gobre and Tkatchenko, 2013).
  Do methods exhibit correct scaling of vdW interactions with system size from dimers to large clusters and extended solids?
- Biological systems provide a rich playground for the assessment of vdW-inclusive methods. Much work has been done evaluating different vdW methods on small peptides (Baldauf and Rossi, 2015), protein secondary-structure elements (Tkatchenko et al., 2011), DNA (DiStasio et al., 2012), crystals of biological molecules (DiStasio et al., 2012; Marom et al., 2013; Reilly and Tkatchenko, 2014b; Otero-de-la-Roza et al., 2014), and ions interacting with biological molecules (Rossi et al., 2013; Ngo et al., 2015), among other systems.
- Can we control intermolecular vdW interactions by the presence of nanostructures? Experiments clearly demonstrate that it is possible to dramatically enhance (Loskill et al., 2012, 2013) or attenuate (Tsoi et al., 2014) vdW interactions by the presence of heterostructured surfaces with complex dielectric profiles. Hence, it seems that it should be possible to design molecular interaction profiles by carefully chosen nanostructures with specific geometries and dielectric properties.
- What is the role of microsolvation to full solvation on vdW interactions between solutes. Similar to the previous point, this field is highly controversial (Yang et al., 2013) and demands systematic experimental and theoretical investigations of a wide range of solutes in solvents of varying polarity and polarizability.

7 Concluding remarks

During the last decade, the atomistic modeling community started to understand the broad implications of van der Waals dispersion interactions for a wide variety of molecules and materials. The development of sophisticated first-principles approximations to model vdW interactions lead to exponentially growing "black-box" use of these approaches in combination with semi-local density functionals. However, as is the case with semi-local density-functional approximations, all existing vdW-inclusive methods have their advantages and limitations, and care must be taken when applying these methods to systems outside of their "comfort zone". The contributions of many-body effects, polarization screening, polarizability anisotropy, multipolar expansion, nontrivial electronic states (metallic or topological), coarse-graining of the electronic response function—all these questions remain open to debate in the modeling of vdW interactions in realistic materials.

In this review, we presented a concise discussion of the ingredients necessary for an accurate description of vdW interactions in a wide range of materials (Section 2). The various existing vdW-inclusive methods have been classified according to their treatment of microscopic polarizability and the interaction potential—the two fundamental quantities required for the modeling of vdW interactions. We discussed systems for which the polarizability can be reasonably approximated with local models, and where such local approximations fail. We emphasized the high accuracy in the polarizabilities (and vdW coefficients) of 5–6% that is required to obtain reliable results for the long-range vdW energy; deviations of just 10% in these quantities can lead to unacceptably large errors.

Based on recent landmark experiments probing the nontrivial nature of vdW interactions at the nanoscale, we argued that the ubiquitous many-body effects are crucial for both qualitative understanding and quantitative description of the vdW energy. Furthermore, these experiments demonstrate that our understanding of the quantum-mechanical vdW effects is still only emerging (see Section 3).

We followed by introducing the theoretical framework for calculating vdW interactions based on the adiabatic-connection fluctuation–dissipation (ACFD) theorem in Section 4. This part also discussed the crucial role of different response functions and the relation between them as used by different approximate vdW methods. We emphasize here that the exact treatment of vdW interactions in arbitrary materials can be formulated exclusively using the microscopic dipolar polarizability of the system.

Finally, we reviewed the performance of widely used vdW-

inclusive methods on a variety of molecular binding or cohesive energy databases in Section 5. Although the performance is generally very good for small molecular dimers, only some available methods perform well for larger more complex supramolecular systems and extended molecular crystals. Current efforts directed at obtaining reliable benchmarks for more realistic systems and to applications of vdW methods to increasingly large molecules will provide significant insights into the successes and limitations of different methods.

In summary, painstaking and systematic work on the concepts, theory, and applications of vdW-inclusive methods should eventually enable us to develop an efficient method for vdW interactions with broad applicability in chemistry, biology, physics, and materials science. Such a unified method should be firmly based in the ACFD formalism and combine the best features of interatomic approaches, nonlocal density functionals, and many-body perturbation theory.

References

a. The divergence theorem relates a volume integral of the divergence of a vector field $\mathbf{F}$ to a surface integral of its normal component,

$$\iiint_V \mathrm{d}\mathbf{r}\, \boldsymbol{\nabla}\cdot\mathbf{F} = \oiint_{\partial V} \mathrm{d}\mathbf{S}\cdot\mathbf{F}.$$

A useful form, which resembles integration by parts, is obtained by substituting $\mathbf{F} = g\mathbf{G}$ (where g and $\mathbf{G}$ are scalar and vector fields, respectively),

$$\iiint_V \mathrm{d}\mathbf{r}\, g\boldsymbol{\nabla}\cdot\mathbf{G} = \oiint_{\partial V} \mathbf{dS}\cdot g\mathbf{G} - \iiint_V \mathrm{d}\mathbf{r}\, \mathbf{G}\cdot\boldsymbol{\nabla}g.$$

Often, the divergence theorem is applied in situations when the surface integral vanishes, which is often the case in physics when the volume integral is over the whole space.

b. $Z = Z_{\mathrm{ab}}/48\pi(3\pi^2)^{\frac{1}{3}}$ where Z_{ab} is the constant used in the original article (Lee et al., 2010).

S. L. Adler. Quantum theory of the dielectric constant in real solids. *Phys. Rev.*, 126(2):413–420, Apr. 1962. doi:10.1103/PhysRev.126.413.

J. A. Alonso and A. Mañanes. Long-Range van der Waals Interactions in Density Functional Theory. *Theor. Chem. Acc.*, 117(4):467–472, 2007. doi:10.1007/s00214-006-0079-3.

A. Ambrosetti and P. L. Silvestrelli. Adsorption of Rare-Gas Atoms and Water on Graphite and Graphene by van der Waals-Corrected Density Functional Theory. *J. Phys. Chem. C*, 115(9):3695–3702, Mar. 2011. doi:10.1021/jp110669p.

A. Ambrosetti, D. Alfè, R. A. DiStasio, Jr., and A. Tkatchenko. Hard Numbers for Large Molecules: Toward Exact Energetics for Supramolecular Systems. *J. Phys. Chem. Lett.*, 5(5):849–855, Mar. 2014a. doi:10.1021/jz402663k.

A. Ambrosetti, A. M. Reilly, R. A. DiStasio, Jr., and A. Tkatchenko. Long-range correlation energy calculated from coupled atomic response functions. *J. Chem. Phys.*, 140(18):18A508, May 2014b. doi:10.1063/1.4865104.

A. Ambrosetti, N. Ferri, R. A. DiStasio, Jr., and A. Tkatchenko. Wavelike charge density fluctuations and van der Waals interactions at the nanoscale. *Science*, 351(6278):1171–1176, Mar. 2016. doi:10.1126/science.aae0509.

Y. Andersson, D. C. Langreth, and B. I. Lundqvist. Van der Waals interactions in density-functional theory. *Phys. Rev. Lett.*, 76(1):102–105, Jan. 1996. doi:10.1103/PhysRevLett.76.102.

L. Andrinopoulos, N. D. M. Hine, and A. A. Mostofi. Calculating dispersion interactions using maximally localized Wannier functions. *J. Chem. Phys.*, 135(15):154105, Oct. 2011. doi:10.1063/1.3647912.

J. G. Ángyán. On the exchange-hole model of London dispersion forces. *J. Chem. Phys.*, 127(2):024108, July 2007. doi:10.1063/1.2749512.

J. G. Ángyán, R.-F. Liu, J. Toulouse, and G. Jansen. Correlation Energy Expressions from the Adiabatic-Connection Fluctuation–Dissipation Theorem Approach. *J. Chem. Theory Comput.*, 7(10):3116–3130, 2011. doi:10.1021/ct200501r.

N. Atodiresei, V. Caciuc, P. Lazić, and S. Blügel. Chemical versus van der Waals Interaction: The Role of the Heteroatom in the Flat Absorption of Aromatic Molecules C_6H_6, C_5NH_5, and $C_4N_2H_4$ on the Cu(110) Surface. *Phys. Rev. Lett.*, 102(13):136809, Apr. 2009. doi:10.1103/PhysRevLett.102.136809.

K. Autumn, Y. A. Liang, S. T. Hsieh, W. Zesch, W. P. Chan, T. W. Kenny, R. Fearing, and R. J. Full. Adhesive force of a single gecko foot-hair. *Nature*, 405(6787):681–685, June 2000. doi:10.1038/35015073.

K. Autumn, M. Sitti, Y. A. Liang, A. M. Peattie, W. R. Hansen, S. Sponberg, T. W. Kenny, R. Fearing, J. N. Israelachvili, and R. J. Full. Evidence for van der Waals adhesion in gecko setae. *Proc. Natl. Acad. Sci.*, 99(19): 12252–12256, Sept. 2002. doi:10.1073/pnas.192252799.

B. Axilrod and E. Teller. Interaction of the van der waals type between three atoms. *J. Chem. Phys.*, 11:299–300, 1943.

R. A. Aziz. A highly accurate interatomic potential for argon. *J. Chem. Phys.*, 99(6):4518–4525, Sept. 1993. doi:10.1063/1.466051.

J. F. Babb. Empirically constructed dynamic electric dipole polarizability function of magnesium and its applications. *Phys. Rev. A*, 92:022712, 2015. doi:10.1103/PhysRevA.92.022712.

W. L. Bade. Drude-Model Calculation of Dispersion Forces. I. General Theory. *J. Chem. Phys.*, 27(6):1280–1284, Dec. 1957. doi:10.1063/1.1743991.

W. L. Bade and J. G. Kirkwood. Drude-Model Calculation of Dispersion Forces. II. The Linear Lattice. *J. Chem. Phys.*, 27(6):1284–1288, Dec. 1957. doi:10.1063/1.1743992.

C. Baldauf and M. Rossi. Going clean: Structure and dynamics of peptides in the gas phase and paths to solvation. *J. Phys.: Condens. Matter*, 27(49): 493002, 2015. doi:10.1088/0953-8984/27/49/493002.

C. A. S. Batista, R. G. Larson, and N. A. Kotov. Nonadditivity of nanoparticle interactions. *Science*, 350(6257):1242477, Sept. 2015. doi:10.1126/science.1242477.

A. D. Becke. On the large-gradient behavior of the density functional exchange energy. *J. Chem. Phys.*, 85(12):7184–7187, Dec. 1986. doi:10.1063/1.451353.

A. D. Becke. A multicenter numerical integration scheme for polyatomic molecules. *J. Chem. Phys.*, 88(4):2547–2553, Feb. 1988a. doi:10.1063/1.454033.

A. D. Becke. Density-functional exchange-energy approximation with correct asymptotic behavior. *Phys. Rev. A*, 38(6):3098–3100, Sept. 1988b. doi:10.1103/PhysRevA.38.3098.

A. D. Becke and E. R. Johnson. A density-functional model of the dispersion interaction. *J. Chem. Phys.*, 123(15):154101, Oct. 2005a. doi:10.1063/1.2065267.

A. D. Becke and E. R. Johnson. Exchange-hole dipole moment and the dispersion interaction. *J. Chem. Phys.*, 122(15):154104, Apr. 2005b. doi:10.1063/1.1884601.

A. D. Becke and E. R. Johnson. Exchange-hole dipole moment and the dispersion interaction: High-order dispersion coefficients. *J. Chem. Phys.*, 124 (1):014104, Jan. 2006. doi:10.1063/1.2139668.

A. D. Becke and E. R. Johnson. Exchange-hole dipole moment and the dispersion interaction revisited. *J. Chem. Phys.*, 127(15):154108, Oct. 2007. doi:10.1063/1.2795701.

A. D. Becke and M. R. Roussel. Exchange holes in inhomogeneous systems: A coordinate-space model. *Phys. Rev. A*, 39(8):3761–3767, Apr. 1989. doi:10.1103/PhysRevA.39.3761.

G. J. O. Beran. Modeling Polymorphic Molecular Crystals with Electronic Structure Theory. *Chem. Rev.*, 116(9):5567–5613, May 2016. doi:10.1021/acs.chemrev.5b00648.

T. Bereau and O. A. von Lilienfeld. Toward transferable interatomic van der waals interactions without electrons: The role of multipole electrostatics and many-body dispersion. *J. Chem. Phys.*, 141(3):034101, 2014.

K. Berland and P. Hyldgaard. Analysis of van der Waals density functional components: Binding and corrugation of benzene and C_{60} on boron nitride and graphene. *Phys. Rev. B*, 87(20):205421, May 2013. doi:10.1103/PhysRevB.87.205421.

K. Berland and P. Hyldgaard. Exchange functional that tests the robustness of the plasmon description of the van der Waals density functional. *Phys. Rev. B*, 89(3):035412, Jan. 2014. doi:10.1103/PhysRevB.89.035412.

K. Berland, V. R. Cooper, K. Lee, E. Schröder, T. Thonhauser, P. Hyldgaard, and B. I. Lundqvist. Van der Waals forces in density functional theory: A review of the vdW-DF method. *Rep. Prog. Phys.*, 78(6):066501, June 2015. doi:10.1088/0034-4885/78/6/066501.

T. Björkman. Van der Waals density functional for solids. *Phys. Rev. B*, 86 (16):165109, Oct. 2012. doi:10.1103/PhysRevB.86.165109.

T. Björkman. Testing several recent van der Waals density functionals for layered structures. *J. Chem. Phys.*, 141(7):074708, Aug. 2014.

doi:10.1063/1.4893329.

T. Björkman, A. Gulans, A. V. Krasheninnikov, and R. M. Nieminen. Are we van der Waals ready? *J. Phys.: Condens. Matter*, 24(42):424218, 2012. doi:10.1088/0953-8984/24/42/424218.

P. Bleiziffer, A. Heßelmann, and A. Görling. Efficient self-consistent treatment of electron correlation within the random phase approximation. *J. Chem. Phys.*, 139(8):084113, Aug. 2013. doi:10.1063/1.4818984.

M. A. Blood-Forsythe, T. Markovich, R. A. DiStasio, Jr., R. Car, and A. Aspuru-Guzik. Analytical nuclear gradients for the range-separated many-body dispersion model of noncovalent interactions. *Chem. Sci.*, 7(3):1712–1728, Feb. 2016. doi:10.1039/C5SC03234B.

O. Bludský, M. Rubeš, P. Soldán, and P. Nachtigall. Investigation of the benzene-dimer potential energy surface: DFT/CCSD(T) correction scheme. *J. Chem. Phys.*, 128(11):114102, Mar. 2008. doi:10.1063/1.2890968.

A. D. Boese. Density Functional Theory and Hydrogen Bonds: Are We There Yet? *ChemPhysChem*, 16(5):978–985, Apr. 2015. doi:10.1002/cphc.201402786.

M. Bordag, B. Geyer, G. L. Klimchitskaya, and V. M. Mostepanenko. Lifshitz-type formulas for graphene and single-wall carbon nanotubes: Van der Waals and Casimir interactions. *Phys. Rev. B*, 74(20):205431, Nov. 2006. doi:10.1103/PhysRevB.74.205431.

J. G. Brandenburg, M. Alessio, B. Civalleri, M. F. Peintinger, T. Bredow, and S. Grimme. Geometrical Correction for the Inter- and Intramolecular Basis Set Superposition Error in Periodic Density Functional Theory Calculations. *J. Phys. Chem. A*, 117(38):9282–9292, Sept. 2013. doi:10.1021/jp406658y.

T. Brinck, J. S. Murray, and P. Politzer. Polarizability and volume. *J. Chem. Phys.*, 98(5):4305–4306, Mar. 1993. doi:10.1063/1.465038.

E. Brémond, N. Golubev, S. N. Steinmann, and C. Corminboeuf. How important is self-consistency for the dDsC density dependent dispersion correction? *J. Chem. Phys.*, 140:18A516, 2014. doi:10.1063/1.4867195.

T. Bučko, S. Lebègue, J. Hafner, and J. G. Ángyán. Improved Density Dependent Correction for the Description of London Dispersion Forces. *J. Chem. Theory Comput.*, 9(10):4293–4299, Oct. 2013a. doi:10.1021/ct400694h.

T. Bučko, S. Lebègue, J. Hafner, and J. G. Ángyán. Tkatchenko-Scheffler van der Waals correction method with and without self-consistent screening applied to solids. *Phys. Rev. B*, 87(6):064110, Feb. 2013b. doi:10.1103/PhysRevB.87.064110.

T. Bučko, S. Lebègue, J. G. Ángyán, and J. Hafner. Extending the applicability of the Tkatchenko-Scheffler dispersion correction via iterative Hirshfeld partitioning. *J. Chem. Phys.*, 141(3):034114, July 2014. doi:10.1063/1.4890003.

T. Bučko, S. Lebègue, T. Gould, and J. G. Ángyán. Many-body dispersion corrections for periodic systems: An efficient reciprocal space implementation. *J. Phys.: Condens. Matter*, 28(4):045201, 2016. doi:10.1088/0953-8984/28/4/045201.

P. Bultinck, C. V. Alsenoy, P. W. Ayers, and R. Carbó-Dorca. Critical analysis and extension of the Hirshfeld atoms in molecules. *J. Chem. Phys.*, 126 (14):144111, Apr. 2007. doi:10.1063/1.2715563.

K. Burke. Perspective on density functional theory. *J. Chem. Phys.*, 136(15): 150901, Apr. 2012. doi:10.1063/1.4704546.

C. Bürker, N. Ferri, A. Tkatchenko, A. Gerlach, J. Niederhausen, T. Hosokai, S. Duhm, J. Zegenhagen, N. Koch, and F. Schreiber. Exploring the bonding of large hydrocarbons on noble metals: Diindoperylene on Cu(111), Ag(111), and Au(111). *Phys. Rev. B*, 87(16):165443, Apr. 2013. doi:10.1103/PhysRevB.87.165443.

L. A. Burns, Á. Vázquez-Mayagoitia, B. G. Sumpter, and C. D. Sherrill. Density-functional approaches to noncovalent interactions: A comparison of dispersion corrections (DFT-D), exchange-hole dipole moment (XDM) theory, and specialized functionals. *J. Chem. Phys.*, 134(8):084107, Feb. 2011. doi:10.1063/1.3545971.

H. B. Callen and T. A. Welton. Irreversibility and generalized noise. *Phys. Rev.*, 83(1):34–40, July 1951. doi:10.1103/PhysRev.83.34.

J. Carrasco, W. Liu, A. Michaelides, and A. Tkatchenko. Insight into the description of van der Waals forces for benzene adsorption on transition metal (111) surfaces. *J. Chem. Phys.*, 140(8):084704, Feb. 2014. doi:10.1063/1.4866175.

D. J. Carter and A. L. Rohl. Benchmarking Calculated Lattice Parameters and Energies of Molecular Crystals Using van der Waals Density Functionals. *J. Chem. Theory Comput.*, 10(8):3423–3437, Aug. 2014. doi:10.1021/ct500335b.

S. D. Chakarova-Käck, E. Schröder, B. I. Lundqvist, and D. C. Langreth. Application of van der Waals Density Functional to an Extended System: Adsorption of Benzene and Naphthalene on Graphite. *Phys. Rev. Lett.*, 96 (14):146107, Apr. 2006. doi:10.1103/PhysRevLett.96.146107.

X. Chu and A. Dalgarno. Linear response time-dependent density functional theory for van der Waals coefficients. *J. Chem. Phys.*, 121(9):4083–4088, Sept. 2004. doi:10.1063/1.1779576.

T. S. Chwee and M. B. Sullivan. Adsorption studies of C6H6 on Cu (111), Ag (111), and Au (111) within dispersion corrected density functional theory. *J. Chem. Phys.*, 137(13):134703, Oct. 2012. doi:10.1063/1.4755993.

A. J. Cohen, P. Mori-Sánchez, and W. Yang. Challenges for Density Functional Theory. *Chem. Rev.*, 112(1):289–320, Jan. 2012. doi:10.1021/cr200107z.

D. J. Cole, J. Z. Vilseck, J. Tirado-Rives, M. C. Payne, and W. L. Jorgensen. Biomolecular force field parameterization via atoms-in-molecule electron density partitioning. *J. Chem. Theory Comput.*, 12:2312–2323, 2016. doi:10.1021/acs.jctc.6b00027.

V. R. Cooper. Van der Waals density functional: An appropriate exchange functional. *Phys. Rev. B*, 81(16):161104, Apr. 2010. doi:10.1103/PhysRevB.81.161104.

V. R. Cooper, T. Thonhauser, and D. C. Langreth. An application of the van der Waals density functional: Hydrogen bonding and stacking interactions between nucleobases. *J. Chem. Phys.*, 128(20):204102, May 2008. doi:10.1063/1.2924133.

A. J. Cruz-Cabeza, S. M. Reutzel-Edens, and J. Bernstein. Facts and fictions about polymorphism. *Chem. Soc. Rev.*, 44:8619–8635, 2015. doi:10.1039/C5CS00227C.

H. G. M. de Wit, J. A. Bouwstra, J. G. Blok, and C. G. de Kruif. Vapor pressures and lattice energies of oxalic acid, mesotartaric acid, phloroglucinol, myoinositol, and their hydrates. *J. Chem. Phys.*, 78(3):1470–1475, 1983. doi:10.1063/1.444836.

M. Del Ben, J. Hutter, and J. VandeVondele. Electron Correlation in the Condensed Phase from a Resolution of Identity Approach Based on the Gaussian and Plane Waves Scheme. *J. Chem. Theory Comput.*, 9(6):2654–2671, June 2013a. doi:10.1021/ct4002202.

M. Del Ben, M. Schönherr, J. Hutter, and J. VandeVondele. Bulk Liquid Water at Ambient Temperature and Pressure from MP2 Theory. *J. Phys. Chem. Lett.*, 4(21):3753–3759, Nov. 2013b. doi:10.1021/jz401931f.

G. A. DiLabio. Accurate treatment of van der Waals interactions using standard density functional theory methods with effective core-type potentials: Application to carbon-containing dimers. *Chem. Phys. Lett.*, 455(4-6): 348–353, Apr. 2008. doi:10.1016/j.cplett.2008.02.110.

M. Dion, H. Rydberg, E. Schröder, D. C. Langreth, and B. I. Lundqvist. Van der Waals density functional for general geometries. *Phys. Rev. Lett.*, 92 (24):246401, June 2004. doi:10.1103/PhysRevLett.92.246401.

J. DiStasio, Robert A., B. Santra, Z. Li, X. Wu, and R. Car. The individual and collective effects of exact exchange and dispersion interactions on the ab initio structure of liquid water. *J. Chem. Phys.*, 141(8):084502, Aug. 2014a. doi:10.1063/1.4893377.

R. A. DiStasio, Jr., G. von Helden, R. P. Steele, and M. Head-Gordon. On the T-shaped structures of the benzene dimer. *Chem. Phys. Lett.*, 437(4-6): 277–283, Apr. 2007. doi:10.1016/j.cplett.2007.02.034.

R. A. DiStasio, Jr., O. A. von Lilienfeld, and A. Tkatchenko. Collective many-body van der Waals interactions in molecular systems. *Proc. Natl. Acad. Sci. U. S. A.*, 109(37):14791–14795, Nov. 2012. doi:10.1073/pnas.1208121109.

R. A. DiStasio, Jr., V. V. Gobre, and A. Tkatchenko. Many-body van der Waals interactions in molecules and condensed matter. *J. Phys.: Condens. Matter*, 26(21):213202, May 2014b. doi:10.1088/0953-8984/26/21/213202.

J. F. Dobson. Beyond pairwise additivity in London dispersion interactions. *Int. J. Quantum Chem.*, 114(18):1157–1161, Sept. 2014. doi:10.1002/qua.24635.

J. F. Dobson and B. P. Dinte. Constraint Satisfaction in Local and Gradient Susceptibility Approximations: Application to a van der Waals Density Functional. *Phys. Rev. Lett.*, 76(11):1780–1783, Mar. 1996. doi:10.1103/PhysRevLett.76.1780.

J. F. Dobson and T. Gould. Calculation of dispersion energies. *J. Phys.: Condens. Matter*, 24(7):073201, Feb. 2012. doi:10.1088/0953-8984/24/7/073201.

J. F. Dobson, A. White, and A. Rubio. Asymptotics of the Dispersion Interaction: Analytic Benchmarks for van der Waals Energy Functionals. *Phys. Rev. Lett.*, 96(7):073201, Feb. 2006. doi:10.1103/PhysRevLett.96.073201.

J. F. Dobson, T. Gould, and G. Vignale. How many-body effects modify the van der waals interaction between graphene sheets. *Phys. Rev. X*, 4:021040, 2014.

A. G. Donchev. Many-body effects of dispersion interaction. *J. Chem. Phys.*, 125(7):074713, Aug. 2006. doi:10.1063/1.2337283.

R. Eisenschitz and F. London. Über das Verhältnis der van der Waalsschen

Kräfte zu den homöopolaren Bindungskräften [On relationship between van der Waals forces and covalent bonds]. *Z. Physik*, 60(7-8):491–527, July 1930. doi:10.1007/BF01341258.

M. Elstner, P. Hobza, T. Frauenheim, S. Suhai, and E. Kaxiras. Hydrogen bonding and stacking interactions of nucleic acid base pairs: A density-functional-theory based treatment. *J. Chem. Phys.*, 114(12):5149–5155, Mar. 2001. doi:10.1063/1.1329889.

H. Eshuis and F. Furche. Basis set convergence of molecular correlation energy differences within the random phase approximation. *J. Chem. Phys.*, 136 (8):084105, Feb. 2012. doi:10.1063/1.3687005.

H. Eshuis, J. E. Bates, and F. Furche. Electron correlation methods based on the random phase approximation. *Theor. Chem. Acc.*, 131(1):1–18, Jan. 2012. doi:10.1007/s00214-011-1084-8.

J. C. Faver, M. L. Benson, X. He, B. P. Roberts, B. Wang, M. S. Marshall, M. R. Kennedy, C. D. Sherrill, and K. M. Merz. Formal Estimation of Errors in Computed Absolute Interaction Energies of Protein-Ligand Complexes. *J. Chem. Theory Comput.*, 7(3):790–797, Mar. 2011. doi:10.1021/ct100563b.

N. Ferri, R. A. DiStasio, Jr., A. Ambrosetti, R. Car, and A. Tkatchenko. Electronic Properties of Molecules and Surfaces with a Self-Consistent Interatomic van der Waals Density Functional. *Phys. Rev. Lett.*, 114(17):176802, Apr. 2015. doi:10.1103/PhysRevLett.114.176802.

R. P. Feynman. Forces in Molecules. *Phys. Rev.*, 56(4):340–343, Aug. 1939. doi:10.1103/PhysRev.56.340.

C. Fiolhais, F. Nogueira, and M. A. L. Marques, editors. *A Primer in Density Functional Theory*. Springer Berlin Heidelberg, 2003. URL http://dx.doi.org/10.1007/3-540-37072-2.

P. W. Fowler, J. H. Harding, and N. C. Pyper. The polarizabilities and dispersion coefficients for ions in the solid group IV oxides. *J. Phys.: Condens. Matter*, 6:10593, 1994. URL http://stacks.iop.org/0953-8984/6/i=48/a=018.

R. H. French, V. A. Parsegian, R. Podgornik, R. F. Rajter, A. Jagota, J. Luo, D. Asthagiri, M. K. Chaudhury, Y.-m. Chiang, S. Granick, S. Kalinin, M. Kardar, R. Kjellander, D. C. Langreth, J. Lewis, S. Lustig, D. Wesolowski, J. S. Wettlaufer, W.-Y. Ching, M. Finnis, F. Houlihan, O. A. von Lilienfeld, C. J. van Oss, and T. Zemb. Long range interactions in nanoscale science. *Rev. Mod. Phys.*, 82:1887–1944, 2010. doi:10.1103/RevModPhys.82.1887.

F. Furche. Molecular tests of the random phase approximation to the exchange-correlation energy functional. *Phys. Rev. B*, 64(19):195120, Oct. 2001. doi:10.1103/PhysRevB.64.195120.

W. Gao and A. Tkatchenko. Electronic Structure and van der Waals Interactions in the Stability and Mobility of Point Defects in Semiconductors. *Phys. Rev. Lett.*, 111(4):045501, July 2013. doi:10.1103/PhysRevLett.111.045501.

W. Gao and A. Tkatchenko. Sliding Mechanisms in Multilayered Hexagonal Boron Nitride and Graphene: The Effects of Directionality, Thickness, and Sliding Constraints. *Phys. Rev. Lett.*, 114(9):096101, Mar. 2015. doi:10.1103/PhysRevLett.114.096101.

X. Ge and D. Lu. Local representation of the electronic dielectric response function. *Phys. Rev. B*, 92(24):241107, Dec. 2015. doi:10.1103/PhysRevB.92.241107.

P. L. Geissler, C. Dellago, D. Chandler, J. Hutter, and M. Parrinello. Autoionization in Liquid Water. *Science*, 291(5511):2121–2124, Mar. 2001. doi:10.1126/science.1056991.

M. J. Gillan, D. Alfè, and A. Michaelides. Perspective: How good is DFT for water? *J. Chem. Phys.*, 144(13):130901, Apr. 2016. doi:10.1063/1.4944633.

V. V. Gobre and A. Tkatchenko. Scaling laws for van der Waals interactions in nanostructured materials. *Nat. Commun.*, 4:2341, Aug. 2013. doi:10.1038/ncomms3341.

A. Görling. Exact exchange kernel for time-dependent density-functional theory. *Int. J. Quantum Chem.*, 69(3):265–277, Jan. 1998. doi:10.1002/(SICI)1097-461X(1998)69:3<265::AID-QUA6>3.0.CO;2-T.

T. Gould. Communication: Beyond the random phase approximation on the cheap: Improved correlation energies with the efficient "radial exchange hole" kernel. *J. Chem. Phys.*, 137(11):111101, Sept. 2012. doi:10.1063/1.4755286.

T. Gould and T. Bučko. C6 Coefficients and dipole polarizabilities for all atoms and many ions in rows 1-6 of the periodic table. *J. Chem. Theory Comput.*, 12(ja):3603–3613, 2016. doi:10.1021/acs.jctc.6b00361.

G. Graziano, J. Klimeš, F. Fernandez-Alonso, and A. Michaelides. Improved description of soft layered materials with van der Waals density functional theory. *J. Phys.: Condens. Matter*, 24(42):424216, Oct. 2012. doi:10.1088/0953-8984/24/42/424216.

S. Grimme. Accurate description of van der Waals complexes by density functional theory including empirical corrections. *J. Comput. Chem.*, 25 (12):1463–1473, Sept. 2004. doi:10.1002/jcc.20078.

S. Grimme. Semiempirical GGA-type density functional constructed with a long-range dispersion correction. *J. Comput. Chem.*, 27(15):1787–1799, Nov. 2006. doi:10.1002/jcc.20495.

S. Grimme. Density functional theory with London dispersion corrections. *Wiley Interdiscip. Rev. Comput. Mol. Sci.*, 1(2):211–228, Mar. 2011. doi:10.1002/wcms.30.

S. Grimme. Supramolecular Binding Thermodynamics by Dispersion-Corrected Density Functional Theory. *Chem. Eur. J.*, 18(32):9955–9964, Aug. 2012. doi:10.1002/chem.201200497.

S. Grimme, J. Antony, S. Ehrlich, and H. Krieg. A consistent and accurate ab initio parametrization of density functional dispersion correction (DFT-D) for the 94 elements H-Pu. *J. Chem. Phys.*, 132(15):154104, Apr. 2010. doi:10.1063/1.3382344.

S. Grimme, A. Hansen, J. G. Brandenburg, and C. Bannwarth. Dispersion-Corrected Mean-Field Electronic Structure Methods. *Chem. Rev.*, 116(9): 5105–5154, May 2016. doi:10.1021/acs.chemrev.5b00533.

A. Gulans, M. J. Puska, and R. M. Nieminen. Linear-scaling self-consistent implementation of the van der Waals density functional. *Phys. Rev. B*, 79 (20):201105, May 2009. doi:10.1103/PhysRevB.79.201105.

I. Hamada. Van der Waals density functional made accurate. *Phys. Rev. B*, 89 (12):121103, Mar. 2014. doi:10.1103/PhysRevB.89.121103.

I. Hamada and M. Otani. Comparative van der Waals density-functional study of graphene on metal surfaces. *Phys. Rev. B*, 82(15):153412, Oct. 2010. doi:10.1103/PhysRevB.82.153412.

A. Hansen, C. Bannwarth, S. Grimme, P. Petrović, C. Werlé, and J.-P. Djukic. The Thermochemistry of London Dispersion-Driven Transition Metal Reactions: Getting the 'Right Answer for the Right Reason'. *ChemistryOpen*, 3(5):177–189, Oct. 2014. doi:10.1002/open.201402017.

E. H. Hardy, A. Zygar, M. D. Zeidler, M. Holz, and F. D. Sacher. Isotope effect on the translational and rotational motion in liquid water and ammonia. *J. Chem. Phys.*, 114(7):3174–3181, Feb. 2001. doi:10.1063/1.1340584.

J. Harris and R. O. Jones. The surface energy of a bounded electron gas. *J. Phys. F: Met. Phys.*, 4(8):1170–1186, 1974. doi:10.1088/0305-4608/4/8/013.

J. Hepburn, G. Scoles, and R. Penco. A simple but reliable method for the prediction of intermolecular potentials. *Chem. Phys. Lett.*, 36(4):451–456, Dec. 1975. doi:10.1016/0009-2614(75)80278-8.

A. Heßelmann. Derivation of the dispersion energy as an explicit density- and exchange-hole functional. *J. Chem. Phys.*, 130(8):084104, Feb. 2009. doi:10.1063/1.3077939.

A. Heßelmann. Long-range correlation energies from frequency-dependent weighted exchange-hole dipole polarisabilities. *J. Chem. Phys.*, 136(1): 014104, Jan. 2012. doi:10.1063/1.3672236.

A. Heßelmann and A. Görling. Random phase approximation correlation energies with exact Kohn–Sham exchange. *Mol. Phys.*, 108(3-4):359–372, Feb. 2010. doi:10.1080/00268970903476662.

F. L. Hirshfeld. Bonded-atom fragments for describing molecular charge densities. *Theoret. Chim. Acta*, 44(2):129–138, June 1977. doi:10.1007/BF00549096.

P. Hobza, H. L. Selzle, and E. W. Schlag. Potential Energy Surface for the Benzene Dimer. Results of ab Initio CCSD(T) Calculations Show Two Nearly Isoenergetic Structures: T-Shaped and Parallel-Displaced. *J. Phys. Chem.*, 100(48):18790–18794, Jan. 1996. doi:10.1021/jp961239y.

J. Hoja, A. F. Sax, and K. Szalewicz. Is Electrostatics Sufficient to Describe Hydrogen-Bonding Interactions? *Chem. Eur. J.*, 20(8):2292–2300, Feb. 2014. doi:10.1002/chem.201303528.

J. Hoja, A. M. Reilly, and A. Tkatchenko. First-principles modeling of molecular crystals: Structures and stabilities, temperature and pressure. *Wiley Interdiscip. Rev. Comput. Mol. Sci.*, 7(1):e1294, 2017. ISSN 1759-0884. doi:10.1002/wcms.1294. e1294.

W. Hujo and S. Grimme. Performance of the van der Waals Density Functional VV10 and (hybrid)GGA Variants for Thermochemistry and Noncovalent Interactions. *J. Chem. Theory Comput.*, 7(12):3866–3871, Dec. 2011. doi:10.1021/ct200644w.

K. L. C. Hunt. Dispersion dipoles and dispersion forces: Proof of Feynman's "conjecture" and generalization to interacting molecules of arbitrary symmetry. *J. Chem. Phys.*, 92(2):1180–1187, Jan. 1990. doi:10.1063/1.458126.

P. Hyldgaard, K. Berland, and E. Schröder. Interpretation of van der Waals density functionals. *Phys. Rev. B*, 90(7):075148, Aug. 2014. doi:10.1103/PhysRevB.90.075148.

T. Ikeshoji, M. Otani, I. Hamada, and Y. Okamoto. Reversible redox reaction

and water configuration on a positively charged platinum surface: First principles molecular dynamics simulation. *Phys. Chem. Chem. Phys.*, 13 (45):20223–20227, Nov. 2011. doi:10.1039/C1CP21969C.

R. L. Jaffe and G. D. Smith. A quantum chemistry study of benzene dimer. *J. Chem. Phys.*, 105(7):2780–2788, Aug. 1996. doi:10.1063/1.472140.

G. Jansen, R.-F. Liu, and J. G. Ángyán. On the equivalence of ring-coupled cluster and adiabatic connection fluctuation-dissipation theorem random phase approximation correlation energy expressions. *J. Chem. Phys.*, 133 (15):154106, Oct. 2010. doi:10.1063/1.3481575.

L. Jensen, P.-O. Åstrand, A. Osted, J. Kongsted, and K. V. Mikkelsen. Polarizability of molecular clusters as calculated by a dipole interaction model. *J. Chem. Phys.*, 116(10):4001–4010, Mar. 2002. doi:10.1063/1.1433747.

L. L. Jensen and L. Jensen. Atomistic Electrodynamics Model for Optical Properties of Silver Nanoclusters. *J. Phys. Chem. C*, 113(34):15182–15190, Aug. 2009. doi:10.1021/jp904956f.

B. Jeziorski, R. Moszynski, and K. Szalewicz. Perturbation Theory Approach to Intermolecular Potential Energy Surfaces of van der Waals Complexes. *Chem. Rev.*, 94(7):1887–1930, Nov. 1994. doi:10.1021/cr00031a008.

E. R. Johnson. Dependence of dispersion coefficients on atomic environment. *J. Chem. Phys.*, 135(23):234109, Dec. 2011. doi:10.1063/1.3670015.

E. R. Johnson and A. D. Becke. A post-Hartree–Fock model of intermolecular interactions. *J. Chem. Phys.*, 123(2):024101, July 2005. doi:10.1063/1.1949201.

E. R. Johnson and A. D. Becke. A post-Hartree-Fock model of intermolecular interactions: Inclusion of higher-order corrections. *J. Chem. Phys.*, 124 (17):174104, May 2006. doi:10.1063/1.2190220.

E. R. Johnson, I. D. Mackie, and G. A. DiLabio. Dispersion interactions in density-functional theory. *J. Phys. Org. Chem.*, 22(12):1127–1135, Dec. 2009. doi:10.1002/poc.1606.

R. Jonchiere, A. P. Seitsonen, G. Ferlat, A. M. Saitta, and R. Vuilleumier. Van der Waals effects in ab initio water at ambient and supercritical conditions. *J. Chem. Phys.*, 135(15):154503, Oct. 2011. doi:10.1063/1.3651474.

A. Jones, F. Cipcigan, V. P. Sokhan, J. Crain, and G. J. Martyna. Electronically Coarse-Grained Model for Water. *Phys. Rev. Lett.*, 110(22):227801, May 2013a. doi:10.1103/PhysRevLett.110.227801.

A. P. Jones, J. Crain, V. P. Sokhan, T. W. Whitfield, and G. J. Martyna. Quantum Drude oscillator model of atoms and molecules: Many-body polarization and dispersion interactions for atomistic simulation. *Phys. Rev. B*, 87(14): 144103, Apr. 2013b. doi:10.1103/PhysRevB.87.144103.

P. Jurečka, J. Šponer, J. Černý, and P. Hobza. Benchmark database of accurate (MP2 and CCSD(T) complete basis set limit) interaction energies of small model complexes, DNA base pairs, and amino acid pairs. *Phys. Chem. Chem. Phys.*, 8(17):1985–1993, Apr. 2006. doi:10.1039/B600027D.

F. O. Kannemann and A. D. Becke. Van der Waals Interactions in Density-Functional Theory: Intermolecular Complexes. *J. Chem. Theory Comput.*, 6(4):1081–1088, Apr. 2010. doi:10.1021/ct900699r.

I. G. Kaplan. *Intermolecular Interactions*. Wiley-Blackwell, Apr. 2006. URL http://dx.doi.org/10.1002/047086334x.

O. Karalti, X. Su, W. A. Al-Saidi, and K. D. Jordan. Correcting density functionals for dispersion interactions using pseudopotentials. *Chem. Phys. Lett.*, 591:133–136, 2014.

M. R. Kennedy, A. R. McDonald, I. DePrince, A. Eugene, M. S. Marshall, R. Podeszwa, and C. D. Sherrill. Communication: Resolving the three-body contribution to the lattice energy of crystalline benzene: Benchmark results from coupled-cluster theory. *J. Chem. Phys.*, 140(12):121104, Mar. 2014. doi:10.1063/1.4869686.

G. L. Klimchitskaya, U. Mohideen, and V. M. Mostepanenko. The Casimir force between real materials: Experiment and theory. *Rev. Mod. Phys.*, 81 (4):1827–1885, Dec. 2009. doi:10.1103/RevModPhys.81.1827.

J. Klimeš and A. Michaelides. Perspective: Advances and challenges in treating van der Waals dispersion forces in density functional theory. *J. Chem. Phys.*, 137(12):120901, Sept. 2012. doi:10.1063/1.4754130.

J. Klimeš, D. R. Bowler, and A. Michaelides. Chemical accuracy for the van der Waals density functional. *J. Phys.: Condens. Matter*, 22(2):022201, 2010. doi:10.1088/0953-8984/22/2/022201.

J. Klimeš, D. R. Bowler, and A. Michaelides. Van der Waals density functionals applied to solids. *Phys. Rev. B*, 83(19):195131, May 2011. doi:10.1103/PhysRevB.83.195131.

J. Klimeš, M. Kaltak, E. Maggio, and G. Kresse. Singles correlation energy contributions in solids. *J. Chem. Phys.*, 143(10):102816, Aug. 2015. doi:10.1063/1.4929346.

W. Koch and M. C. Holthausen. *A Chemist's Guide to Density Functional Theory*. John Wiley & Sons, 2015.

M. Kohtani, T. C. Jones, J. E. Schneider, and M. F. Jarrold. Extreme Stability of an Unsolvated α-Helix. *J. Am. Chem. Soc.*, 126(24):7420–7421, June 2004. doi:10.1021/ja048766c.

J. Kong, Z. Gan, E. Proynov, M. Freindorf, and T. R. Furlani. Efficient computation of the dispersion interaction with density-functional theory. *Phys. Rev. A*, 79(4):042510, Apr. 2009. doi:10.1103/PhysRevA.79.042510.

A. Krishtal, K. Vannomeslaeghe, D. Geldof, C. Van Alsenoy, and P. Geerlings. Importance of anisotropy in the evaluation of dispersion interactions. *Phys. Rev. A*, 83(2):024501, Feb. 2011. doi:10.1103/PhysRevA.83.024501.

L. Kronik and A. Tkatchenko. Understanding Molecular Crystals with Dispersion-Inclusive Density Functional Theory: Pairwise Corrections and Beyond. *Acc. Chem. Res.*, 47(11):3208–3216, Nov. 2014. doi:10.1021/ar500144s.

S. Kurth and J. P. Perdew. Density-functional correction of random-phase-approximation correlation with results for jellium surface energies. *Phys. Rev. B*, 59(16):10461–10468, Apr. 1999. doi:10.1103/PhysRevB.59.10461.

L. D. Landau and E. M. Lifschitz. *Statistical Physics*, volume 5. Pergamon Press, Oxford, 3rd edition, Jan. 1980. ISBN 978-0-7506-3372-7.

D. Langbein. *Theory of Van Der Waals Attraction*, volume 72 of *Springer Tracts in Modern Physics*. Springer Berlin Heidelberg, 1974. ISBN 978-3-540-06742-9 978-3-540-38332-1. doi:10.1007/BFb0042407. URL http://link.springer.com/chapter/10.1007/BFb0042407.

D. C. Langreth and B. I. Lundqvist. Comment on "Nonlocal Van Der Waals Density Functional Made Simple". *Phys. Rev. Lett.*, 104(9):099303, Mar. 2010. doi:10.1103/PhysRevLett.104.099303.

D. C. Langreth and J. P. Perdew. Exchange-correlation energy of a metallic surface: Wave-vector analysis. *Phys. Rev. B*, 15(6):2884–2901, Mar. 1977. doi:10.1103/PhysRevB.15.2884.

D. C. Langreth, M. Dion, H. Rydberg, E. Schröder, P. Hyldgaard, and B. I. Lundqvist. Van der Waals density functional theory with applications. *Int. J. Quantum Chem.*, 101(5):599–610, 2005. doi:10.1002/qua.20315.

D. C. Langreth, B. I. Lundqvist, S. D. Chakarova-Käck, V. R. Cooper, M. Dion, P. Hyldgaard, A. Kelkkanen, J. Kleis, L. Kong, S. Li, P. G. Moses, E. Murray, A. Puzder, H. Rydberg, E. Schröder, and T. Thonhauser. A density functional for sparse matter. *J. Phys.: Condens. Matter*, 21(8):084203, Feb. 2009. doi:10.1088/0953-8984/21/8/084203.

H. Larsen, J. Olsen, C. Hättig, P. Jørgensen, O. Christiansen, and J. Gauss. Polarizabilities and first hyperpolarizabilities of HF, Ne, and BH from full configuration interaction and coupled cluster calculations. *J. Chem. Phys.*, 111(5):1917–1925, July 1999. doi:10.1063/1.479460.

S. Lebègue, J. Harl, T. Gould, J. G. Ángyán, G. Kresse, and J. F. Dobson. Cohesive Properties and Asymptotics of the Dispersion Interaction in Graphite by the Random Phase Approximation. *Phys. Rev. Lett.*, 105(19):196401, Nov. 2010. doi:10.1103/PhysRevLett.105.196401.

K. Lee, É. D. Murray, L. Kong, B. I. Lundqvist, and D. C. Langreth. Higher-accuracy van der Waals density functional. *Phys. Rev. B*, 82(8):081101, Aug. 2010. doi:10.1103/PhysRevB.82.081101.

E. M. Lifshitz. The theory of molecular attractive forces between solids (M. Hamermesh, transl.). *Sov. Phys. JEPT*, 2(1):73–83, 1956. URL http://www.jetp.ac.ru/cgi-bin/e/index/e/2/1/p73?a=list.

O. A. v. Lilienfeld and A. Tkatchenko. Two- and three-body interatomic dispersion energy contributions to binding in molecules and solids. *J. Chem. Phys.*, 132(23):234109, June 2010. doi:10.1063/1.3432765.

I.-C. Lin, A. P. Seitsonen, M. D. Coutinho-Neto, I. Tavernelli, and U. Rothlisberger. Importance of van der Waals Interactions in Liquid Water. *J. Phys. Chem. B*, 113(4):1127–1131, Jan. 2009. doi:10.1021/jp806376e.

W. Liu, V. G. Ruiz, G.-X. Zhang, B. Santra, X. Ren, M. Scheffler, and A. Tkatchenko. Structure and energetics of benzene adsorbed on transition-metal surfaces: Density-functional theory with van der Waals interactions including collective substrate response. *New J. Phys.*, 15(5):053046, 2013. doi:10.1088/1367-2630/15/5/053046.

W. Liu, A. Tkatchenko, and M. Scheffler. Modeling adsorption and reactions of organic molecules at metal surfaces. *Acc. Chem. Res.*, 47(11):3369–3377, 2014.

W. Liu, F. Maaß, M. Willenbockel, C. Bronner, M. Schulze, S. Soubatch, F. S. Tautz, P. Tegeder, and A. Tkatchenko. Quantitative Prediction of Molecular Adsorption: Structure and Binding of Benzene on Coinage Metals. *Phys. Rev. Lett.*, 115(3):036104, July 2015. doi:10.1103/PhysRevLett.115.036104.

F. London. Zur Theorie und Systematik der Molekularkräfte [On theory and classification of molecular forces]. *Z. Physik*, 63(3-4):245–279, Mar. 1930. doi:10.1007/BF01421741.

F. London. The general theory of molecular forces. *Trans. Faraday Soc.*, 33

(0):8–26, Jan. 1937. doi:10.1039/TF937330008B.

P. Loskill, H. Hähl, T. Faidt, S. Grandthyll, F. Müller, and K. Jacobs. Is adhesion superficial? Silicon wafers as a model system to study van der Waals interactions. *Adv. Colloid Interface Sci.*, 179–182:107–113, Nov. 2012. doi:10.1016/j.cis.2012.06.006.

P. Loskill, J. Puthoff, M. Wilkinson, K. Mecke, K. Jacobs, and K. Autumn. Macroscale adhesion of gecko setae reflects nanoscale differences in subsurface composition. *J. R. Soc. Interface*, 10(78):20120587, Jan. 2013. doi:10.1098/rsif.2012.0587.

D. Lu, Y. Li, D. Rocca, and G. Galli. Ab initio Calculation of van der Waals Bonded Molecular Crystals. *Phys. Rev. Lett.*, 102(20):206411, May 2009. doi:10.1103/PhysRevLett.102.206411.

A. Lucas. Collective contributions to the long-range dipolar interaction in rare-gas crystals. *Physica*, 35(3):353–368, 1967. doi:10.1016/0031-8914(67)90184-X.

Z. Ma, Y. Zhang, and M. E. Tuckerman. Ab initio molecular dynamics study of water at constant pressure using converged basis sets and empirical dispersion corrections. *J. Chem. Phys.*, 137(4):044506, July 2012. doi:10.1063/1.4736712.

G. D. Mahan. Van der Waals Forces in Solids. *J. Chem. Phys.*, 43(5):1569–1574, Sept. 1965. doi:10.1063/1.1696973.

N. Mardirossian and M. Head-Gordon. Mapping the genome of meta-generalized gradient approximation density functionals: The search for B97M-V. *J. Chem. Phys.*, 142(7):074111, Feb. 2015. doi:10.1063/1.4907719.

A. Marini, P. García-González, and A. Rubio. First-Principles Description of Correlation Effects in Layered Materials. *Phys. Rev. Lett.*, 96(13):136404, Apr. 2006. doi:10.1103/PhysRevLett.96.136404.

N. Marom, A. Tkatchenko, M. Rossi, V. V. Gobre, O. Hod, M. Scheffler, and L. Kronik. Dispersion Interactions with Density-Functional Theory: Benchmarking Semiempirical and Interatomic Pairwise Corrected Density Functionals. *J. Chem. Theory Comput.*, 7(12):3944–3951, Dec. 2011. doi:10.1021/ct2005616.

N. Marom, R. A. DiStasio, Jr., V. Atalla, S. Levchenko, A. M. Reilly, J. R. Chelikowsky, L. Leiserowitz, and A. Tkatchenko. Many-Body Dispersion Interactions in Molecular Crystal Polymorphism. *Angew. Chem.*, 125(26):6761–6764, June 2013. doi:10.1002/ange.201301938.

M. A. L. Marques, A. Castro, G. Malloci, G. Mulas, and S. Botti. Efficient calculation of van der Waals dispersion coefficients with time-dependent density functional theory in real time: Application to polycyclic aromatic hydrocarbons. *J. Chem. Phys.*, 127(1):014107, July 2007. doi:10.1063/1.2746031.

N. Marzari, A. A. Mostofi, J. R. Yates, I. Souza, and D. Vanderbilt. Maximally localized Wannier functions: Theory and applications. *Rev. Mod. Phys.*, 84(4):1419–1475, Oct. 2012. doi:10.1103/RevModPhys.84.1419.

R. J. Maurer, V. G. Ruiz, and A. Tkatchenko. Many-body dispersion effects in the binding of adsorbates on metal surfaces. *J. Chem. Phys.*, 143(10):102808, 2015.

A. Mayer. Formulation in terms of normalized propagators of a charge-dipole model enabling the calculation of the polarization properties of fullerenes and carbon nanotubes. *Phys. Rev. B*, 75(4):045407, Jan. 2007. doi:10.1103/PhysRevB.75.045407.

A. D. McLachlan and M. A. Ball. Time-Dependent Hartree–Fock Theory for Molecules. *Rev. Mod. Phys.*, 36(3):844–855, July 1964. doi:10.1103/RevModPhys.36.844.

G. Mercurio, E. R. McNellis, I. Martin, S. Hagen, F. Leyssner, S. Soubatch, J. Meyer, M. Wolf, P. Tegeder, F. S. Tautz, and K. Reuter. Structure and Energetics of Azobenzene on Ag(111): Benchmarking Semiempirical Dispersion Correction Approaches. *Phys. Rev. Lett.*, 104(3):036102, Jan. 2010. doi:10.1103/PhysRevLett.104.036102.

A. J. Misquitta, J. Spencer, A. J. Stone, and A. Alavi. Dispersion interactions between semiconducting wires. *Phys. Rev. B*, 82:075312, 2010.

A. J. Misquitta, R. Maezono, N. D. Drummond, A. J. Stone, and R. J. Needs. Anomalous nonadditive dispersion interactions in systems of three one-dimensional wires. *Phys. Rev. B*, 89(4):045140, Jan. 2014. doi:10.1103/PhysRevB.89.045140.

J. Mitroy and J.-Y. Zhang. Long-range dispersion interactions. II. Alkali-metal and rare-gas atoms. *Phys. Rev. A*, 76(3):032706, Sept. 2007. doi:10.1103/PhysRevA.76.032706.

F. Mittendorfer, A. Garhofer, J. Redinger, J. Klimeš, J. Harl, and G. Kresse. Graphene on Ni(111): Strong interaction and weak adsorption. *Phys. Rev. B*, 84(20):201401, Nov. 2011. doi:10.1103/PhysRevB.84.201401.

J. Moellmann and S. Grimme. DFT-D3 Study of Some Molecular Crystals. *J. Phys. Chem. C*, 118(14):7615–7621, Apr. 2014. doi:10.1021/jp501237c.

J. Moellmann, S. Ehrlich, R. Tonner, and S. Grimme. A DFT-D study of structural and energetic properties of TiO2 modifications. *J. Phys.: Condens. Matter*, 24(42):424206, 2012. doi:10.1088/0953-8984/24/42/424206.

A. Møgelhøj, A. K. Kelkkanen, K. T. Wikfeldt, J. Schiøtz, J. J. Mortensen, L. G. M. Pettersson, B. I. Lundqvist, K. W. Jacobsen, A. Nilsson, and J. K. Nørskov. Ab Initio van der Waals Interactions in Simulations of Water Alter Structure from Mainly Tetrahedral to High-Density-Like. *J. Phys. Chem. B*, 115(48):14149–14160, Dec. 2011. doi:10.1021/jp2040345.

É. D. Murray, K. Lee, and D. C. Langreth. Investigation of Exchange Energy Density Functional Accuracy for Interacting Molecules. *J. Chem. Theory Comput.*, 5(10):2754–2762, Oct. 2009. doi:10.1021/ct900365q.

Y. Muto. Force between nonpolar molecules. *J. Phys.-Math. Soc. Japan*, 17:629–631, 1943.

V. Ngo, M. C. da Silva, M. Kubillus, H. Li, B. Roux, M. Elstner, Q. Cui, D. R. Salahub, and S. Y. Noskov. Quantum effects in cation interactions with first and second coordination shell ligands in metalloproteins. *J. Chem. Theory Comput.*, 11(10):4992–5001, 2015. doi:10.1021/acs.jctc.5b00524.

R. Nimalakirthi and K. L. C. Hunt. Nonlocal polarizability density of a model system: A homogeneous electron gas at T=0. *J. Chem. Phys.*, 98(4):3066–3075, Feb. 1993. doi:10.1063/1.464133.

T. Olsen and K. S. Thygesen. Extending the random-phase approximation for electronic correlation energies: The renormalized adiabatic local density approximation. *Phys. Rev. B*, 86(8):081103, Aug. 2012. doi:10.1103/PhysRevB.86.081103.

T. Olsen and K. S. Thygesen. Beyond the random phase approximation: Improved description of short-range correlation by a renormalized adiabatic local density approximation. *Phys. Rev. B*, 88(11):115131, Sept. 2013a. doi:10.1103/PhysRevB.88.115131.

T. Olsen and K. S. Thygesen. Random phase approximation applied to solids, molecules, and graphene-metal interfaces: From van der Waals to covalent bonding. *Phys. Rev. B*, 87(7):075111, Feb. 2013b. doi:10.1103/PhysRevB.87.075111.

T. Olsen and K. S. Thygesen. Accurate Ground-State Energies of Solids and Molecules from Time-Dependent Density-Functional Theory. *Phys. Rev. Lett.*, 112(20):203001, May 2014. doi:10.1103/PhysRevLett.112.203001.

T. Olsen, J. Yan, J. J. Mortensen, and K. S. Thygesen. Dispersive and Covalent Interactions between Graphene and Metal Surfaces from the Random Phase Approximation. *Phys. Rev. Lett.*, 107(15):156401, Oct. 2011. doi:10.1103/PhysRevLett.107.156401.

A. Otero-de-la-Roza and E. R. Johnson. A benchmark for non-covalent interactions in solids. *J. Chem. Phys.*, 137(5):054103, Aug. 2012a. doi:10.1063/1.4738961.

A. Otero-de-la-Roza and E. R. Johnson. Van der Waals interactions in solids using the exchange-hole dipole moment model. *J. Chem. Phys.*, 136(17):174109, May 2012b. doi:10.1063/1.4705760.

A. Otero-de-la-Roza and E. R. Johnson. Many-body dispersion interactions from the exchange-hole dipole moment model. *J. Chem. Phys.*, 138(5):054103, Feb. 2013. doi:10.1063/1.4789421.

A. Otero-de-la-Roza and E. R. Johnson. Predicting Energetics of Supramolecular Systems Using the XDM Dispersion Model. *J. Chem. Theory Comput.*, 11(9):4033–4040, Sept. 2015. doi:10.1021/acs.jctc.5b00044.

A. Otero-de-la-Roza, B. H. Cao, I. K. Price, J. E. Hein, and E. R. Johnson. Predicting the relative solubilities of racemic and enantiopure crystals by density-functional theory. *Angew. Chem. Int. Ed.*, 53:7879–7882, 2014.

Y. C. Park and J. S. Lee. Accurate ab Initio Binding Energies of the Benzene Dimer. *J. Phys. Chem. A*, 110(15):5091–5095, Apr. 2006. doi:10.1021/jp0582888.

R. M. Parrish, J. F. Gonthier, C. Corminbœuf, and C. D. Sherrill. Communication: Practical intramolecular symmetry adapted perturbation theory via Hartree-Fock embedding. *J. Chem. Phys.*, 143(5):051103, Aug. 2015. doi:10.1063/1.4927575.

V. A. Parsegian. *Van der Waals Forces: A Handbook for Biologists, Chemists, Engineers, and Physicists*. Cambridge University Press, Cambridge, 2005. ISBN 978-0-511-61460-6. URL `http://ebooks.cambridge.org/ref/id/CBO9780511614606`.

J. P. Perdew and W. Yue. Accurate and simple density functional for the electronic exchange energy: Generalized gradient approximation. *Phys. Rev. B*, 33(12):8800–8802, June 1986. doi:10.1103/PhysRevB.33.8800.

J. P. Perdew, K. Burke, and M. Ernzerhof. Generalized Gradient Approximation Made Simple. *Phys. Rev. Lett.*, 77(18):3865–3868, Oct. 1996. doi:10.1103/PhysRevLett.77.3865.

K. Pernal, R. Podeszwa, K. Patkowski, and K. Szalewicz. Dispersionless Density Functional Theory. *Phys. Rev. Lett.*, 103(26):263201, Dec. 2009.

doi:10.1103/PhysRevLett.103.263201.

R. Peverati and D. G. Truhlar. Improving the Accuracy of Hybrid Meta-GGA Density Functionals by Range Separation. *J. Phys. Chem. Lett.*, 2(21): 2810–2817, Nov. 2011. doi:10.1021/jz201170d.

D. Pines. *Elementary Excitations in Solids*. Westview Press, Reading, Mass, Mar. 1999. ISBN 978-0-7382-0115-3.

R. Podeszwa, B. M. Rice, and K. Szalewicz. Predicting Structure of Molecular Crystals from First Principles. *Phys. Rev. Lett.*, 101(11):115503, Sept. 2008. doi:10.1103/PhysRevLett.101.115503.

S. L. Price. Predicting crystal structures of organic compounds. *Chem. Soc. Rev.*, 43(7):2098–2111, Mar. 2014. doi:10.1039/C3CS60279F.

E. Prodan and W. Kohn. Nearsightedness of electronic matter. *Proc. Natl. Acad. Sci. U. S. A.*, 102(33):11635–11638, Aug. 2005. doi:10.1073/pnas.0505436102.

A. Puzder, M. Dion, and D. C. Langreth. Binding energies in benzene dimers: Nonlocal density functional calculations. *J. Chem. Phys.*, 124(16):164105, Apr. 2006. doi:10.1063/1.2189229.

L. Rajchel, P. S. Żuchowski, M. M. Szcześniak, and G. Chałasiński. Density Functional Theory Approach to Noncovalent Interactions via Monomer Polarization and Pauli Blockade. *Phys. Rev. Lett.*, 104(16):163001, Apr. 2010. doi:10.1103/PhysRevLett.104.163001.

G. A. Rance, D. H. Marsh, S. J. Bourne, T. J. Reade, and A. N. Khlobystov. Van der Waals Interactions between Nanotubes and Nanoparticles for Controlled Assembly of Composite Nanostructures. *ACS Nano*, 4(8):4920–4928, Aug. 2010. doi:10.1021/nn101287u.

W. Reckien, M. Eggers, and T. Bredow. Theoretical study of the adsorption of benzene on coinage metals. *Beilstein J. Org. Chem.*, 10(1):1775–1784, Aug. 2014. doi:10.3762/bjoc.10.185.

C. R. C. Rêgo, L. N. Oliveira, P. Tereshchuk, and J. L. F. Da Silva. Comparative study of van der Waals corrections to the bulk properties of graphite. *J. Phys.: Condens. Matter*, 27(41):415502, 2015. doi:10.1088/0953-8984/27/41/415502.

A. M. Reilly and A. Tkatchenko. Understanding the role of vibrations, exact exchange, and many-body van der Waals interactions in the cohesive properties of molecular crystals. *J. Chem. Phys.*, 139(2):024705, July 2013a. doi:10.1063/1.4812819.

A. M. Reilly and A. Tkatchenko. Seamless and Accurate Modeling of Organic Molecular Materials. *J. Phys. Chem. Lett.*, 4(6):1028–1033, Mar. 2013b. doi:10.1021/jz400226x.

A. M. Reilly and A. Tkatchenko. Role of dispersion interactions in the polymorphism and entropic stabilization of the aspirin crystal. *Phys. Rev. Lett.*, 113:055701, July 2014a. doi:10.1103/PhysRevLett.113.055701.

A. M. Reilly and A. Tkatchenko. Role of Dispersion Interactions in the Polymorphism and Entropic Stabilization of the Aspirin Crystal. *Phys. Rev. Lett.*, 113(5):055701, July 2014b. doi:10.1103/PhysRevLett.113.055701.

A. M. Reilly and A. Tkatchenko. Van der Waals dispersion interactions in molecular materials: Beyond pairwise additivity. *Chem. Sci.*, 6(6):3289–3301, May 2015. doi:10.1039/C5SC00410A.

A. M. Reilly, R. I. Cooper, C. S. Adjiman, S. Bhattacharya, A. D. Boese, J. G. Brandenburg, P. J. Bygrave, R. Bylsma, J. E. Campbell, R. Car, D. H. Case, R. Chadha, J. C. Cole, K. Cosburn, H. M. Cuppen, F. Curtis, G. M. Day, R. A. DiStasio Jr, A. Dzyabchenko, B. P. van Eijck, D. M. Elking, J. A. van den Ende, J. C. Facelli, M. B. Ferraro, L. Fusti-Molnar, C.-A. Gatsiou, T. S. Gee, R. de Gelder, L. M. Ghiringhelli, H. Goto, S. Grimme, R. Guo, D. W. M. Hofmann, J. Hoja, R. K. Hylton, L. Iuzzolino, W. Jankiewicz, D. T. de Jong, J. Kendrick, N. J. J. de Klerk, H.-Y. Ko, L. N. Kuleshova, X. Li, S. Lohani, F. J. J. Leusen, A. M. Lund, J. Lv, Y. Ma, N. Marom, A. E. Masunov, P. McCabe, D. P. McMahon, H. Meekes, M. P. Metz, A. J. Misquitta, S. Mohamed, B. Monserrat, R. J. Needs, M. A. Neumann, J. Nyman, S. Obata, H. Oberhofer, A. R. Oganov, A. M. Orendt, G. I. Pagola, C. C. Pantelides, C. J. Pickard, R. Podeszwa, L. S. Price, S. L. Price, A. Pulido, M. G. Read, K. Reuter, E. Schneider, C. Schober, G. P. Shields, P. Singh, I. J. Sugden, K. Szalewicz, C. R. Taylor, A. Tkatchenko, M. E. Tuckerman, F. Vacarro, M. Vasileiadis, A. Vazquez-Mayagoitia, L. Vogt, Y. Wang, R. E. Watson, G. A. de Wijs, J. Yang, Q. Zhu, and C. R. Groom. Report on the sixth blind test of organic crystal structure prediction methods. *Acta Crystallogr.*, B72(4):439–459, Aug. 2016. doi:10.1107/S2052520616007447.

X. Ren, A. Tkatchenko, P. Rinke, and M. Scheffler. Beyond the Random-Phase Approximation for the Electron Correlation Energy: The Importance of Single Excitations. *Phys. Rev. Lett.*, 106(15):153003, Apr. 2011. doi:10.1103/PhysRevLett.106.153003.

X. Ren, P. Rinke, C. Joas, and M. Scheffler. Random-phase approximation and its applications in computational chemistry and materials science. *J. Mater. Sci.*, 47(21):7447–7471, June 2012. doi:10.1007/s10853-012-6570-4.

X. Ren, P. Rinke, G. E. Scuseria, and M. Scheffler. Renormalized second-order perturbation theory for the electron correlation energy: Concept, implementation, and benchmarks. *Phys. Rev. B*, 88(3):035120, July 2013. doi:10.1103/PhysRevB.88.035120.

M. J. Renne and B. R. A. Nijboer. Microscopic derivation of macroscopic Van der Waals forces. *Chem. Phys. Lett.*, 1(8):317–320, Oct. 1967. doi:10.1016/0009-2614(67)80004-6.

J. Řezáč, K. E. Riley, and P. Hobza. S66: A Well-balanced Database of Benchmark Interaction Energies Relevant to Biomolecular Structures. *J. Chem. Theory Comput.*, 7(8):2427–2438, Aug. 2011. doi:10.1021/ct2002946.

J. Řezáč, K. E. Riley, and P. Hobza. Benchmark Calculations of Noncovalent Interactions of Halogenated Molecules. *J. Chem. Theory Comput.*, 8(11): 4285–4292, Nov. 2012. doi:10.1021/ct300647k.

J. Řezáč, Y. Huang, P. Hobza, and G. J. O. Beran. Benchmark Calculations of Three-Body Intermolecular Interactions and the Performance of Low-Cost Electronic Structure Methods. *J. Chem. Theory Comput.*, 11(7):3065–3079, July 2015. doi:10.1021/acs.jctc.5b00281.

T. Risthaus and S. Grimme. Benchmarking of London Dispersion-Accounting Density Functional Theory Methods on Very Large Molecular Complexes. *J. Chem. Theory Comput.*, 9(3):1580–1591, Mar. 2013. doi:10.1021/ct301081n.

A. W. Rodriguez, F. Capasso, and S. G. Johnson. The Casimir effect in microstructured geometries. *Nat. Photonics*, 5(4):211–221, Apr. 2011. doi:10.1038/nphoton.2011.39.

G. Román-Pérez and J. Soler. Efficient Implementation of a van der Waals Density Functional: Application to Double-Wall Carbon Nanotubes. *Phys. Rev. Lett.*, 103(9):096102, Aug. 2009. doi:10.1103/PhysRevLett.103.096102.

M. Rossi, V. Blum, P. Kupser, G. von Helden, F. Bierau, K. Pagel, G. Meijer, and M. Scheffler. Secondary Structure of Ac-Alan-LysH+ Polyalanine Peptides (n = 5,10,15) in Vacuo: Helical or Not? *J. Phys. Chem. Lett.*, 1 (24):3465–3470, Dec. 2010. doi:10.1021/jz101394u.

M. Rossi, A. Tkatchenko, S. B. Rempe, and S. Varma. Role of methyl-induced polarization in ion binding. *Proc. Natl. Acad. Sci. USA*, 110:12978–12983, 2013.

M. Rossi, S. Chutia, M. Scheffler, and V. Blum. Validation Challenge of Density-Functional Theory for Peptides—Example of Ac-Phe-Ala5-LysH+. *J. Phys. Chem. A*, 118(35):7349–7359, Sept. 2014. doi:10.1021/jp412055r.

M. Rossi, W. Fang, and A. Michaelides. Stability of Complex Biomolecular Structures: Van der Waals, Hydrogen Bond Cooperativity, and Nuclear Quantum Effects. *J. Phys. Chem. Lett.*, 6(21):4233–4238, Nov. 2015. doi:10.1021/acs.jpclett.5b01899.

B. Rozitis, E. MacLennan, and J. P. Emery. Cohesive forces prevent the rotational breakup of rubble-pile asteroid (29075) 1950 DA. *Nature*, 512: 174–176, 2014.

V. G. Ruiz, W. Liu, E. Zojer, M. Scheffler, and A. Tkatchenko. Density-Functional Theory with Screened van der Waals Interactions for the Modeling of Hybrid Inorganic-Organic Systems. *Phys. Rev. Lett.*, 108(14):146103, Apr. 2012. doi:10.1103/PhysRevLett.108.146103.

V. G. Ruiz, W. Liu, and A. Tkatchenko. Density-functional theory with screened van der Waals interactions applied to atomic and molecular adsorbates on close-packed and non-close-packed surfaces. *Phys. Rev. B*, 93(3):035118, Jan. 2016. doi:10.1103/PhysRevB.93.035118.

A. Ruzsinszky and J. P. Perdew. Twelve outstanding problems in ground-state density functional theory: A bouquet of puzzles. *Comput. Theor. Chem.*, 963(1):2–6, Jan. 2011. doi:10.1016/j.comptc.2010.09.002.

A. Ruzsinszky, J. P. Perdew, J. Tao, G. I. Csonka, and J. M. Pitarke. Van der Waals Coefficients for Nanostructures: Fullerenes Defy Conventional Wisdom. *Phys. Rev. Lett.*, 109(23):233203, Dec. 2012. doi:10.1103/PhysRevLett.109.233203.

R. Sabatini, T. Gorni, and S. de Gironcoli. Nonlocal van der Waals density functional made simple and efficient. *Phys. Rev. B*, 87(4):041108, Jan. 2013. doi:10.1103/PhysRevB.87.041108.

J. C. Sancho-García and Y. Olivier. Reliable DFT-based estimates of cohesive energies of organic solids: The anthracene crystal. *J. Chem. Phys.*, 137(19): 194311, Nov. 2012. doi:10.1063/1.4766933.

J. C. Sancho-García, A. J. Pérez-Jiménez, and Y. Olivier. Determining the cohesive energy of coronene by dispersion-corrected DFT methods: Periodic boundary conditions vs. molecular pairs. *J. Chem. Phys.*, 142(5):054702, Feb. 2015. doi:10.1063/1.4907268.

B. Santra, A. Michaelides, M. Fuchs, A. Tkatchenko, C. Filippi, and M. Scheffler. On the accuracy of density-functional theory exchange-correlation functionals for H bonds in small water clusters. II. The water hexamer and

van der Waals interactions. *J. Chem. Phys.*, 129(19):194111, Nov. 2008. doi:10.1063/1.3012573.

T. Sato and H. Nakai. Density functional method including weak interactions: Dispersion coefficients based on the local response approximation. *J. Chem. Phys.*, 131(22):224104, Dec. 2009. doi:10.1063/1.3269802.

T. Sato and H. Nakai. Local response dispersion method. II. Generalized multicenter interactions. *J. Chem. Phys.*, 133(19):194101, Nov. 2010. doi:10.1063/1.3503040.

D. J. Scheeres, C. M. Hartzell, P. Sánchez, and M. Swift. Scaling forces to asteroid surfaces: The role of cohesion. *Icarus*, 210:968–984, 2010.

J. Schmidt, J. VandeVondele, I.-F. W. Kuo, D. Sebastiani, J. I. Siepmann, J. Hutter, and C. J. Mundy. Isobaric-Isothermal Molecular Dynamics Simulations Utilizing Density Functional Theory: An Assessment of the Structure and Density of Water at Near-Ambient Conditions. *J. Phys. Chem. B*, 113(35): 11959–11964, Sept. 2009. doi:10.1021/jp901990u.

F. Schubert, M. Rossi, C. Baldauf, K. Pagel, S. Warnke, G. v. Helden, F. Filsinger, P. Kupser, G. Meijer, M. Salwiczek, B. Koksch, M. Scheffler, and V. Blum. Exploring the conformational preferences of 20-residue peptides in isolation: Ac-Ala19-Lys + H+vs. Ac-Lys-Ala19 + H+ and the current reach of DFT. *Phys. Chem. Chem. Phys.*, 17(11):7373–7385, Mar. 2015. doi:10.1039/C4CP05541A.

G. E. Scuseria, T. M. Henderson, and D. C. Sorensen. The ground state correlation energy of the random phase approximation from a ring coupled cluster doubles approach. *J. Chem. Phys.*, 129(23):231101, Dec. 2008. doi:10.1063/1.3043729.

R. Sedlak, T. Janowski, M. Pitoňák, J. Řezáč, P. Pulay, and P. Hobza. Accuracy of Quantum Chemical Methods for Large Noncovalent Complexes. *J. Chem. Theory Comput.*, 9(8):3364–3374, Aug. 2013. doi:10.1021/ct400036b.

Y. V. Shtogun and L. M. Woods. Many-body van der waals interactions between graphitic nanostructures. *J. Phys. Chem. Lett.*, 1:1356, 2010.

P. L. Silvestrelli. Van der Waals Interactions in DFT Made Easy by Wannier Functions. *Phys. Rev. Lett.*, 100(5):053002, Feb. 2008. doi:10.1103/PhysRevLett.100.053002.

P. L. Silvestrelli. Improvement in hydrogen bond description using van der Waals-corrected DFT: The case of small water clusters. *Chem. Phys. Lett.*, 475(4-6):285–288, June 2009a. doi:10.1016/j.cplett.2009.05.049.

P. L. Silvestrelli. Van der Waals Interactions in Density Functional Theory Using Wannier Functions. *J. Phys. Chem. A*, 113(17):5224–5234, Apr. 2009b. doi:10.1021/jp811138n.

P. L. Silvestrelli. Van der Waals interactions in density functional theory by combining the quantum harmonic oscillator-model with localized Wannier functions. *J. Chem. Phys.*, 139(5):054106, Aug. 2013. doi:10.1063/1.4816964.

P. L. Silvestrelli, K. Benyahia, S. Grubisiĉ, F. Ancilotto, and F. Toigo. Van der Waals interactions at surfaces by density functional theory using Wannier functions. *J. Chem. Phys.*, 130(7):074702, Feb. 2009. doi:10.1063/1.3077288.

P. L. Silvestrelli, A. Ambrosetti, S. Grubisiĉ, and F. Ancilotto. Adsorption of rare-gas atoms on Cu(111) and Pb(111) surfaces by van der Waals corrected density functional theory. *Phys. Rev. B*, 85(16):165405, Apr. 2012. doi:10.1103/PhysRevB.85.165405.

M. O. Sinnokrot and C. D. Sherrill. Highly Accurate Coupled Cluster Potential Energy Curves for the Benzene Dimer: Sandwich, T-Shaped, and Parallel-Displaced Configurations. *J. Phys. Chem. A*, 108(46):10200–10207, Nov. 2004. doi:10.1021/jp0469517.

M. O. Sinnokrot, E. F. Valeev, and C. D. Sherrill. Estimates of the Ab Initio Limit for π-π Interactions: The Benzene Dimer. *J. Am. Chem. Soc.*, 124 (36):10887–10893, Sept. 2002. doi:10.1021/ja025896h.

L. B. Skinner, C. Huang, D. Schlesinger, L. G. M. Pettersson, A. Nilsson, and C. J. Benmore. Benchmark oxygen-oxygen pair-distribution function of ambient water from x-ray diffraction measurements with a wide Q-range. *J. Chem. Phys.*, 138(7):074506, Feb. 2013. doi:10.1063/1.4790861.

V. P. Sokhan, A. P. Jones, F. S. Cipcigan, J. Crain, and G. J. Martyna. Signature properties of water: Their molecular electronic origins. *Proc. Natl. Acad. Sci.*, 112(20):6341–6346, May 2015. doi:10.1073/pnas.1418982112.

P. Sony, P. Puschnig, D. Nabok, and C. Ambrosch-Draxl. Importance of Van Der Waals Interaction for Organic Molecule-Metal Junctions: Adsorption of Thiophene on Cu(110) as a Prototype. *Phys. Rev. Lett.*, 99(17):176401, Oct. 2007. doi:10.1103/PhysRevLett.99.176401.

A. K. Soper and C. J. Benmore. Quantum Differences between Heavy and Light Water. *Phys. Rev. Lett.*, 101(6):065502, Aug. 2008. doi:10.1103/PhysRevLett.101.065502.

D. C. Sorescu, E. F. C. Byrd, B. M. Rice, and K. D. Jordan. Assessing the Performances of Dispersion-Corrected Density Functional Methods for Predicting the Crystallographic Properties of High Nitrogen Energetic Salts. *J. Chem. Theory Comput.*, 10(11):4982–4994, Nov. 2014. doi:10.1021/ct5005615.

L. Spanu, S. Sorella, and G. Galli. Nature and Strength of Interlayer Binding in Graphite. *Phys. Rev. Lett.*, 103(19):196401, Nov. 2009. doi:10.1103/PhysRevLett.103.196401.

G. Starkschall and R. G. Gordon. Calculation of Coefficients in the Power Series Expansion of the Long-Range Dispersion Force between Atoms. *J. Chem. Phys.*, 56(6):2801–2806, Mar. 1972. doi:10.1063/1.1677610.

S. N. Steinmann and C. Corminboeuf. A System-Dependent Density-Based Dispersion Correction. *J. Chem. Theory Comput.*, 6(7):1990–2001, July 2010. doi:10.1021/ct1001494.

S. N. Steinmann and C. Corminboeuf. A generalized-gradient approximation exchange hole model for dispersion coefficients. *J. Chem. Phys.*, 134(4): 044117, Jan. 2011a. doi:10.1063/1.3545985.

S. N. Steinmann and C. Corminboeuf. Comprehensive Benchmarking of a Density-Dependent Dispersion Correction. *J. Chem. Theory Comput.*, 7 (11):3567–3577, Nov. 2011b. doi:10.1021/ct200602x.

A. J. Stone. *The Theory of Intermolecular Forces*. Oxford University Press, 2nd edition, Jan. 2013. ISBN 978-0-19-967239-4. URL http://www.oxfordscholarship.com/view/10.1093/acprof:oso/9780199672394.001.0001/acprof-9780199672394.

D. Stradi, S. Barja, C. Díaz, M. Garnica, B. Borca, J. J. Hinarejos, D. Sánchez-Portal, M. Alcamí, A. Arnau, A. L. Vázquez de Parga, R. Miranda, and F. Martín. Role of Dispersion Forces in the Structure of Graphene Monolayers on Ru Surfaces. *Phys. Rev. Lett.*, 106(18):186102, May 2011. doi:10.1103/PhysRevLett.106.186102.

M. Stöhr, G. Michelitsch, J. Tully, K. Reuter, and R. Maurer. Communication: Charge-population based dispersion interactions for molecules and materials. *J. Chem. Phys.*, 144:151101, 2016.

J. Sun, A. Ruzsinszky, and J. P. Perdew. Strongly Constrained and Appropriately Normed Semilocal Density Functional. *Phys. Rev. Lett.*, 115(3):036402, July 2015. doi:10.1103/PhysRevLett.115.036402.

J. Sun, R. C. Remsing, Y. Zhang, Z. Sun, A. Ruzsinszky, H. Peng, Z. Yang, A. Paul, U. Waghmare, X. Wu, M. L. Klein, and J. P. Perdew. Accurate first-principles structures and energies of diversely bonded systems from an efficient density functional. *Nat. Chem.*, 8(9):831–836, Sept. 2016. doi:10.1038/nchem.2535.

R. Sure and S. Grimme. Comprehensive Benchmark of Association (Free) Energies of Realistic Host–Guest Complexes. *J. Chem. Theory Comput.*, 11(8):3785–3801, Aug. 2015. doi:10.1021/acs.jctc.5b00296.

A. Szabo and N. S. Ostlund. *Modern Quantum Chemistry*. McGraw-Hill, New York, 1989.

K. Szalewicz. Symmetry-adapted perturbation theory of intermolecular forces. *Wiley Interdiscip. Rev. Comput. Mol. Sci.*, 2(2):254–272, Mar. 2012. doi:10.1002/wcms.86.

K. T. Tang and J. P. Toennies. An improved simple model for the van der Waals potential based on universal damping functions for the dispersion coefficients. *J. Chem. Phys.*, 80(8):3726–3741, Apr. 1984. doi:10.1063/1.447150.

K. T. Tang and J. P. Toennies. The van der Waals potentials between all the rare gas atoms from He to Rn. *J. Chem. Phys.*, 118(11):4976–4983, Mar. 2003. doi:10.1063/1.1543944.

J. Tao, J. P. Perdew, and A. Ruzsinszky. Long-range van der Waals attraction and alkali-metal lattice constants. *Phys. Rev. B*, 81(23):233102, June 2010. doi:10.1103/PhysRevB.81.233102.

J. Tao, J. P. Perdew, and A. Ruzsinszky. Accurate van der Waals coefficients from density functional theory. *Proc. Natl. Acad. Sci. U. S. A.*, 109(1): 18–21, Mar. 2012. doi:10.1073/pnas.1118245108.

J. Tao, Y. Fang, P. Hao, G. E. Scuseria, A. Ruzsinszky, and J. P. Perdew. Van der Waals coefficients beyond the classical shell model. *J. Chem. Phys.*, 142(2):024312, Jan. 2015. doi:10.1063/1.4905259.

E. Tapavicza, I.-C. Lin, O. A. von Lilienfeld, I. Tavernelli, M. D. Coutinho-Neto, and U. Rothlisberger. Weakly Bonded Complexes of Aliphatic and Aromatic Carbon Compounds Described with Dispersion Corrected Density Functional Theory. *J. Chem. Theory Comput.*, 3(5):1673–1679, Sept. 2007. doi:10.1021/ct700049s.

J. R. Tessman, A. H. Kahn, and W. Shockley. Electronic polarizabilities of ions in crystals. *Phys. Rev.*, 92:890–895, 1953. doi:10.1103/PhysRev.92.890.

A. J. Thakkar. Higher dispersion coefficients: Accurate values for hydrogen atoms and simple estimates for other systems. *J. Chem. Phys.*, 89(4):2092–2098, Aug. 1988. doi:10.1063/1.455105.

B. T. Thole. Molecular polarizabilities calculated with a modified dipole interaction. *Chem. Phys.*, 59(3):341–350, Aug. 1981. doi:10.1016/0301-0104(81)85176-2.

T. Thonhauser, V. R. Cooper, S. Li, A. Puzder, P. Hyldgaard, and D. C. Langreth. Van der Waals density functional: Self-consistent potential and the nature of the van der Waals bond. *Phys. Rev. B*, 76(12):125112, Sept. 2007. doi:10.1103/PhysRevB.76.125112.

A. Tkatchenko. Current Understanding of Van der Waals Effects in Realistic Materials. *Adv. Funct. Mater.*, 25(13):2054–2061, Apr. 2015. doi:10.1002/adfm.201403029.

A. Tkatchenko and M. Scheffler. Accurate Molecular Van Der Waals Interactions from Ground-State Electron Density and Free-Atom Reference Data. *Phys. Rev. Lett.*, 102(7):073005, Feb. 2009. doi:10.1103/PhysRevLett.102.073005.

A. Tkatchenko and O. A. von Lilienfeld. Popular Kohn-Sham density functionals strongly overestimate many-body interactions in van der Waals systems. *Phys. Rev. B*, 78(4):045116, July 2008. doi:10.1103/PhysRevB.78.045116.

A. Tkatchenko, L. Romaner, O. T. Hofmann, E. Zojer, C. Ambrosch-Draxl, and M. Scheffler. Van der Waals Interactions Between Organic Adsorbates and at Organic/Inorganic Interfaces. *MRS Bull.*, 35(06):435–442, June 2010. doi:10.1557/mrs2010.581.

A. Tkatchenko, M. Rossi, V. Blum, J. Ireta, and M. Scheffler. Unraveling the Stability of Polypeptide Helices: Critical Role of van der Waals Interactions. *Phys. Rev. Lett.*, 106(11):118102, Mar. 2011. doi:10.1103/PhysRevLett.106.118102.

A. Tkatchenko, R. A. DiStasio, Jr., R. Car, and M. Scheffler. Accurate and Efficient Method for Many-Body van der Waals Interactions. *Phys. Rev. Lett.*, 108(23):236402, June 2012. doi:10.1103/PhysRevLett.108.236402.

A. Tkatchenko, A. Ambrosetti, and R. A. DiStasio, Jr. Interatomic methods for the dispersion energy derived from the adiabatic connection fluctuation-dissipation theorem. *J. Chem. Phys.*, 138(7):74106, Feb. 2013. doi:10.1063/1.4789814.

G. Tocci, L. Joly, and A. Michaelides. Friction of Water on Graphene and Hexagonal Boron Nitride from Ab Initio Methods: Very Different Slippage Despite Very Similar Interface Structures. *Nano Lett.*, 14(12):6872–6877, Dec. 2014. doi:10.1021/nl502837d.

K. Tonigold and A. Groß. Adsorption of small aromatic molecules on the (111) surfaces of noble metals: A density functional theory study with semiempirical corrections for dispersion effects. *J. Chem. Phys.*, 132(22): 224701, June 2010. doi:10.1063/1.3439691.

J. Toulouse, F. Colonna, and A. Savin. Long-range–short-range separation of the electron-electron interaction in density-functional theory. *Phys. Rev. A*, 70(6):062505, Dec. 2004. doi:10.1103/PhysRevA.70.062505.

J. Toulouse, I. C. Gerber, G. Jansen, A. Savin, and J. G. Ángyán. Adiabatic-Connection Fluctuation-Dissipation Density-Functional Theory Based on Range Separation. *Phys. Rev. Lett.*, 102(9):096404, Mar. 2009. doi:10.1103/PhysRevLett.102.096404.

K. Toyoda, Y. Nakano, I. Hamada, K. Lee, S. Yanagisawa, and Y. Morikawa. First-principles study of benzene on noble metal surfaces: Adsorption states and vacuum level shifts. *Surf. Sci.*, 603(18):2912–2922, Sept. 2009. doi:10.1016/j.susc.2009.07.039.

S. Tsoi, P. Dev, A. L. Friedman, R. Stine, J. T. Robinson, T. L. Reinecke, and P. E. Sheehan. Van der Waals Screening by Single-Layer Graphene and Molybdenum Disulfide. *ACS Nano*, 8(12):12410–12417, Dec. 2014. doi:10.1021/nn5050905.

S. Tsuzuki, T. Uchimaru, K. Matsumura, M. Mikami, and K. Tanabe. Effects of the higher electron correlation correction on the calculated intermolecular interaction energies of benzene and naphthalene dimers: Comparison between MP2 and CCSD(T) calculations. *Chem. Phys. Lett.*, 319(5–6): 547–554, Mar. 2000. doi:10.1016/S0009-2614(00)00170-6.

S. Tsuzuki, K. Honda, T. Uchimaru, M. Mikami, and K. Tanabe. Origin of Attraction and Directionality of the π/π Interaction: Model Chemistry Calculations of Benzene Dimer Interaction. *J. Am. Chem. Soc.*, 124(1): 104–112, Jan. 2002. doi:10.1021/ja0105212.

A. Unsöld. Quantentheorie des Wasserstoffmolekülions und der Born-Landéschen Abstoßungskräfte. *Z. Physik*, 43(8):563–574, Aug. 1927. doi:10.1007/BF01397633.

M. Vanin, J. J. Mortensen, A. K. Kelkkanen, J. M. Garcia-Lastra, K. S. Thygesen, and K. W. Jacobsen. Graphene on metals: A van der Waals density functional study. *Phys. Rev. B*, 81(8):081408, Feb. 2010. doi:10.1103/PhysRevB.81.081408.

T. Verstraelen, E. Pauwels, F. De Proft, V. Van Speybroeck, P. Geerlings, and M. Waroquier. Assessment of Atomic Charge Models for Gas-Phase Computations on Polypeptides. *J. Chem. Theory Comput.*, 8(2):661–676, Feb. 2012. doi:10.1021/ct200512e.

O. A. von Lilienfeld, I. Tavernelli, U. Rothlisberger, and D. Sebastiani. Optimization of Effective Atom Centered Potentials for London Dispersion Forces in Density Functional Theory. *Phys. Rev. Lett.*, 93(15):153004, Oct. 2004. doi:10.1103/PhysRevLett.93.153004.

O. A. von Lilienfeld, I. Tavernelli, U. Rothlisberger, and D. Sebastiani. Performance of optimized atom-centered potentials for weakly bonded systems using density functional theory. *Phys. Rev. B*, 71(19):195119, May 2005. doi:10.1103/PhysRevB.71.195119.

O. A. Vydrov and T. Van Voorhis. Improving the accuracy of the nonlocal van der Waals density functional with minimal empiricism. *J. Chem. Phys.*, 130(10):104105, Mar. 2009a. doi:10.1063/1.3079684.

O. A. Vydrov and T. Van Voorhis. Nonlocal van der Waals Density Functional Made Simple. *Phys. Rev. Lett.*, 103(6):063004, Aug. 2009b. doi:10.1103/PhysRevLett.103.063004.

O. A. Vydrov and T. Van Voorhis. Implementation and assessment of a simple nonlocal van der Waals density functional. *J. Chem. Phys.*, 132(16):164113, Apr. 2010a. doi:10.1063/1.3398840.

O. A. Vydrov and T. Van Voorhis. Nonlocal van der Waals density functional: The simpler the better. *J. Chem. Phys.*, 133(24):244103, Dec. 2010b. doi:10.1063/1.3521275.

O. A. Vydrov and T. Van Voorhis. Dispersion interactions from a local polarizability model. *Phys. Rev. A*, 81(6):062708, June 2010c. doi:10.1103/PhysRevA.81.062708.

O. A. Vydrov and T. Van Voorhis. Vydrov and Van Voorhis Reply. *Phys. Rev. Lett.*, 104(9):099304, Mar. 2010d. doi:10.1103/PhysRevLett.104.099304.

O. A. Vydrov and T. Van Voorhis. Benchmark Assessment of the Accuracy of Several van der Waals Density Functionals. *J. Chem. Theory Comput.*, 8 (6):1929–1934, June 2012. doi:10.1021/ct300081y.

O. A. Vydrov, Q. Wu, and T. Van Voorhis. Self-consistent implementation of a nonlocal van der Waals density functional with a Gaussian basis set. *J. Chem. Phys.*, 129(1):014106, July 2008. doi:10.1063/1.2948400.

C. Wagner, N. Fournier, V. G. Ruiz, C. Li, K. Müllen, M. Rohlfing, A. Tkatchenko, R. Temirov, and F. S. Tautz. Non-additivity of molecule-surface van der Waals potentials from force measurements. *Nat. Commun.*, 5:5568, Nov. 2014. doi:10.1038/ncomms6568.

J. P. Wagner and P. R. Schreiner. London Dispersion in Molecular Chemistry—Reconsidering Steric Effects. *Angew. Chem. Int. Ed.*, 54(42):12274–12296, Oct. 2015. doi:10.1002/anie.201503476.

J. Wang, G. Román-Pérez, J. M. Soler, E. Artacho, and M.-V. Fernández-Serra. Density, structure, and dynamics of water: The effect of van der Waals interactions. *J. Chem. Phys.*, 134(2):024516, Jan. 2011. doi:10.1063/1.3521268.

S. C. Wang. Die gegenseitige Einwirkung zweier Wasserstoffatome [Mutual influence of two hydrogen atoms]. *Phys. Z.*, 28:663–666, 1927.

J. Wellendorff, K. T. Lundgaard, A. Møgelhøj, V. Petzold, D. D. Landis, J. K. Nørskov, T. Bligaard, and K. W. Jacobsen. Density functionals for surface science: Exchange-correlation model development with Bayesian error estimation. *Phys. Rev. B*, 85(23):235149, June 2012. doi:10.1103/PhysRevB.85.235149.

S. Wen and G. J. O. Beran. Accurate Molecular Crystal Lattice Energies from a Fragment QM/MM Approach with On-the-Fly Ab Initio Force Field Parametrization. *J. Chem. Theory Comput.*, 7(11):3733–3742, Nov. 2011. doi:10.1021/ct200541h.

N. Wiser. Dielectric constant with local field effects included. *Phys. Rev.*, 129 (1):62–69, Jan. 1963. doi:10.1103/PhysRev.129.62.

J. Witte, M. Goldey, J. B. Neaton, and M. Head-Gordon. Beyond Energies: Geometries of Nonbonded Molecular Complexes as Metrics for Assessing Electronic Structure Approaches. *J. Chem. Theory Comput.*, 11(4):1481–1492, Apr. 2015. doi:10.1021/ct501050s.

L. M. Woods, D. A. R. Dalvit, A. Tkatchenko, P. Rodriguez-Lopez, A. W. Rodriguez, and R. Podgornik. Materials perspective on Casimir and van der Waals interactions. *Rev. Mod. Phys.*, 88(4):045003, Nov. 2016. doi:10.1103/RevModPhys.88.045003.

Q. Wu and W. Yang. Empirical correction to density functional theory for van der Waals interactions. *J. Chem. Phys.*, 116(2):515–524, Jan. 2002. doi:10.1063/1.1424928.

Z. Yan, J. P. Perdew, and S. Kurth. Density functional for short-range correlation: Accuracy of the random-phase approximation for isoelectronic energy changes. *Phys. Rev. B*, 61(24):16430–16439, June 2000. doi:10.1103/PhysRevB.61.16430.

J. Yang, W. Hu, D. Usvyat, D. Matthews, M. Schütz, and G. K.-L. Chan. Ab initio determination of the crystalline benzene lattice energy to sub-kilojoule/mole accuracy. *Science*, 345(6197):640–643, Aug. 2014. doi:10.1126/science.1254419.

L. Yang, C. Adam, G. S. Nichol, and S. L. Cockroft. How much do van der

waals dispersion forces contribute to molecular recognition in solution? *Nat. Chem.*, 5:1006–1010, 2013.

E. Zaremba and W. Kohn. Van der Waals interaction between an atom and a solid surface. *Phys. Rev. B*, 13(6):2270–2285, Mar. 1976. doi:10.1103/PhysRevB.13.2270.

C. Zhang, J. Wu, G. Galli, and F. Gygi. Structural and Vibrational Properties of Liquid Water from van der Waals Density Functionals. *J. Chem. Theory Comput.*, 7(10):3054–3061, Oct. 2011a. doi:10.1021/ct200329e.

G.-X. Zhang, A. Tkatchenko, J. Paier, H. Appel, and M. Scheffler. Van der Waals Interactions in Ionic and Semiconductor Solids. *Phys. Rev. Lett.*, 107 (24):245501, Dec. 2011b. doi:10.1103/PhysRevLett.107.245501.

J.-Y. Zhang and J. Mitroy. Long-range dispersion interactions. I. Formalism for two heteronuclear atoms. *Phys. Rev. A*, 76(2):022705, Aug. 2007. doi:10.1103/PhysRevA.76.022705.

Y. Zhang and W. Yang. Comment on "Generalized Gradient Approximation Made Simple". *Phys. Rev. Lett.*, 80(4):890–890, Jan. 1998. doi:10.1103/PhysRevLett.80.890.

W. Zhu, J. Toulouse, A. Savin, and J. G. Ángyán. Range-separated density-functional theory with random phase approximation applied to noncovalent intermolecular interactions. *J. Chem. Phys.*, 132(24):244108, June 2010. doi:10.1063/1.3431616.

U. Zimmerli, M. Parrinello, and P. Koumoutsakos. Dispersion corrections to density functionals for water aromatic interactions. *J. Chem. Phys.*, 120: 2693–2699, 2004.

F. Zipoli, R. Car, M. H. Cohen, and A. Selloni. Simulation of Electrocatalytic Hydrogen Production by a Bioinspired Catalyst Anchored to a Pyrite Electrode. *J. Am. Chem. Soc.*, 132(25):8593–8601, June 2010. doi:10.1021/ja910694p.